Republic of Iraq
Ministry of Higher Education
And Scientific Research
University of Babylon –College of Science
Department of Chemistry

Synthesis of Cu/ZnO/rGO tertiary Nanocomposite and its applications to removal of the Rhodamine 6G dye from the aqueous solution and antibacterial activity

A thesis

Submitted to the Council of the College of Science

University of Babylon

In Partial Fulfillment of the Requirements for

The Degree of Master in Chemistry Science

BY

Adel Hamza Abbas Hassoun

B.Sc. University of AL-Qadisiyah 2013

Supervised by

Prof .Dr . Nada Yahiya Fairooz

2021 AD **1443 H**

بِسْمِ اللَّهِ الرَّحْمَٰنِ الرَّحِيمِ

" وَلَقَدْ آتَيْنَا دَاوُودَ وَسُلَيْمَانَ عِلْمًا ۖ وَقَالَا الْحَمْدُ لِلَّهِ الَّذِي فَضَّلَنَا عَلَىٰ كَثِيرٍ مِّنْ عِبَادِهِ الْمُؤْمِنِينَ ۝ "

صدق الله العلي العظيم

سورة النمل (الآية ١٥)

Supervisor Certification

I certify that this thesis entitled, " **Synthesis of (Cu/ZnO/rGO) tertiary Nanocomposite and its applications to removal of the Rhodamine 6G dye from the aqueous solution and antibacterial activity"** was prepared under my supervision, by " Adel hamza Abbas Al-zurfy" It was done at the Department of Chemistry, College of Science at the University of Babylon as a partial fulfillment for requirement for the degree of Master in science of chemistry (Physical Chemistry) at the University of Babylon and this work has never been published anywhere else.

Signature:

Name: Prof .Dr. Nada Yahya Fairooz

Title: Professor

Address: Babylon University, College of Science, Chemistry Department

Date: / / 2021

In the view of the available recommendation, I forward this thesis for

debate by the examining committee.

Signature:

Name: Dr. Saadon Abdulla Aowda

Title: Professor

Address: Head of Department

Date : / / 2021

Committee Certification

We, the examiner committee, certify that we have read the thesis entitled " **Synthesis of Cu/ZnO/rGO tertiary Nanocomposite and its applications to removal of the Rhodamine 6G dye from the aqueous solution and antibacterial activity** " and examined the student (**Adel Hamza Abbas)** in its contents at 21/ 11/ 2021, and that in our opinion it is accepted as a thesis for a **Master's** degree in chemistry with (**Excellent**) estimation.

Signature:

Name: **Dr. Abbas Jasim Atiyah**

Title: Professor

Address: Babylon University

College of Science, Chemistry

Date: / / 2021

(Chairman)

Signature:

Name: **Dr. Qahtan Adnan Youssef**

Title: Professor

Address: Al-Qadisiyah University

College of Education

Date: / / 2021

(Member)

Signature:

Name: **Dr. Hazem Yahya Muhammad Ali**

Title: Professor

Address: Babylon University

College of Science, Chemistry

Date: / / 2021

(Member)

Signature:

Name: **Dr. Nada Yahya Fairooz**

Title: Professor

Address: Babylon University

College of Science, Chemistry

Date: / / 2021

(Member and supervisor)

Approved for the College Committee of Graduate Studies

Signature:

Name: **Dr. Enas M . AL-Robayi**

Title: Professor

Address: Dean of the College of Science - University of Babylon

Date: / / 2021

Dedications

To our martyrs who sacrificed their blood for our lives

To spirt of my father ..... Who persevered for my academic career

To my mother …that sacrificed enough

To my brothers… who Support me all the time

To my wife ……. that supported me and was patient

To my friends … who supported me all time

Adel Hamza 2021

Acknowledgements

First of all, I would like to express my great appreciation to the almighty Allah for his support enabling me to complete this work. Special thanks are due to ***Dr. Nada Yahya Fairoz*** my supervisor who enriched my knowledge.

I would like to express my deep and special thanks to , my father, my mother, my brothers, my wife. In addition, I would like to thank all people who introduced direct or indirect assistance for me in Babylon University, College of science, and Department of Chemistry.

I would like to thank everyone who has, in one way or another, contributed to the completion of my project. In particular, me wish to express my appreciation to the people who have provided technical, experimental and graphical assistance.

Finally, I would like to express my deep and special gratefulness to my best friends, who help and encourage me a lot during 1 years ago, and who support me in happy times and sad times when I needed them to help me.

Adel

Summery

The present study represents synthesis of Copper nanoparticles (Cu NPs) alone by using root Ginger extract by combination with anhydrous copper sulfate (Cu SO_4) as an eco-friendly method, and synthesis of Zinc Oxide (ZnO NPs) alone by precipitation Method using zinc sulfate heptahydrate ($ZnSO_4$. $7H_2O$) . then synthesis ZnONPs was doped with copper to synthesize modified ZnONPs (Cu/ZnO NPs) binary Nanocomposite .These binary Nanocomposite systems were combined with reduce graphene oxide (rGO) to obtain tertiary systems of (Cu/ZnO/rGO) and measure part of its physical and biological action These prepared materials were . investigated using different techniques such as X- rays diffraction (XRD),Fourier transform infrared (FTIR), Energy Dispersive X-Ray(EDX), Scanning electron microscopy (FE-SEM) ,Zeta-potential, Brunauer-Emmett-Teller (BET) Surface Area ,Ultra-Sonic, and Zeta Potential. The zeta strength was measured at about (-27.4 mV) BET surface area was [29.833 m^2 g^{-1}] and average crystal size (23.77 nm) The adsorption efficiency of Rhodamine(6G) dye on all of these materials was also examined. The best removal percentage of Rhodamine 6G dye (80.7 %) over used suspension of these materials was recorded using the Cu-ZnO/rGO Tertiary Nanocomposite at a weight of 0.1 gm , pH= 9 and a temperature of 30°C for 60 minutes. In this context, different adsorption conditions were considered such as effect of temperature, mass dosage of the used materials, contact time, and the pH of reaction mixture.

The best removal efficiency of Rhodamine (6G) dye over used suspension of these materials was recorded using of Cu/ZnO/rGO reduced graphene oxide (rGO). In terms of adsorption isotherms both of Langmuir and Freundlich adsorption isotherms were investigated and the obtained results showed that it was more fitted with Freundlich adsorption isotherm and the kinetics of the reaction were pseudo-first order.

A study of the inhibition of the activity of two strains of gram-negative bacterial Escherichia coli (E.coli) and gram-positive bacterial Staphylococcus aurous (S. aurous) bacteria by all synthezied Nanoparticles and Nanocomposites at a concentration of (10 mg/ml). The best inhibition zone for Cu-ZnO/rGO Tertiary Nanocomposite showed highest inhibition zone (13.2 mm) against E. coli bacterial and ZnO NPs showed highest inhibition zone (9.6mm) against S. aurous.

Table of Contents

Chapter One / Introduction

Chapter Two / Experimental Part

List of Tables

List of Figures

Table of Abbreviations and Symbols

Abbreviations and Symbols	The Meaning
A	Absorbance
A_0	Absorption at Time Zero
A_t	Absorption at Different Time
BET	Brunauer–Emmett– Teller
C	Concentration of Reactant.
C_o	Initial Concentration
C_t	Concentration of Substance at Different Times
Cu	Copper
D	Mean Crystalline Size
DI	Deionized Water
Ea	Activation Energy
Eq	Equation
Exp	Experimental
FESEM	Field Emission Electron Microscopy
FTIR	Fourier Transform Infrared
FWHM	Full Width at Half-Maximum
G^0	Gibbs energy
GO	Graphene Oxide
H^0	Enthalpy changes
K	Scherer Constant
Log	Logarithm
mg	Milligram
Min	Minute

nm	Nano meter
^{o}C	Centigrade
R 6G	Rhodamine 6G
rGO	reduced Graphene Oxide
S^{0}	standard entropy of reaction
UV	Ultraviolet
UV-Vis	Ultraviolet-visible
V	Volume
W	weight
XRD	X-ray Diffraction
ZnO	Zinc Oxide
Θ	Diffraction angle (Bragg's angle)
λ	Wavelength
λ max	Maximum Wavelength

Chapter One

Introduction

1. Introduction

1.1.Background of Nanotechnology Science .

A nanomaterial's primary purpose is the exact management of atoms, molecules and their chemical interactions with each other. As the Greek word for dwarf or someone who is unusually short suggests, the word nano is derived from that word. There are billions (10^{-9}) of any unit prefixed with this. An individual nanometer is therefore one billionth of an inch or centimeter. A wide definition of nanomaterials is a material with grain or particle sizes ranging from 1 to 100 nanometers in at least one direction. Science and technology involved in creating and utilizing nanostructures and nanomaterials are collectively known as "nanotechnology." As the barrier between atoms/moleculars and the macro world, it is a critical component of any design. Biomineralization (in an abalone shell or human bone) lotus leaves photosynthesis (in plants) spider silk, peacock feather, etc. are all instances of nanotechnology in nature [1].Naturally, we are curious as to what this crucial technology is. If we go back to Richard Feynman's presentation on "Plenty of Room at the Bottom" in 1959, we can see that the nanoprocess is already in progress. Later on, Professor Norio Taniguchi (1974) proposed the term "nanotechnology." After that, nanotechnology evolves in a more vivid method as more recent tools develop to accurately consider or isolate nanoparticles [2]. Nanotechnology has been used in many fields of science like physics, chemistry, pharmaceutical science, material science, medicine, and agriculture[3]. Nanotechnology is the manipulation of matter on a microscopic scale to create useful materials, devices, and systems. Nanotechnology brings together scientists from a variety of fields, including physicists, chemists,

engineers, and biologists. Although the term nanotechnology is relatively new, the “natural version” of nanotechnology was already in the lead thousands of millions of years ago with the spawning of life itself. At the nanoscale, all-natural materials and systems lay their foundation. Nano-entities, the biological building blocks of life, have distinct features dictated by their size, folding, and patterning at Nanoscale. [4]. This technology's most distinguishing feature is its small size, which allows it to be applied to a wide range of applications. The nanoscale size of the materials has some advantages, such as a large surface area and a low number of surface flaws, which improves the materials' qualities. Nanomaterials, which are manufactured at the Nanoscale and exhibit properties that are considerably different from their "bulk" counterpart, are a vital feature of nanotechnology. Nanomaterials can be found in nearly any product, including sunscreens and other cosmetics, fabrics, paint, and so forth. Silver Nanomaterials, carbon nanotubes, Nano metal oxides (iron oxides, titanium dioxide, zinc oxide), silica, and gold are some of the most often used Nanomaterials in consumer items.

1.2. Types and Classification of Nanomaterials

Most current nanoparticle and nanomaterial can be organized into four materials:

1.2.1. Inorganic-based nanomaterials

Inorganic nano materials involve metal and metal oxide NPs and NMs. These NMs can be synthesized into metals such as silver nanoparticles (Ag NPs) or gold nanoparticles (Au NPs), metal oxides such as Titanium dioxide nanoparticles (TiO_2 NPs) and zinc oxide nanoparticles (ZnO NPs), and semiconductors such as ceramics and silicon.

1.2.2. Organic-based nanomaterials

They are nanomaterials that are mostly made from organic materiales, they are found in many different forms such as dendrimers, liposomes, micelles ferritin and polymer NPs etc. These nanoparticles are non-toxic and biodegradable some particles has a hollow core like liposomes and micelles also known as nanocapsules it are sensitive to electro-magnetic radiation and thermal such as light and heat, These unique properties makes them an ideal choice for drug delivery where the organic nanoparticles are most widely used in the biomedical field.

1.2.3. Carbon- based nanomaterials

Carbon- based nano materials generally made completely of carbon they are found

in several morphologies such as carbon nanotubes (CNT), fullerenes(C_{60}), graphene, carbon nanofibers and hollow tubes etc.

1.2.4. Composite-based nanomaterials

During the period 1982- 1983 the term of nanocomposite was introduced by Roy, Komarneni, and co-workers in order to indicate a change in the conceptual direction of the sol-gel process. Nano composites refer to composites of more than one solid phase where at least one dimension is in the nanometre scale and typically all solids phases are in the (1-20) nm domain, its use for make rather heterogeneous than homogeneous materials[5].

1.3 Nanopartical Synthesis Methodologies

The capacity to create and process nanoparticles and nanostructures is the fundamental cornerstone in nanotechnology for exploring novel physical properties and phenomena and realizing future applications of nanostructures and nanomaterials. The synthesis of nanomaterials and the manufacturing of nanostructures can be done in two ways Figure(1-1) top-down and bottom-up[6]. Slicing or successive cutting of a bulk substance to obtain nanosized particles is referred to as a top-down technique. The term "bottom-up approach" relates to the construction of a substance from the ground up: atom-by-atom, molecule-by-molecule, or cluster-by-cluster, to name a few methods. Milling, for example, is a top-down way for creating nanoparticles, whereas colloidal dispersion is an excellent example of a bottom-up strategy in nanoparticle synthesis. Both In nanotechnology, approaches play a critical role.

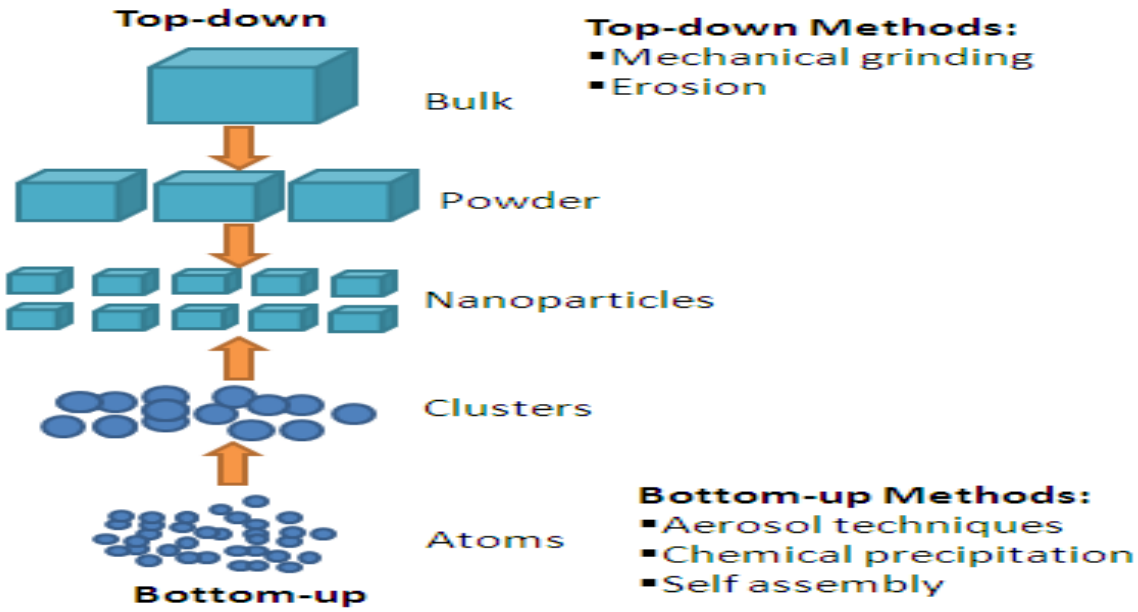

Figure (1-1) :The 'bottom-up' and 'top-down' approaches to synthesis of nanomaterials [6].

These technical approaches can also be classified based on the growing medium used:

1- Vapour phase growth for nanoparticle production, incorporating laser reaction pyrolysis for thin film deposition, atomic layer deposition (ALD) is used.

2-Growth in the liquid phase, including hydrothermal and colloidal processes Formation of nanoparticles and monolayer self-assembly

3-Formation of solid phases, including phase segregation to produce metallic particles construction of a glass matrix and two-photon induced polymerization Photonic crystals in three dimensions

4-Hybrid growth of nanofibres, including vapour-liquid-solid (VLS) growth.Because of the variation in exposed crystalline surface, controlled development of nanomaterials with diverse morphologies is critical.

Specifically,This control is required in catalytic applications to improve selectivity .reported on the tuning of selectivity in the generation of cis olefins by changing particle shape to reduce the production of harmful trans fats during partial hydrogenation of edible oils [7].

1.4 Nanocomposite.

As the name suggests, nanocomposites are mixtures in which at least single component has a diameter in the nanometer range (1 nm = 10^{-9}m). There are a number of preparation problems associated with nanocomposite materials, including elemental composition and stoichiometry in the nanocluster state [8].At a nanoscale, nature has traditionally mixed organic and inorganic components to create smart

materials with extraordinary properties and functionalities (mechanics, density, permeability, colour, hydrophobicity, etc). Organic-inorganic natural materials include crustacean carapaces, mollusk shells, bone, and tissues. In the realm of material science, nanocomposites are expected to be made up of solid structures dispersed at the nano size in a matrix, often an organic matrix incorporating inorganic nanoparticles in the case of polymers. The nanostructure phases of nanocomposite structures are: zero-dimensional (embedded cluster), 1D (one-dimension; e.g. nanot) and 2D (two-dimension; e.g. nanotubes) 3D (embedded network) [9].

Table 1.1: Different dimensions of nanomaterials with an examples

Elementary units	**Examples**
0D Units (3 dimensions in the monometric range)	Molecules, Clusters, fullerenes, rings, metal carbides, powders, grains.
1D Units (2 dimensions in the monometric range)	Nanotubes, fibres, filaments, whiskers, spirals, belts, springs, needles.
2D Units (1 dimensions in the monometric range)	Layers

1.5.General approaches to nanocomposite fabrication

For the formation of nanocomposites, many techniques can be utilized to build nanostructures of various materials. In order to construct a metal nanoparticles on a ceramic supporting, for example, one can vaporize metal onto the proper substrate or disperse metal oxide nanoparticles with aqueous chemistry Nanocomposites containing ceramic and polymers phases are difficult to fabricate using normal

methods, and so splitting processing techniques are required [10]. Research on nanostructures is still needed despite the fact that there are many different ways to create them. Development methods for producing nanostructures that are uniform and free of templates. Simple and efficient, such a production method relies merely on the mixing of components to generate an ordered structure. The advantages of template-free nanostructure synthesis include ease of synthesis and purification without the need for template removal. Homogeneous nanofibers that are scalable and repeatable are also created. Nanomaterials operate better as sensors because they have a nanoscale width and are water-dispersible, allowing for more environmentally friendly biological usage and processing. [11].

1.6. Types of nan composite

1.6.1. Non-Polymer Based Nanocomposites

The following can be classified as non-polymer-based nano composite materials:

1.6.1.1. Metal / Metal Nanocomposite

Bimetallic nanoparticles in the form of alloys or core-shell structures are being studied in depth due to their improved catalytic qualities and improved electronic/optical properties associated to various, independent metals. As a result of blending two types of metals with fine structures, they are believed to exhibit unique physical-chemical properties[12].

1.6.1.2. Metal/Ceramic Nanocomposites

Within the category of composites, the electrical, chemical, magnetic, mechanical, and optical The combined qualities of both stages

are used to create the product. The nanoscale reduction of parts improves the above-mentioned qualities and opens up new possibilities. These composites have an appealing rough that is chemically inert and durable ceramic matrix thanks to the polymer precursor systems [13].

1.6.1.3. Ceramic/Ceramic Nanocomposites

1.6.2. Polymer-Based Nanocomposites

Ceramic Nanocomposites tackle the problem of crack failures in artificial joint implants, however they can increase the high cost of surgery and the patient's mobility. [14].Nanocomposite polymers consist of a polymer matrix and a filler with a minimum dimension of 100 nanometers. A high aspect ratio clay, nanotubes or nanoparticles are examples of fillers[15].

1.6.2.1. Ceramic/Polymer Nanocomposite

They are composed of 1 nm-thick ceramic layers that are consistently distributed in a constant matrix. In part, this is due to the dipole-dipole coupling between the host ceramic layers [16]

1.6.2.2. Nanocomposites of inorganic/organic polymers

Because with the metal clusters distributed throughout the polymer matrix, metal-polymer nanocomposites draw attention. (1-2) nanometers is the size of the average metal cluster. Aspects such as electron transit and bandgap are very different between larger particles and individual atom or molecule clusters and nanoparticles. Because metal atoms move around, particle and grain size is affected. The degree of cross-linking in polymethyl methacrylate polymer, for example, determines the size of the clusters[17].

1.6.2.3. Inorganic/Organic hybrid nanocomposite

Are nano composites made up of closely integrated organic and inorganic components. Hybrids can be heterogeneous systems (nano composites) having at least one nanometer-sized component or homogeneous systems made up of monomers and miscible organic/inorganic components[25].

1.6.2.4. Polymer/ Layered Silicate Nanocomposites

Composite materials made of nan In polymer science, polymer / layered silicate (PLS) attracts a lot of attention. When compared to virgin polymer and modern nano- and nano-composites, the PLS nan composites have sparked a lot of interest in the manufacturing world as well as in academia. Hectoliter is one of the most extensively used smectite-type layered silicates for the manufacture of nan composites[18]. More than ever, the gap between block co-polymer self-assembly and nanostructured plastics endowed with yet-to-be-discovered combinations of qualities is narrowing. Polymers under pressure to be cheap and property profiles given are becoming increasingly tight. Even when their monomers are homogeneously combined, mixtures of dissimilar polymers frequently phase independently [13].

1.6.2.5. Polymer/polymer Nanocomposites

The distance between self-assembling co-polymer blocks and plastic nanostructured is narrowing, with still unknown product combinations. Polymers are under more pressure than ever to be inexpensive and sell immobilized profiles. Even if their monomers are combined homogeneously, miscellaneous polymers can sometimes separate phases**[**13].

1.6.2.6. Biocomposites

Both polymers are employed in soft tissue replacement and a variety of other non-structural applications. Metals alloys are commonly utilized in orthopedics, other load-bearing uses include dental and dentistry. All of us are made up of composites in some way. Collagen is a relatively ubiquitous protein that comes in over 14 different types[19].

1.7. NANOCOMPOSITE SYNTHESIS

1.7.1 Nanocomposites

The term nanocomposite refers to a multiphase solid substance that has one, two, or three dimensions less than 100 nm in one of the phases, the material's phases are separated by nanoscale intervals, or Nanocomposite solids include porous media, gels, colloids, and copolymers in their fullest sense [20]. Figure (2-1) shows how ceramic, metallic mixed polymer nanocomposites can be made.

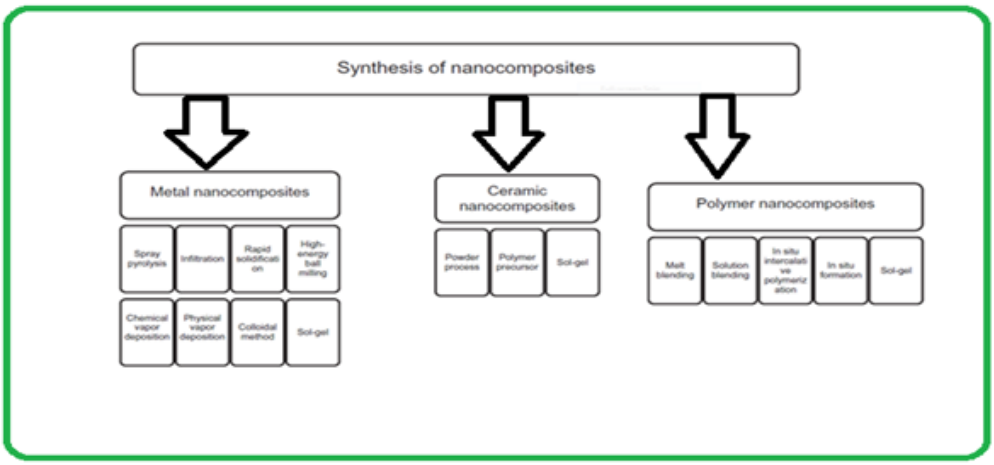

Figure 2-1: Nanocomposite fabrication techniqe

1.7.2 Nanocomposites made of metal

These materials consist of a metal or alloy matrix and a nanoscale reinforcing agent. Metallic alloys having ceramic strength and modulus

are known as metalloceramic materials. MMC is therefore ideal for the High shear/compression intensity and quality service temperature characteristics can be achieved by manufacturing materials [21].
These material can be synthesized as following:

1.7.2.1. Spray Pyrolysis

Is a technique for depositing a thin coating on a heated surface by spraying a solution over it, in which the ingredients react to produce a chemical product. When selecting chemical reactants, care is taken to ensure that every products that aren't the goal chemical are flammable at the heating rate [22]. The steps involved in the fabrication process are as follows:

1. dissolving inorganic progenitors (starting materials) in a solvent system to get a liquid source.
2. Using an ultrasonic atomizer, create a mist from this liquid source;
3. The mist is transported into a heated chamber using a carrier gas.
4. metal oxides are reduced selectively to produce the corresponding metallic compounds; and
5. Locked in by a filter in the chamber the droplets can be vaporized, promoting their decomposition to produce the oxides formed [23].

1.7.2.2. Infiltration

When ceramic particles or fibers are created, they're immersed in molten metal matrix, which fills in the gaps between the scattered phase inclusion. This procedure is used to fabricate composite materials. Particle concentration of dispersed liquid phase (dramatic infiltration) as well as external pressure (mechanical, gaseous,, ultrasonics, centrifugal, or electromagnetic) [24].

1.7.2.3. Rapid Solidification

At high temperature, when transitioning to a solid environment, the temperature of the liquid is high or substance at room temperature, fast solidification involves the extraction of thermal energy quickly Ultrasonics are utilized to mixing the polymer and reinforcement with increase their wetability [25].

1.7.2.4. High-Energy Balls Milling

An explosive powder mixture is subjected to high-energy ball mill collisions. It is possible to obtain thin and homogenous oxide dispersions in nickel-base superalloys by mechanical alloying, commonly known as long ball milling. Grinding with high-energy ball mills alters the conditions under either altering the reactivity of milled nanoparticles, or by activating biological reactions during milling [26].

1.7.2.5. Chemical Vapor Deposition method

Produces high-performance solid materials. Thin films are often produced using this technology in the semiconductor sector. Semiconductor (substrate) is treated by volatile precursors and dissolve (and/or react) In a conventional chemical vapor deposition, the desired deposit is deposited on the substrate's surface. This chamber is used to remove volatile waste material on a regular basis[27].

1.7.2.6. Physical Vapor Deposition method

thin films and coatings are produced using a series of vacuum deposition processes. An electrochemical method in which materials are converted to condensed to vapor and then back to thin film condensed phase, is known as Physical Vapour Deposition (PVD) Sputtering and evaporation are the two most frequent physical vapor deposition mechanisms [28].

This is how physical vapor deposition is conducted:

(i) forming a vapor phase by sputtering/evaporating certain components; (ii) metal nanoparticle condensation by supersaturating the vapor phase in an inert atmosphere;

(iii) To consolidate the nanocomposite, it is subjected to thermal treatment in an inert environment [29]. Pb/Cu, Al/Mo, Al/Pb, Al/SiC, Fe/MgO, Cu/Al_2O_3, and Ag/Au are other examples.

1.7.2.7. Colloidal Method

Chemical reduction of inorganic salts to synthesis metal particles, followed by drying and heat treatment in a reducing environment (such as hydrogen) to facilitate selective oxide reduction and produce the metal component [30]. Chemical method for generating composite polymer composites(sol-gel method) [31] .

1.7.3 Nanocomposites made of ceramics

platelets, Fibers, or whiskers are combined with a ceramic system to form ceramic nanocomposites..

1.7.3.1. Powder Process

Such as processes, compression, rolling, and extrusion are used in manufacturing of ceramic nanocomposites. The powder is fed into a two-walled conduit and squeezed vertically by a fixed horizontal punch in a simple compression process. A sintering furnace then heats the compressed bulk to a high temperature to complete the process. It is fed into a two-story rolling mill, where it is crushed into strips, sintered and then rerolled. During the first type of extrusion, Binding or plasticizer is added to the mixture and heated at room temperature Other methods include non-fortified powder extrusion at high temperatures, as well as fortified powder extrusion at low temperatures [32].

1.7.3.2. Polymer Precursor and Sol-Gel

The polymer precursor approach involves mixing a polymeric precursor with the matrix material, then pyrolyzing the combination in a microwave oven to produce reinforcing particles [33]. Sol-gel is also a ceramic nanocomposites fabrication technology in which:

The following processes would be involved in this

(i) hydrolysis and polycondensation processes .

(ii) Precursor of an organic compound dispersed in organic medium ,

which results in the creation of three-dimensional polymers with metal-oxygen linkages (sol or gel),

(iii) subsequent drying to obtain a solid substance consolidation by thermal treatment [21]

(iv) at a later stage. Al_2O_3/SiC, ZnO/Co, and SiO_2/Ni are some examples of these materials.

1.7.4 Composites made of polymer nanoparticles

There are two main groups of nanomaterials, namely nanostructured materials and bulk materials, respectively. While nanostructured bulk materials consist of nanometer-sized clusters, nanophase materials consist of nanoparticles that are distributed throughout a material's surface. Adding inorganic nanoparticles to a polymer matrix offer advantages over typical polymer composites in terms of chemical resistance, lower permeability, There are number of properties that make a material heat resistant, such as moisture and charge dissipation. The area of contact between the nanostructure and the host polymer matrices is unusually large per volume as a result of a homogeneous and constant filler particles dispersion. Unlike normal polymer composites, polymer nanocomposites have a large interfacial area and nanoscale particle sizes [34].

1.7.4.1. Melt Blending

For making nanocomposites comprising thermoplastic polymers and elastic polymeric matrix made of clay, are described melt blending is the recommended approach [35]. Typically, a banbury or an extruder is used to melt the polymer and blend it with the necessary amount of intercalated clay. Inert gas, such as nitrogen, neon or argon is used to combine the melts. Alternatively, the polymer and the intercalant can be mixed. Then heated in a mixer and sheared to generate the clay polymer nanocomposites. Melt blending outperforms in *situ* polymerizations for polymer solution intercalation. Because organic solvents aren't used, melt blending is environmentally friendly. Extrusion and injection molding, for example, are both compatible with melt blending. Melt mixing has gained popularity as a result of its potential for industrial applications.

1.7.4.2. Solution Mixing

Soluble polymer or prepolymer solution mixing is a solvent-based method in which nanofillers can swell (for layered nanofillers). Water, chloroform, or toluene are used to swell the nanofillers before they are employed. Solvent is displaced from the silicate interlayer mixed with nanofiller. Intercalated/exfoliated polymer nanocomposites remain after the solvent has been removed Solutions include the vigorous agitation of nanofiller in a polymer solution and the controllable solvent evaporation as well as the composite film casting stage [36].

1.7.4.3. In *situ* intercalative polymerization.

The first approach used to create polymer clay nanocomposites based on nylon 6. A liquid monomer solution inflates a layered silicate, allowing polymer to develop between the intercalated sheets. Before the

swelling stage, heat or radiation, diffusion of a suitable initiator, or cation exchange might induce polymerization [37].

1.7.4.4. Sol-Gel and In *Situ* Formation

Is it possible to make an aqueous phase of this composite material subjected to in *situ* formation, which results in the development of an inorganic material layered structure. Layers are created by using the water-soluble polymer as a template. Nanocomposites made from layered double hydroxides (LDH) are quite well, but those made from layered silicates are less well-known[38].Sol-gel matrix are used to embed monomers and organic molecules. During the sol-gel process, a polymer and silicate building block solution is employed to produce clay minerals within the polymer matrix [39]. They become imprisoned within layers when they expand.

1.8. Applications of Nanotechnology

Nanotechnology is a comprehensive technology that has evolved dramatically that is widely applied in various fields of our daily life [40], such as medicine and pharmacology (nanomedicine), chemistry, environment, and agriculture [41]. For example, nanotechnology is widely used in the medical field such as diagnostics as show in Figure (3-1) tissue regeneration, cell culture, biosensors [42] antimicrobials [43], employed to encapsulate the drug, high drug loading capacity, drug delivery, and targeted delivery to specific sites or organs, detection, Excellent tool in the field of biological imaging, magnetic resonance imaging [44]. Nanotechnology plays an important role in the field of manufacturing such as information, techniques, energy sources, environment [45], dendrimers,metal-containing nanoparticles, zeolites,

and carbonaceous nanomaterials, Also used in water purification where there are four classes of nanomaterials: metal-containing nanoparticles, zeolites, and carbonaceous nanomaterials These have a broad range of chemical and physical properties that make them special materials attractive for water purification [46]. Nanomaterials utilize in a variety of consumer products such as cosmetics, paints, food, and suntan lotions, remediation of the polluted environment [47]. possibility applications of nanoparticles have been exploited in several fields such as sensors, energy batteries, automobile components, high-power, formable ceramics, magnets, Smart structures, catalyst, dielectrics cells, optical devices, Cutting tools, Aerospace components, etc [48]. Fuel oil and gas industry [49], improving the performance of solar cell technologies [50], textile industry [51] and applications in agriculture through detection of pathogens and contaminants in food products, genetic enhance of plants and animals efficient delivery systems for agrochemicals like fertilizers and pesticides [52], catalysis and analysis[53].

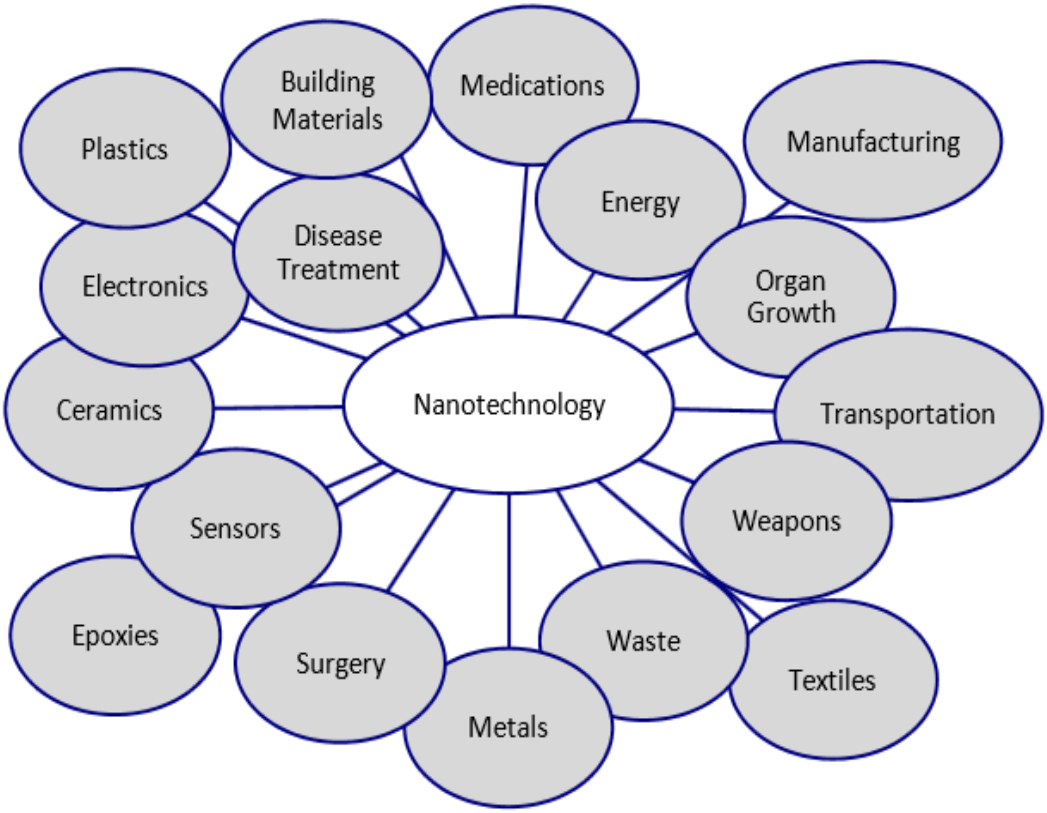

Figure(3-1): Scheme of Application of Nanotechnology

1.9 Adsorption process

In Figure (4-1), four steps in the adsorption process are shown. In the first step, bulk solution transportation will be undertaken. Substances to be adsorbed must be moved from large volumes of bulk liquid to a small adsorbent surface layer. In the second stage, film diffusion transport, the material diffuses to the pore entrance of the adsorbent through a stationary liquid film. In the third stage, pore transport will occur. Adsorbent pores and surface absorb the substance during this process. Adsorption is completed when the adsorbate adheres to the adsorbent's surface and takes up space on the surface. [54]

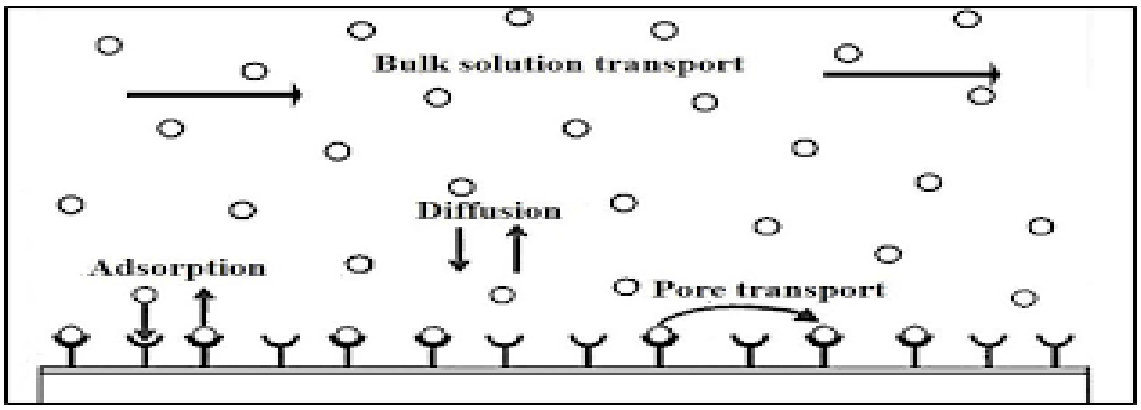

Figure (4 – 1): diagram of the adsorption process [54]

At the solid-liquid interface, adsorption occurs when molecular species (either gas or liquid) accumulate in excess The term adsorbent refers to the material on which the substance is deposited. adsorption happens because the adsorbent's surface nanoparticles are in the same phase as its bulk counterparts. Not up to standard: solids with surface valence forces as shown Figure(5-1). It is possible to see how the adsorption process works. Graphene-Based Composites and atoms operate as activators on the surface of the material. Activated surfaces may attract other chemicals, reducing entropy (S). The Gibbs free energy of any process is triggered by a small amount of it (G),which can be written as:

$$\Delta G = \Delta H - T\Delta S \qquad \ldots\ldots\ldots\ldots \qquad (1\text{-}1)$$

As a result, adsorption is fundamentally an exothermic process, and the magnitude of the enthalpy change (H) must be larger than the magnitude of the term 'TS.' As the adsorption progresses, H gets less negative and eventually equals TS, causing G to become zero and equilibrium to be reached. On the surface of an adsorbent, the definition adsorption refers to the capturing of the adsorbate alone. Physisorption (which includes van der Waals binding forces) and chemisorption are the two basic forms of adsorption based on the type of physically interacting between both the

adsorbent and adsorbate [55]. As far as chemistry is concerned, they are all related. Adsorption, its process, and the thermodynamic factors that affect adsorption capability and rate require a thorough analysis. Adsorption types include homogeneous and heterogeneous [56].

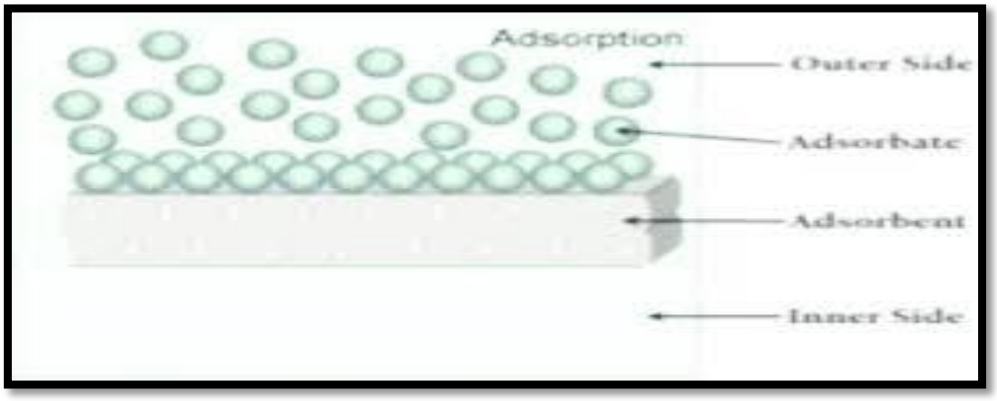

Figure (5-1): Pictorial representation of adsorption process[55]

1.10 Types of Adsorption

Physical adsorption (Physiosorption) and chemical adsorption (Chemisorption) are the two forms of adsorption (Fig 6-1).

1.10.1 Physical Adsorption's

It involves weak van der Waal's forces adsorption of gases on solid surfaces.

1.10.1.A. Characteristics of Physical Adsorption's

• Physical adsorption has no specificity. Every gas is adsorbed onto the solid's surface. Nature of the adsorbate. Easily liquefiable gases are strongly adsorbed physically.

• Adsorption is a reduction reaction that can be reversed. Pressure increases cause gas volume to decrease, allowing more gas to be absorbed. This allows gases to escape from solid surfaces by decreasing pressure. At low temperatures, physical adsorption is enhanced, while at high temps, adsorption is slowed down.

• The higher the surface area, the faster the absorption rate. Porous materials and finely split metals work well as adsorbents. The process of physical adsorption is exothermic.

• There is no need for activation energy.

Chemical adsorption, also known as chemisorption, occurs when gas molecules or atoms are bound to a solid surface by chemical bonding [57]

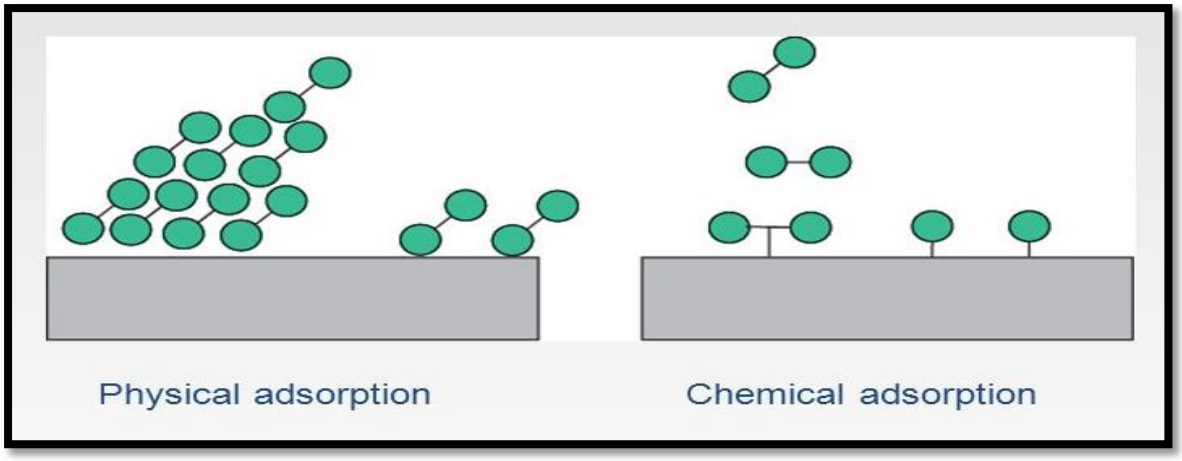

Figure (6-1): Types of adsorption[57]

1.10.1.B. Characteristics of Chemical Adsorption

In Comparatively, physical adsorption it a selective. Chemical adsorption is permanent. Although it's an exothermic reaction, cold temperatures cause it to occur more slowly. In addition to chemisorption, there is also a temperature rise. High pressure aids in chemisorption, As the surface area of a surface grows, so does chemisorption .

● Chemisorption enthalpy is high due to chemical bond formation .

●There is a requirement for activation energy.

The unimolecular layer is the consequence.

1.10.2 Adsorption Influencing Factors

The temperature has a significant impact on adsorption. Low temperatures are ideal for adsorption. Because adsorption is an exothermic process, the forward reaction will be derived at a low temperature. Up to a point, a rise in pressure causes an increase in adsorption until saturation is attained. No additional adsorption will occur after saturation has been attained, regardless of the pressure applied. Adsorption Isobar[62]. is the relationship between the extent of adsorption and temperature at any fixed pressure. Because adsorption is a surface phenomenon, a larger surface area, a faster the adsorption rate. Liquefied liquefiable liquefied**.**

1.10.3 Adsorption Applications

• The adsorption approach can be used to achieve a high vacuum. activated charcoal is utilized to make the vacuum.

• Adsorption is the basis for gas masks used in coal mines. The purpose of these gas masks is to adsorb hazardous gases. This purifies the air for breathing.

• To minimize humidity, silica, and aluminum gels are utilized to absorb moisture.

• Using charcoal as an adsorbent, noble gases can be separated.

• Drug adsorption is used to kill bacteria.

• Chromatographic analysis is based on the adsorption phenomena.

• Sugar is decolorized by adding the charcoal powder to a sugar solution. The latter absorbs the unwanted colors that are present.

• In the paint industry, adsorption also plays a significant role. If the paint contains dissolved gases, it will not adhere effectively to the surface to be painted, resulting in poor coverage.

• Adsorption is responsible for the cleansing action of soaps and detergents, as well as the generation of stable emulsions in cosmetics and syrups[57].

1.11. Dyes

Dyes are defined as organic compounds used in many industrial fields and tissues also can be used as sensitizers for light to improve the efficiency of some types of semiconductors, by absorbing the energy of light and this leads to exactions of electrons dye from the ground state to Homo state. Therefore, these electrons are injected in the conduction band of the semiconductor particle that is used in a photocatalytic process to increase efficiency for it, therefore, it will move the reaction into a visible region[58]. To accomplish the heterogeneous photocatalytic reactions, photosensitizers are used with high efficiency and must own some properties such as having high stability towards the light and heat. Strong adsorption on the surface of the catalyst, has an absorption band within the visible region and interferes with the absorption region for the catalyst used, and can transfer electrons to the conduction band larger than recombination reaction for it [59]. Dyes possess high stability, which is due to the presence of the aromatic ring in their chemical structure. Dye molecules consist of two important components that are known as chromophores and auxochromes. Chromophores are functional groups responsible for color depend on an electronic transition in the presence of some groups and bonds, such as (C = C, C = O, C-S) and the other that is known chromophores dyes shows absorption in a region located in the ultraviolet near region or the visible region. When their chromophores

groups present more than once in the conjugated state for the same molecule. The absorption region for this molecule shifts to the long wave's length, sometimes located in the visible region of the spectrum to show specified colors[60]. The phenomenon of absorption shifts to the longer wavelength knowing (Bathochromic shift) or red shift[61].

1.12 Rhodamine 6G (R6G)

Rhodamine 6G (R6G) is an organic laser dye with a high quantum yield for fluorescence that can be used to examine probes. It can be used as a fluorescence tracker to aid in the definition of spectroscopic features to achieve high conversion efficiency and measurement precision. R6G absorbs between 400 and 700 nanometers in various solvents[62]. Figure 1-5 shows the chemical structure of the R6G molecule, which is soluble in ethanol,methanol, the use of organic solvents, etc. In environmental flow investigations, water is widely utilized as a tracer medium. For example, Nd:YAG lasers operating at 532 nanometers absorb most of R6energy, G's while copper-vapor lasers at 511 nanometers absorb most of R6energy, G's and argon-iodine lasers at 514 nanometers absorb most of R6energy. G's 510 to 710 nanometers is the range of wavelengths in the emission spectrum, having a maximum at 550 nanometers. the concentration of solvent and dye While the laser emission range is much lower, with a peak wavelength of around 575 nm, the laser absorption range is much wider. Energy conversion efficiency of more than 50% are feasible [63]. Rhodamine 6G is a fluorescent dye that can penetrate living cells. Rhodamine 6G attaches to mitochondria's inner membranes as soon as it enters the cell. Rhodamine6G dye may be utilized to provide fluorescent pictures of mitochondria with low background noise and excellent resolution, based on these findings, Rhodamine 6G at ultra-low

concentrations appears to selectively kill cancer cells in vitro while leaving normal cells unaffected[64].

specification		Structure of dye
Emprical formula	$C_{28}H_{31}N_2O_3Cl$	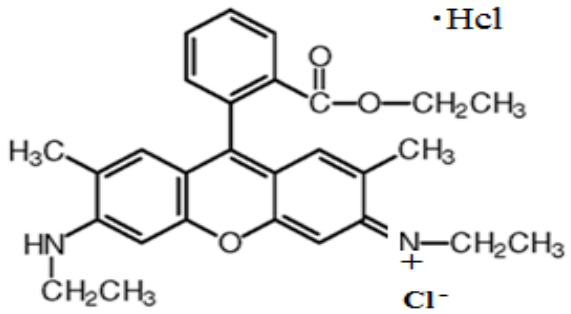
Molar mass	479.02	
Soruce	Chem. -supply	
Class	Xanthane	Rhodamine 6G

Figure (7-1): chemical structure of R6G dye

1.13 Zinc Oxide (ZnO)

Because of its broad bandgap (3.37 eV) and substantial exciton binding energy (60 meV), zinc oxide (ZnO) has gotten a lot of attention for nanoscale electrical and optoelectronic device applications [65]. It's also common knowledge that ZnO is a polar crystal with a hexagonal phase, and that its strong anisotropy causes it to grow oriented along the c axis [66]. ZnO is a good alternative to TiO_2 in terms of band energy [67]. Zinc oxide (ZnO) nanoparticles are materials with a wide range of uses in a variety of industries, including fluorescent tube luminescence, laser-active medium, sensors, and antibacterial [68]. As a result, the researcher is quite interested in the synthesis of ZnO nanoparticles. Sol-gel, sonochemical, solvothermal, hydrothermal, and mechanochemical approaches have all been used in the synthesis of ZnO nanoparticles using chemical methods [69].

1.13.1 Crystal Structure of ZnO

ZnO is a versatile material with a wide range of morphologies and two unique crystal structures, hexagonal and cubic zinc mix of which the wurtzite structure is the most stable for a variety of applications, including DMS [70] (Figure 8-1 a and b). The crystal structure of crystalline ZnO is wurtzite (B4), with a hexagonal unit cell with two lattice parameters and, each anion in this wurtzite hexagonal structure is surrounded by four cations at the tetrahedron's corners, displaying tetrahedral coordination and so sp^3 covalent bonding. The noncentrosymmetric structure of ZnO is due to its tetrahedral configuration[71] in Figure (8-1c).

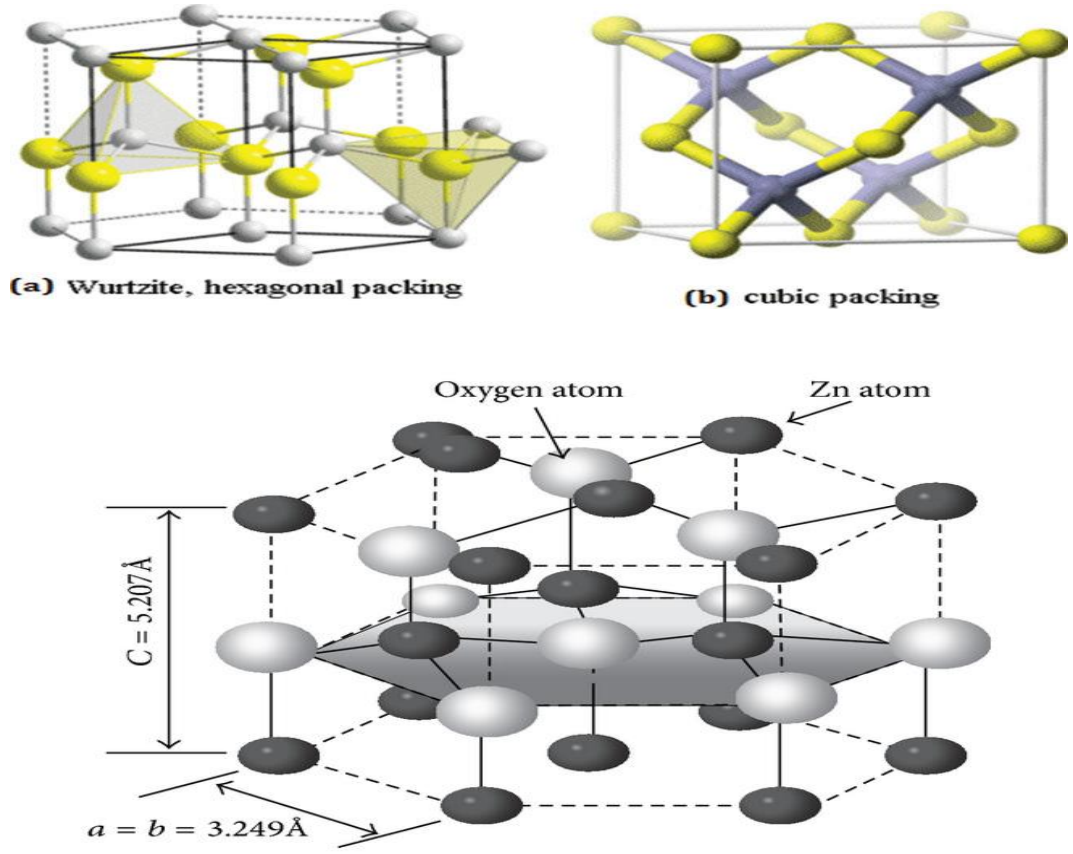

Figure (8-1): a ,b and c wurtzite structure of ZnO [71] .

1.14 Copper (Cu)

In addition to its physical and chemical features, copper is also a transition metal in the third dimension. A wide variety of reactions can be initiated and carried out in copper-based materials due to Cu's show multiple oxidation states (Cu^0, Cu^{+1}, and Cu^{+2}). They can be used in catalytic organic transformations as well as in electrocatalysis and photocatalysis because of their distinct features and properties.The most difficult aspect of developing catalytic NPS is creating nanoparticles those that are extremely active, selective, steady, sturdy, and reasonably priced. Making complex Cu-based nanoparticles for catalysis by anchoring Cu NPs (e.g., Cu, CuO or Cu_2O) on iron oxides, SiO2, carbon-based materials, or polymers is a cheap approach. Its high boiling point makes it suitable for high-temperature and high-pressure chemical reactions[72].Copper metals were absorbed efficiently in a continuous flow mode from polluted water by application of alginate immobilized water hyacinth, i.e., Eichhorniacrassipes, which acts as a promising biosorbent in an acidic environment, and a review on natural dyes and antimicrobials [73]. Due to their significant physicochemical, optical, catalytic, and heat transfer properties, copper nanoparticles (CuNPs) have attracted a lot of attention. CuNPs have been used in a variety of fields, including solar cells, energy storage, dye degradation, chemical manufacturing, and medicinal applications[74].

1.15 Graphene Oxide (GO) and reduced Graphene Oxide(rGO)

As one of the most prevalent materials, carbon may be used in a wide variety of applications, from electronics to biotechnology. It is generally created by oxidizing and exfoliating graphite-bearing oxygen functional groups such as carboxyl (-OOH), hydroxyl (-OH), or epoxy on

its basal planes and edges (-O). Figure (9-1) show a Graphene (G), graphene oxide (GO), and reduced graphene oxide (rGO) structures were created using a modified Hummers process. being a gold standard approach for manufacturing it, To reduce the oxygen content of GO and produce so-called reduced graphene oxide (rGO), chemical, microwave, thermal, photo-chemical, microbial/bacterial treatments, or photo-thermal can be applied. Some oxygen-containing functional groups almost always remain after graphene oxide is completely reduced because not all sp^3 bonds revert to sp^2 state. Varied reductive agents can create graphene oxide with different carbon-to-oxygen levels and chemical compositions [75].Due to its remarkable features, such as a huge surface area volume ratio and low cost of manufacture, graphene oxides are of tremendous interest as another carbon-based nanoscale particle that offers an alternative path to graphene [76].

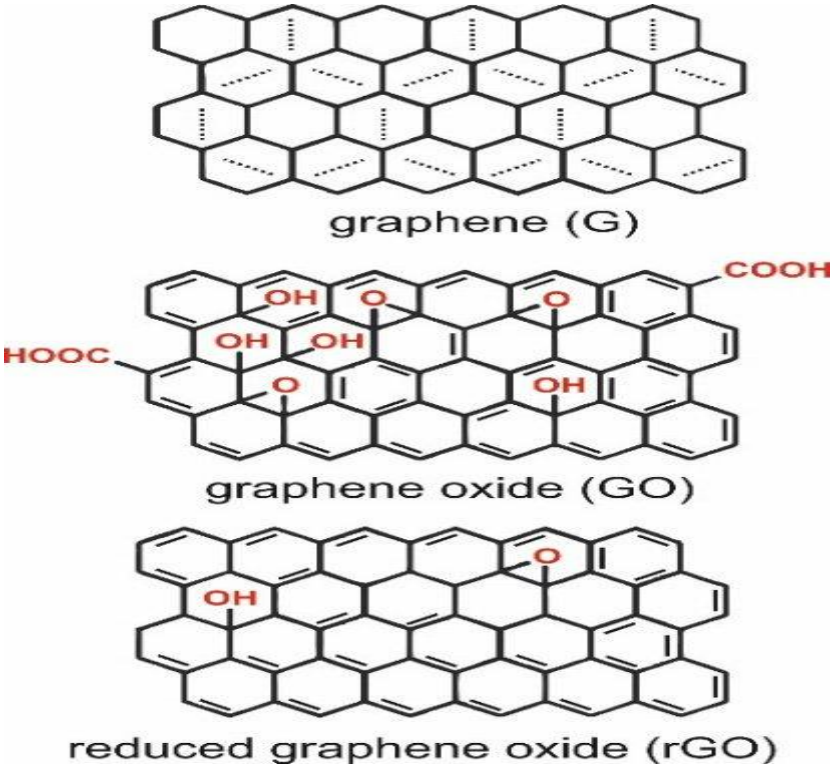

Figure (9-1): Structures of graphene (G), graphene oxide (GO), and reduced graphene oxide (rGO)[77]

This is a single-layered substance made of oxidizing graphite that can be produced in large quantities at a low cost. Graphene oxide resembles a graphene sheet in appearance, with oxygen groups such as hydroxyl, carbonyl, carboxylic, and epoxy groups in its base[77]. These groups may be deposited informally on a broad range of substrates in the form of thin films because they have a high affinity for water molecules, i.e. they are hydrophilic, and they can be quickly dissolved in water and other solvents, making them potentially suitable for microelectronics. Graphene oxide has recently grown in popularity as a result of its efficacy in fluorescence tests[78]. Because of its one-of-a-kind characteristics, GO is a promising bioapplication nanomaterial. Solar cells, hydrogen storage, transparent conductive films, polymer composites, paper such as plastics, biomedicine, nanoelectronic device manufacturing, energy storage devices, biosensors, catalysis, and transparent electrodes are just a few of the applications for graphene oxide developed in the industry[79].

1.16. Doping of Zinc Oxide Nanoparticles

1.16.1. Doping of Zinc Oxide Nanoparticles with copper nanoparticles

Control of specific properties such as chemical composition, purity, morphology, and particle size is very important to obtain metal-doped ZnO powders suitable for their intended applications. ZnO powder has various shapes such as ellipsoidal ,prismatic, dumbbell-like, and bipyramidal, nanorod, nanowire by different synthesis methods [80]. The synthesis of nanopowder can be done in a variety of ways, including sol-gel, hydrothermal, gas condensation, and spray pyrolysis. The hydrolysis synthesis approach has the benefit of producing high-crystallized powders quickly. The hydrolysis approach for making metal-doped ZnO nanorods,

in particular, is a straightforward one-step procedure. This approach allows for easy control of crystallization of target materials as well as dopants without the use of surfactants[81]. Some metals can change their valency depending on their chemical environment; for example, any copper salt doped in ZnO with an organometallic solution can result in a variety of copper oxidation states. Film-based gas sensors use n-type semiconducting metal oxides like ZnO to detect variations in some electrical property of the film, such as resistance or capacitance. Metal oxides are also stable in the air at high temperatures [82]. Despite the enormous number of papers on transition metal-doped ZnO systems, Cu-doped ZnO receives very little attention. Photocatalytic activity, gas sensitivity, and magnetic semiconductivity have all been found to improve when copper is substituted into the ZnO lattice[83].

1.16.B. Doping of Zinc Oxide Nanoparticles with reduced Graphene Oxide (rGO)

Scientists have given graphene-based compounds a lot of thought because of its efficacy in removing contaminants via electrostatic attraction (multi prep-interactions and functional groups that are found on the surface of graphene). Graphene oxide (GO) has been shown to be particularly effective in removing heavy metal ions such as (Cd^{+2},Pd^{+2}, \Cr^{+2}, As^{+3}, Hg^{+2}, etc.). Because metal ions have a positive charge that alternates with negative functional groups and oxygen on the GO, cation capture is improved. Tan *et al.* [84] demonstrated effective Cd^{+2},Ni^{+2} , and Cu^{+2} adsorption on GO/PVA films .To employ in the low layer method of Torlon support, the composite membrane for GO nano-filtration. In an aqueous environment, the percentage removal efficiency for Ni^{+2}, Zn^{+2}, and Pd^{+2} was over 95%, with long-term stability in the

150-h NF test [85]. The rGO/ZnO nanocomposite has a high specific capacitance and cyclic stability, making it suitable for use as an electrode material in energy storage and wastewater treatment. Nanomaterials have been made in a variety of ways for various applications. Drumset et al. devised a two-step sol-gel deposition process for creating thermally expanded and chemically oxidized GO sheets with ZnO nanoparticles [86]. Photodegradation mechanism in Figure (10-1)

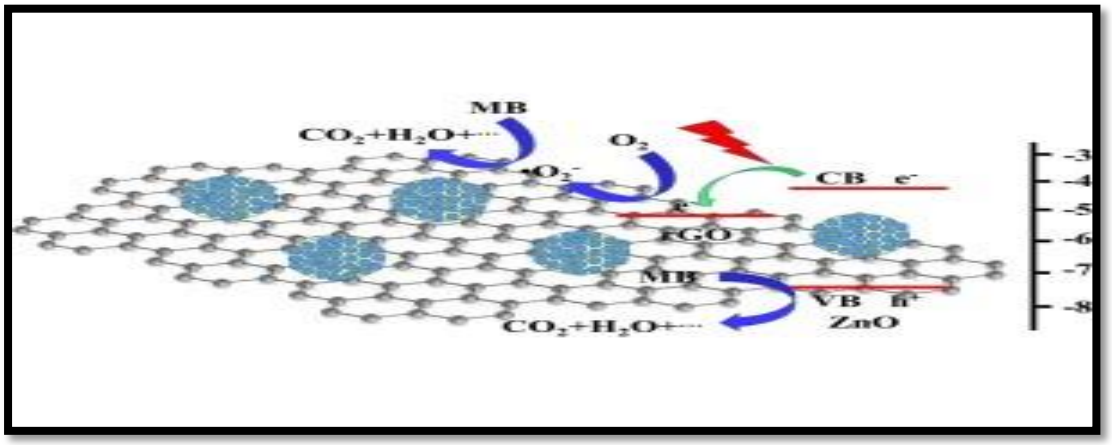

Figure (10-1): Mechanism of photodegradation of methyl blue [97].

1.16.3. Doping of Cu / ZnO with reduce Grephen Oxide (rGO)

A combination of metal, metal oxide nanoparticles, and reduced graphene oxide is helpful among these sensing materials because of its chemical and mechanical stability, low cost, strong mechanical strength, and wide dynamic range[87]. These materials have recently attracted a great deal of attention due to their simplicity of synthesis and innovative uses [88]. For high-performance sensors, recent advances have shown that coating graphene with metal oxide nanoparticles is a viable option [89]. Even stronger sensing capability can be achieved with rGO due to its strongly conducting sp^2 carbon atoms, which can act as electron

anchors in proximal metal oxide nanoparticles [90]. By boosting light absorption and decreasing recombination, doping or adding GO to ZnO improves photocatalytic efficiency, according to numerous studies conducted in the past few decades Combining the advantages of Cu doping with those of graphene support, a Cu/ZnO/rGO nanocomposite may theoretically enhance visible-light-driven photocatalysis. Cu/ZnO/rGO composite applications for catalysis are currently poorly understood, notably in the case of nutrient remediation from water, where our expertise is limited [91].

1.17 Application of (Cu ⁄ ZnO ⁄ rGO) nanocomposite

1.17.A. Antibacterial Application of nanocomposite

Humans are continually infected by microbes, which can lead to a variety of significant illnesses. Antibacterial drugs are commonly employed to destroy germs in a range of healthcare and residential settings, and hence play a critical role in infection management. Nanomaterials have been employed as an antibacterial agent in recent years [92]. By comparing Cu–ZnO/rGO to context rGO, the antimicrobial activities of the latter was further demonstrated. As a result of the synergistic action of metal oxides, all nanocomposite material exhibited good antimicrobial activity against both(gram positive) and (negative bacteria) [93]. This is due to the incorporation of Cu–ZnO into the thin films of GO, indicating that GO has a favorable impact in suppressing bacteria growth in comparison to Cu–ZnO alone, according to the study's findings. Graphene-based materials can also be made more antibacterial by forming electron-hole pairs in conjunction with hydroxide and carboxylic groups throughout the basal plane [94].

1.17.B The application of Adsorption

Adsorption is a surface-based equilibrium process also known as adsorption or chemical adsorption. Chemical adsorption attaches to the surface of the absorbent material by forming a chemical bond, whereas adsorption adheres to the surface through weak intermolecular interactions such as Van der Waals (VDW) forces. Reversible physical adsorption is the most common type of adsorption. Adsorption is not the same as adsorption on a surface, and it is not a surface-based process. Adsorption occurs at low temperatures and uses low-energy heat sources. On the other hand, adsorption is the polar opposite [95]. Dyestuff wastewater can be treated using physical, chemical, or biological approaches. As a technique of eliminating pollutants, photolysis, adsorption, chemical coagulation, liquid membrane separation, electrolysis, and biological treatments have all been examined. The efficiency, cost, and environmental impact of different technologies, on the other hand, differ. The adsorption method is more competitive than the others due to its widespread availability, lower cost, and wider range of applications. The technique of trapping soluble substances in an aqueous solution using a porous solid is known as adsorption (sorbent material) solution in water (e.g. dyes) [96] .

1.18 Literature survey:

In 2013 Sharma *et al*. Adsorption was carried out using graphene oxide nanosheets (GO). Carboxyl, epoxy, keton and hydroxyl groups in the graphite structure provide GO nano sheets their negative charge density in water over a wide pH range. Due to this, GO nano sheets should be a good adsorbent material for cationic species, according to the study's findings. Methylene green was adsorbed onto GO nanosheets under a variety of circumstances, including kinetics, pH and concentration of the adsorbate. The pseudofirst-order model, pseudosecond-order model, intraparticle diffusion, and Boyd model were used to examine the adsorption data. After 60 minutes, the maximum adsorption was obtained, and the pseudo-order kinetics followed a linear pattern. It was also possible to monitor changes in various thermodynamic parameters, including Gibbs free energy (G°), enthalpy (H°), and entropy (S°). This means the adsorption process in the methyl green–GO combination is spontaneous, as indicated by G's negative value. Metabolic interactions of methylation[97].

In 2017 Modwi *et al*. They were made using a simple sol-gel process and then heated to various temperatures (TC). Analytical techniques were used to characterize the nanoparticles. In order to investigate the photocatalytic performance of nanomaterials, malachite green solutions (300 ppm) were irradiated with UV light. Cu/ZnO nanoparticles have crystallite sizes ranging from 15.86 to 24.25 nm. According to the findings, depending of the annealing temperature, wurtzite forms. Copper doping has an impact on ZnO, according to adsorption and degradation studies. On pure ZnO and Cu/ZnO, respectively, 14.49 and 23.55 percent of MG was adsorbed at the same TA (550 °C). Cu/ZnO exhibits a rapid

adsorption isotherm. ZnO degrades quicker than pure ZnO when Cu/MG is present, with a rate constant of 10 x 103 min1. Cu/ZnO nanoparticles were optimally annealed at 550 °C, based on adsorption and degradation rate constants. Cu/ZnO nanocomposite is therefore a potential and good alternative for wastewater treatment when dye concentrations are high, as a result of this. [98].

In 2018 Khain *et al*. X-ray diffraction, FESEM, FESEM-FESEM, and TEM were utilized to study biosynthesized Cu-NPs in 2018. (XRD). Aqueous crystal violet (CV) was effectively removed from aqueous solutions using Cu-NPs. We studied the effects of pH, initial dye concentration, adsorbent dosage and stirring time on CV removal using a central composite design (CCD). Desirability function linked response surface methods was used to optimize variables for maximum dye adsorption (RSM). An 80-mg dosage was found to remove 95 percent of CV with a high-adsorption capacity (37.5 mg g1) in under one hour (7.5 min). E. coli and S. aureus were also evaluated for antibacterial activity with CuNPs however, the results were inconclusive[99] .

In 2019 Wong *et al*. examined the impact of ZnO nanoparticle characteristics on dye-sensitized solar cell performance. The optical properties of nanoparticles of various sizes and shapes were examined. We observed a complex link between native defects, dye adsorption, charge transfer, and solar cell efficiency. Photovoltaic performance was found to be harmed by the presence of a substantial concentration of nonradiative flaws, however samples emitting orange-red defects performed better than samples emitting green defects (when the samples had similar emission intensities). The characteristics of nanoparticles and

their relation to dye adsorption, electron lifespan, solar cell performance, electron injection, and electron transit time are addressed in detail [100].

In 2019 Aragaw *et al.* For a number of applications, copper nanoparticles put on reduced graphene oxide (rGO) have been examined. However, rGO is utilized as both a support and an electron collector. A study of the photocatalytic activity of Cu nanoparticles on the surface of semiconducting RGO as a light absorber has not been conducted. In situ photoreduction was used to deposit Cu nanoparticles on rGO sheets. UV-Visible spectroscopy, FT-IR, and X-rays powder diffraction were used to assess the Cu/rGO nanocomposite photocatalyst. Photodegradation of a model organic dye is also investigated. The photocatalytic degradation efficiency of Cu/rGO nanocomposites was 94 percent after 50 minutes of light irradiation at pH=7. Cu catalytic activity is responsible for the nanocomposite's remarkable photocatalytic performance. In addition to trapping photoelectrons, Cu nanoparticles also reduce the recombination rate of photoelectron-hole pairs. For low-cost environmental protection, our findings can be applied to graphene oxide-based composites including metallic or metal oxide nanoparticles [101].

In 2019 Mandal *et al.* Researchers have effectively implanted ZnO on a reduced graphene oxide (rGO) surface, as demonstrated by XRD and Raman tests and solvothermal methods. In ZnO/rGO composites, rGO luminescence is suppressed by charge transfer from the lowest unoccupied molecular orbital of the rGO layer to the conduction band of ZnO. Safranin O, Methylene blue, Rhodamine 6G, and other toxic medicinal and textile dyes were degraded by ZnO or ZnO/rGO composites in a comprehensive investigation. Upon UV irradiation, ZnO QD exhibited substantial photocatalytic activity towards dye degradation.

After 15-30 minutes, a ZnO/rGO composite exposed to UV light destroyed virtually all colors. This indicates that the composite's dye degradation effectiveness is good. UV-induced electron-hole recombination in ZnO/rGO composites was revealed by photoluminescence longevity experiments [102].

In 2019 Jilani *et al*. Hydroxide, carbonyl, and carboxylic moieties are found on its basal plane, giving a honeycomb structure. rGO has fewer functionalities, which enhances graphene oxide's inherent features, according to the company (rGO). We evaluated the physical and chemical properties of copper-doped zinc oxide thin films (Cu–ZnO) for the first time using DC/RF sputtering. As a result of Cu–ZnO plane's hydrophobic character, Cu–d-spacing ZnO/rGO increased. The band gap of composite thin films was reduced by the surface electric charge of GO or rGO Lead to an increase in electron–hole pairs, the dielectric constant increases as sp^2 hybridization occurs. It has been determined by AFM morphological analysis that Cu–ZnO/rGO films have such a larger optical absorption than their counterparts Cu–ZnO/rGO films. XPS examination of Cu-ZnO/GO/rGO thin films revealed surface chemistry that was impacted by COOH, C=O, C–OH, and C–C bonding ratios. As a result, antimicrobial activities of the thin films produced was improved against E. coli and E. faecalis [103]

1.19. Aims of the Present Work

This work involves the following main objects:

1- Synthesis and characterization of zinc oxide nanoparticles (ZnONPs) using chemical method.

2- Doping and characterization of ZnONPs with metals (Copper) nonpartisan to yield Cu-doped ZnONPs.

3- Synthesis, characterizating, and modification of reducing Grephen Oxide(rGO) by Hummer methods.

4- Synthesis and characterization of composites of Cu-ZnO/rGO

5- Study of adsorption processes of Rhodamine 6G over some prepared materials.

6- Investigation of antibacterial activity of some of the prepared materials.

2. Experimental

2.1 Chemicals

Chemical used in the present work with their purity and suppliers are given in (Table 1.2).

Table (1.2): Chemicals used in this work and their purity .

No	Chemicals	Chemical formula	Company Supplied	Purity
1	zinc sulfate heptahydrate	$ZnSO_4.7H_2O$	Hi Media	**99%**
2	Hydrochloric Acid	HCl	B.D.H	**33 %**
3	Sodium Hydroxide	NaOH	B.D.H	**99 %**
4	Ethanol	C_2H_5OH	United Kingdom	**98%**
5	Sulfuric Acid	H_2SO_4	B.D.H	**99%**
6	Rhodamine 6G	$C_{28}H_{31}N2O_3Cl$	Germany	**95%**
7	Graphite	C	India	**99%**
8	anhydrous copper sulfate	Cu So4	Germany	**98%**
9	Sodium Nitrate	$NaNO_3$	B.D.H	**99%**
10	Potassium permanganate	$KMnO_4$	Sigma Chemical	**99.5%**
11	Hydrogen Peroxide	H_2O_2	B.D.H	**30%**
12	Copper sulfate pentahydrate	$CuSO_4 \cdot 5H_2O$	Germany	**98%**
13	Ammonia	NH_3	B.D.H	**99%**
14	Zinc acetate dihydrate	$Zn(CH_3CO_2)_2 \cdot 2H_2O$	B.D.H	**99%**
15	Cupric nitrate hydrate	$Cu(NO_3)_2 .H_2O$	B.D.H	**99%**
16	sodium oxalate	$Na_2C_2O_4$	Germany	**99.5%**

2.2 Instruments

Used the instruments used in this work are listed in (Table 2.2)

Table (2.1): Instruments and their models and worksite use this work

No	Instrument	Model	Location
1	Fourier Transform Infrared (FTIR) spectroscopy	Fourier Transform Infrared FTIR 8400S Shimadzu. Japan	Babylon University College of science Department of Chemistry
2	T80 UV/VIS Spectrometer Double Beam	PG Instruments Ltd	Babylon University College of science Department of Chemistry
3	X-Rays Diffraction(XRD)	Lab XXRD 6000 SHIMADZU	University of Kashan
4	Field Emission Scanning Electron Microscopy (FESEM)	Advanced Angstrom (2000A)	Kashan University Iran country
5	U.V-Vis Spectrophotometer Energy	U.V.2600 series	Babylon University College of Science for women Department of Chemistry
6	Furnace (300 - 1200)°C	Muffle Furnace Size two, Gallenkamp	Babylon University College of science Department of Chemistry
7	(Brunauer – Emmett- Teller) BET	NOVA instruments ©1994-2006, Quantachrome Instruments version 2.2	Kashan University Iran country
8	Thermo-Stirred Heater	Heidolph MR Hei Standard, IKA-RH Basic 2	Babylon University College of science Department of Chemistry
9	Magnetic-Stirred Hot Plate	Gallenkamp, England	Babylon University College of science Department of Chemistry

10	Oven	Memmert	Babylon University College of science Department of Chemistry
11	Circulating Thermostat	Lab Tech	Babylon University College of science Department of Chemistry
12	Shaker	GFL(D-3006) Germany	Babylon University College of science Department of Chemistry
13	Sensitive Balance	Sartorius	Babylon University College of science Department of Chemistry
14	pH – Meter	WTW inolab pH 7110	Babylon University College of science Department of Chemistry
15	Ultra-sonic	Sold State (T-14B)	Babylon University College of science Department of Chemistry
16	Autocleave	Steam Sterilizer-001	Babylon University College of Science for women Department of Chemistry

2.3 Synthesis of Zinc Oxide nanoparticles by precipitation Method (ZnO NPs)

Zinc sulfate heptahydrate ($ZnSO_4$. $7H_2O$) and sodium hydroxide (NaOH) were used in this experiment. A 1:2 molar ratio of sodium hydroxide solution was steadily added drop by drop with vigorous stirring for 12 hours to generate an aqueous solution of zinc sulfate. The resultant precipitate was filtered three times with deionized water before being used. Before being dried in at 100°C in oven, the precipitate was completely filtered. The dry sample was pulverized with an agate pestle and mortar to get the fine powder. The resulting powder was calcined for 2 hours at 700 °C in a muffle furnace under air condation [104].

Figure (1-2) depicts a schematic picture of the manufacture of zinc oxide nanoparticles using sodium hydroxide as the reducing agent [105].

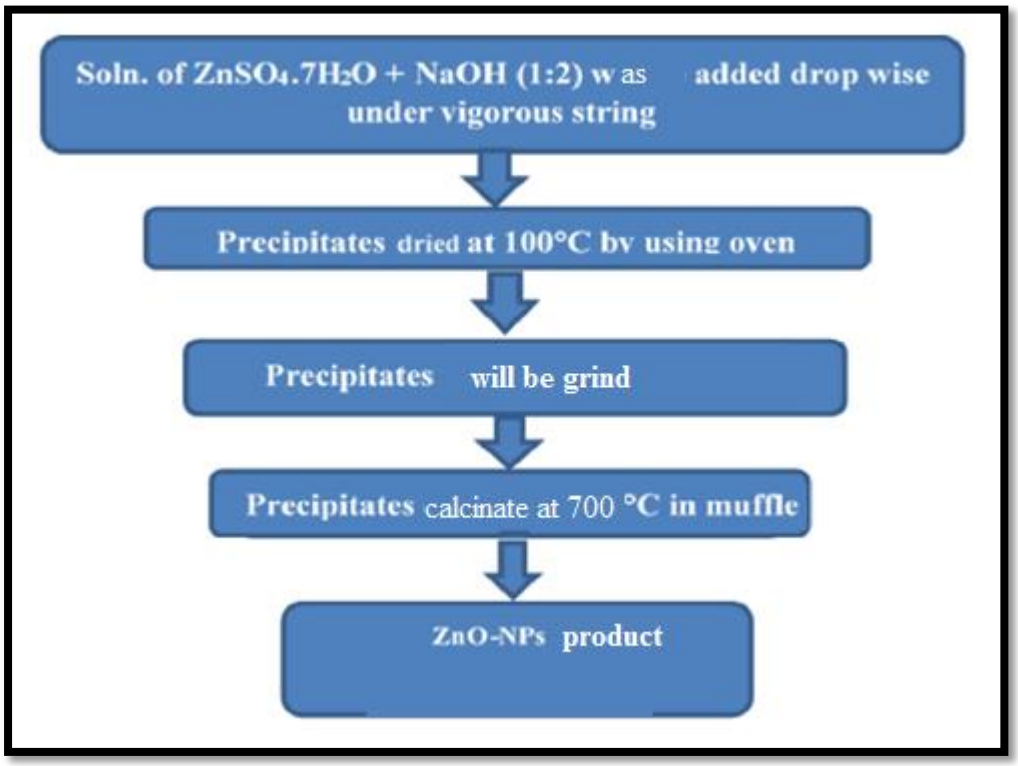

Figure (1-2): Schematic diagram for the synthesis of zinc oxide nanoparticles

2.4 Synthesis of Copper nanoparticles (Cu NPs)

It is a greener chemistry-based approach that combines plants and pathogens to biosynthesize nanoparticle as a non-toxic, clean, and environmentally - friendly technology for synthesizing nanoparticles (NPs) with a wide range of sizes, characteristics, and contents A number of physical and chemical technologies, involving laser irradiation and microwave-aided techniques, are employed by scientists in the production of nanoparticles, Nanoparticles are well delineated and pured, but the hazardous chemicals used in their process of production make them neither cost-effective nor environmentally benign." Developing non-

toxic, clean green biological mechanisms one of the most significant criteria for nanostructures [106].

2.4.1 Synthesis of Copper nanoparticles by Biological Method (Cu NPs)

2.4.1.A. Plant material and its extraction

The ginger was purchased from a local market and is known as Zingiber Officinale. To thoroughly remove moisture from the plant roots, dry them in a shaded area. The roots are then ground into a fine powder using a grinder. The mixture was then heated on a magnetic heater for 6-8 minutes at a temperature of 50 to 60 degrees Celsius, with 1 gram of dried ginger powder added to 100 ml of Deionized water in a 250 mL conical flask. For a period of no more than 10 minutes, the full amount is dissolved. The final step is to filter the solution via filter paper to obtain the plant extract[107].

2.4.1.B. Synthesis of copper nanoparticles

After dissolving 0.7605 g of anhydrous copper sulfate ($CuSO_4$) in 140 mL of Deionized water, the sulfate solution was added to a 250 ml conical flask holding 45 ml of the produced plant extract. The mixture was then placed on a starting magnetic stirrer after the conical flask was clogged with paper. Figure (2-2) shows how gradually change in the color of the sulfate solution from light blue to yellowish blues, then dry the product and heat it for 12 hours in an electric oven at 90 °C. The solid product was obtained, and a sample was taken for this investigation [107].

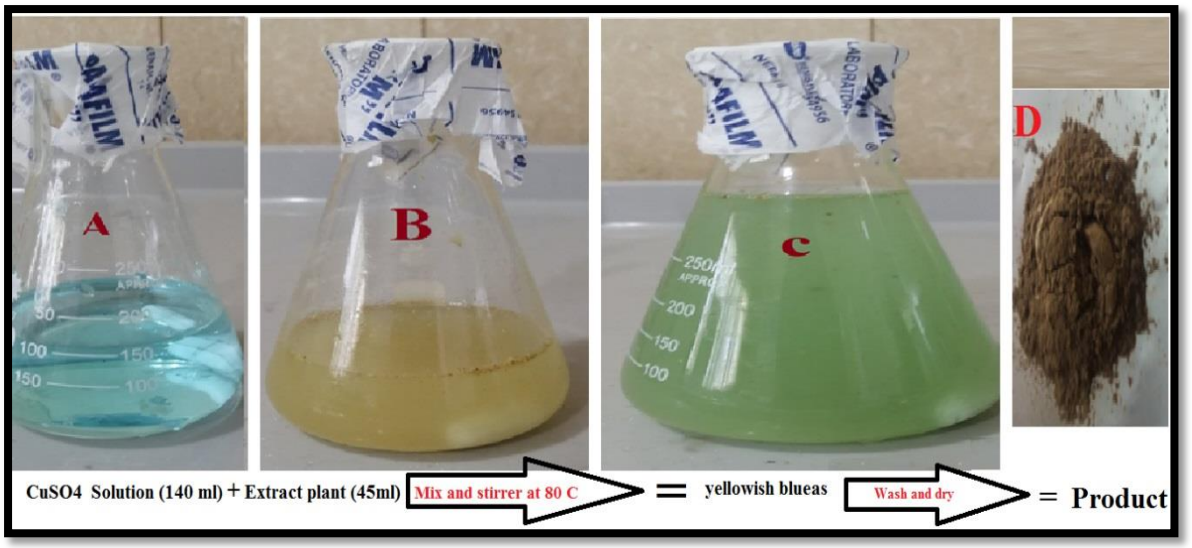

Figure (2-2): Biosynthesis of Copper nanoparticles

2.5 Synthesis of Graphene Oxide nanoparticles by modified hummer's method (GO NPS)

The modified Hummers method is used to prepare graphene oxide. To synthesize graphene oxide (GO) of purified graphite powder, the modified Hummers process was employed. For 15 minutes, sulfuric acid ($H2SO_4$) 27 mL and 3 mL phosphoric acid (H3PO4) (volume ratio 9:1) was mixing together. After that, amid tumultuous events 0.225 g graphite powder is added to the mixed solution. Potassium permanganate ($KMnO_4$), 1.32 g, was gradually added to the solution. The solution was agitated for 6 hours at a low temperature until it turned dark green, as shown in Figure (3-2). 0.675 mL hydrogen peroxide (H2O2) was progressively dropped and agitated for 10 minutes to remove excess KMnO4. Allow for an exothermic reaction to develop before allowing it to cool. 10 mL hydrochloric acid (HCl) and 30 mL deionized water (DIW) were mixed together and centrifuged for 7 minutes at 5000 rpm. A supernatant was then drained aways, and the residue were washed

three times with DIW and HCl (3-2) times . To make GO powder ,the cleaned GO solution was dried at 90 °C in oven for 24 hours [108,109].

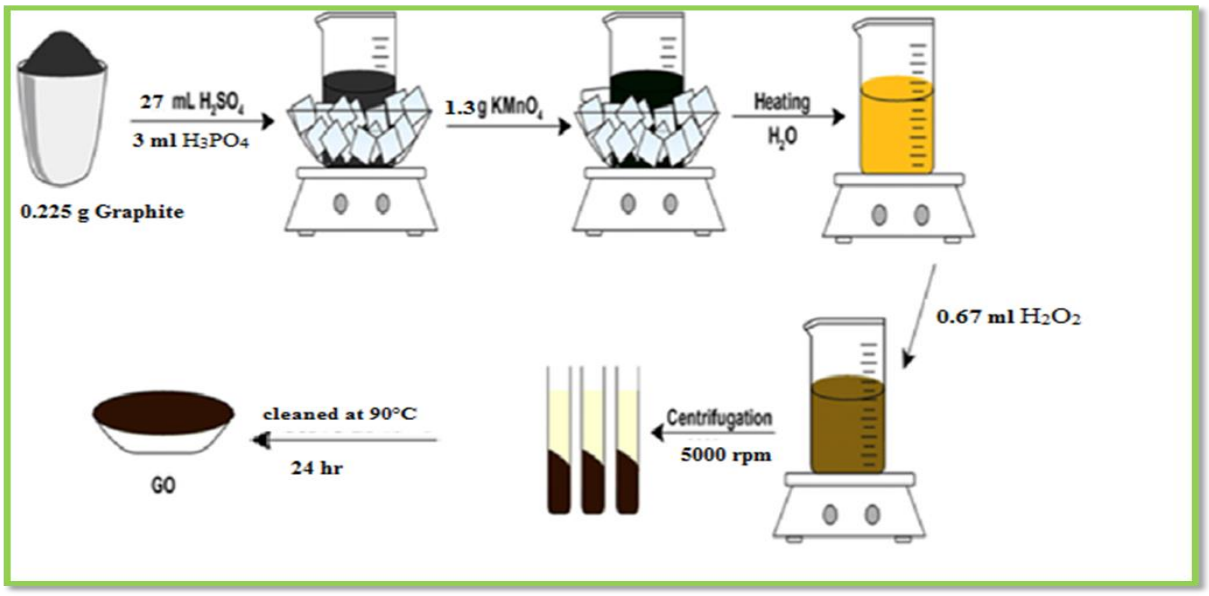

Figure 3-2 :Diagram of the synthesis of graphene oxide nanoparticles by modified hummer's method

2.6. Synthesis of Copper Doped Zinc Oxide nanoparticle's by precipitation Method (Cu/ZnO NPs)

In deionized water, $ZnSO_4 \cdot 7H_2O$ (0.8 M) was dissolved with dropwise addition of NaOH (0.8 M) solution and CuSO4 • $5H_2O$ (0.02M) solution to $ZnSO_4 \cdot 7H_2O$ with continual stirring produced Cu-ZnO NPs. The stirring was kept going until the precipitation was complete. The mother liquid was aged for 12 hours prior to filtration. The resulting residue was dried at 80 °C for 12 hours before being calcined at 350 °C for 3 hours [110].

2.7 Synthesis of Zinc Oxide Doped with GO nanoparticle's by precipitation Method to produce (ZnO/rGO Nanopcomposite)

In a typical synthesis, 50 mg GO was mixed with 10 mL zinc acetate (0.1 M) solution and 10 mL NaOH aqueous solution for 30 minutes.Then the slurry solutions were placed into Teflonlined autoclaves and hydrothermally heated at 180 °C for 24 hours. The yield was rinsed with water, then ethanol, centrifuged, and dried in the oven overnight (see Figure(4-2). The same process was used to prepare pure ZnO without the use of GO [111].

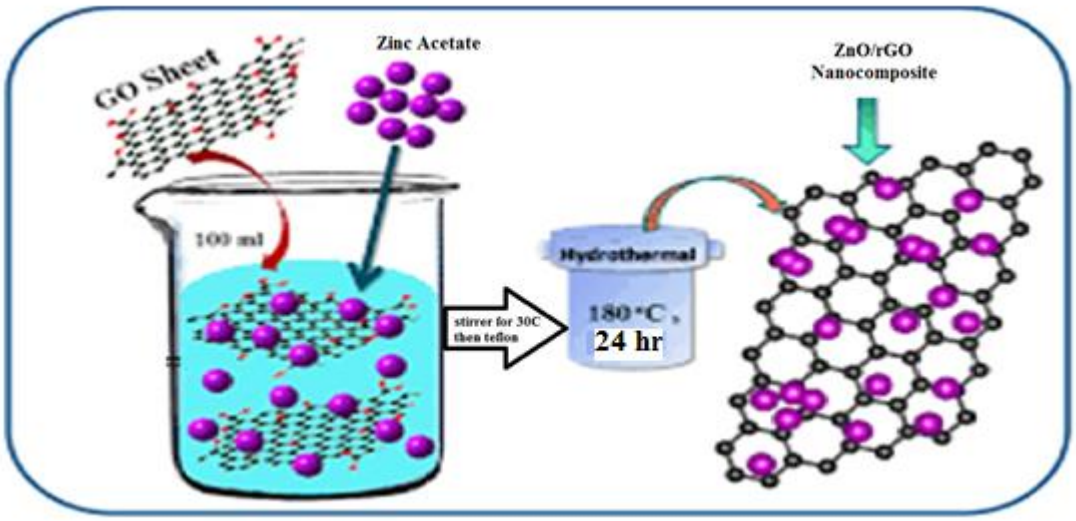

Figure.(4-2) diagram of the synthesis of ZnO/rGO binary nanocomposite

2.8. Synthesis of Copper Doped with rGO nanoparticle's by precipitation Method to produce (Cu/rGO Nanopcomposite)

Cu-rGO powders were prepare using a simple one-step reduction process. The GO was diluted in deionized water to a 0.5 mg/mL stable solution by ultrasonic dispersion during a two-hour period. This was followed by the

addition of aqueous Go to $CuSO_4 5H_2O$ (1 M, 62.5 mL) and agitation to produce the Cu^{+2} -GO solution. CuO-GO was generated by adding ammonia to the emulsion after it had been heated to 90 C without even any gas being introduced into the mixture. Ascorbic acid (1 M, 75 mL) was used as a reducing agent, while vigorous stirring was performed to incorporate it into the reaction. CuO nanoparticles were converted to copper by coagulation and growth. We obtained Cu-RGO powder after 3 hours of reduction ,This was followed by many washes with deionized water and a vacuum drying oven [112].

2.9.Synthesis of Cu/ZnO-doped with Reduce Graphene Oxide to produce (Cu/ZnO/rGO) Nanocomposites By hydrothermal method.

Cu/ZnO/rGO nanocomposite was prepared by tow different hydrothermal techniqes . $ZnAcO_4$, $CuNiO_4$, and NaO were mixed in room tempe. until homogenization were achieved (magnetic stirrer). KOH (20 mL, 1M) was then added drop by drop. We obtained a homogeneous white solution (200 mL) after 2 hours of stirring and sealing, followed by 10 hours of autoclave sterilization (0.8 filled fraction, 120°C, for 10 hours). It was necessary to make a white precipitate, filter it, and then remove residues by washing three times with DI water and twice with ethanol. It was then exposed to air after 12 hours of drying in an oven at 80 °C. After 30 minutes of ultrasonic dispersion, To 50 mL of Deionised water, 25mg of GO powder were added. 0.4 gram of Cu/ZnO (as produced) and 30 mL Deionized water were added to the GO solution for 30 minutes. It was boiled at 160 °C for 12 hours in a 100 mL Teflon liner (autocleave).In Figure (5-2) demonstrates the transformation of Cu/white ZnO's hue into a dark gray tone (see below) ,Hydrothermal GO was thermally reduced,

Finally, deionized water and ethanol were used to filtrate and rinse the grayish precipitation multiple times It took 10 hours at 70 °C to prepare the final product (Cu/ZnO/rGO) [113].

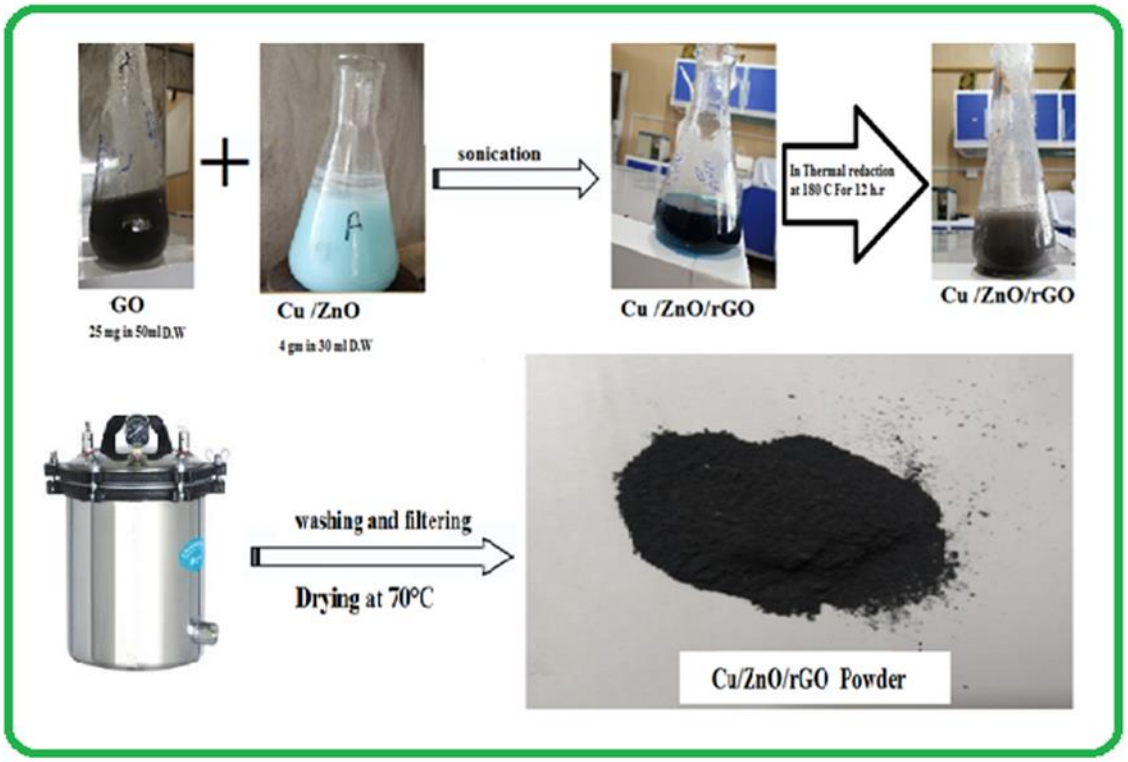

Figure (5-2): Synthesis of Cu/ZnO/rGO tertiary nanocomposite by hydrothermal method

2.10.Characterizations of the Prepared Materials

To analyze synthetic samples and commercial materials this investigation, Field Emission Scanning electron microscope (FE-SEM), X-rays diffraction, Brunauer–Emmett–Teller (BET),Energy Dispersive X-rays (EDX), Fourier transform infrared spectroscopy (FTIR), and Zeta-potential.

2.10.1. X-rays Diffraction Patterns (XRD)

The crystallite structure of the synthezied nanomaterials was measured using X-ray diffractometers,with the parameters of measurement being an Anode Material Cu, k-alpha (K=1.54 A°) source. Scanning step time (s) 1.0000, step size [°2Th.] 0.0500, measurement temperature 25°C. Diffractograms of nanostructures provide information on crystallite size, phase composition, crystallographic orientation, and lattice parameter, among other factors. The distance d separates the lattice planes of a crystal. This law relates the wavelength (**λ**), the distance between atomic planes (d), and the angle of reflection (**θ**) of an incident X-ray.

$n\lambda = 2d\sin\theta$ …….. (2-1)

Using the Debye-Scherer formula in the following equation, find the crystal structure and crystallite size of the produced materials at room temperature:

$D=k\lambda/\beta\cos\Theta$ …… 2-2

Where D denotes the average crystal size, and k denotes the form factor with a value near unity. For heterogeneous shape 0.90, while for homogeneous shape 0.94 = 0.154 nm is Cuk's X-ray wavelength, is the diffraction peaks' full width at half-maximum intensity (FWHM), and is the peak's Bragg's angle[114].

2.10.2. Field Scanning Electron Microscopy (FE-SEM)

The surface morphological properties of prepared materials were revealed using the field scanning electron microscopy (FE-SEM) approach , The specimens were studied using a Scanning Electron Microscope (FE-SEM, Zeiss, Germany) at electron high tension EHT 10 Kv and 60 kx magnification [115].

2.10.3. Fourier Transform Infrared Spectroscopy (FTIR)

Fourier transforms infrared spectroscopy (FT-IR) spectra were acquired using the potassium bromide KBr pellets method at room temperature on a SpactraIR-2, Perkin Elmer Instrument, Functional groups on the surface of the materials under study can be identified using a spectrometer and a spectrophotometer, respectively.Between the waves number of (400 - 4000 cm1) the FT-IR spectrum was acquired [116].

2.10.4. Brunauer–Emmett–Teller (BET)

The amount of N_2 sorption over the surface of the catalyst was measured using a (BEL sorp- mini II, Japan) nitrogen adsorption analyzer with adsorptive N_2 at 77 K, utilizing the Brunauer–Emmett–Teller (BET) model to examine surface area, pore size, and pore volume of produced Nanocomposite materials. The surface area and porosity of the produced composite materials can be examined using the results [117].

2.10.5. UV-Vis. Spectrophotometry

(UV-Vis 1650PC Shimadzu, Japan).The Rhodamine 6G dye degradation behavior over composite is studied using a double beam spectrophotometer. Then determine maximum amount of (R 6G) dye.

2.11. Adsorption Activity of the Prepared Nanomaterials

Adsorption of Rhodamine 6G dye of aqueous solution onto nanomaterials removes the dye in aqueous solution, the adsorption ability of the nanomaterials was studied. All of the experiments were carried out with Rhodamine 6G dye at a concentration of 50 ppm, a volume of 100 mL, a weight of 0.1 g, and a pH of 9 in the dye solution.

Then, removal efficiency was calculated using the following equation:

$$\textbf{\textit{Removal}}\ \% = \frac{A_0 - A_t}{A_0} \times 100 \qquad \text{…….. (2-3)}$$

$$\textbf{\textit{Remaining percentage}} = \text{At /AO} \qquad \text{…….. (2-4)}$$

2.11.1. Calibration Curve

Standard Rhodamine 6G dye aqueous solutions were used to create the calibration curves. Using a UV-visible spectrophotometer, the absorbance of each concentration was measured at 524 nm (UV-1650PC Shimadzu, Japan). Rhodamine 6G is an azo dye with the formula $C_{28}H_{31}N2O_3.Cl$ or $C_{28}H_{31}C_lN_2O_3$ with a molar mass of 479.01 g/mol [118]. Table (3-2) and Figure (6-2) show typical calibration values (7-2).

Table (2-3): Calibration curve for Rhodamine 6G record at 524 nm.

Concentration (ppm)	Absorbance
0	0.00
1	0.25
2	0.51
3	0.74
4	0.91
5	1.13
6	1.32
7	1.5
8	1.64
9	1.78
10	1.97
11	2.23
12	2.44

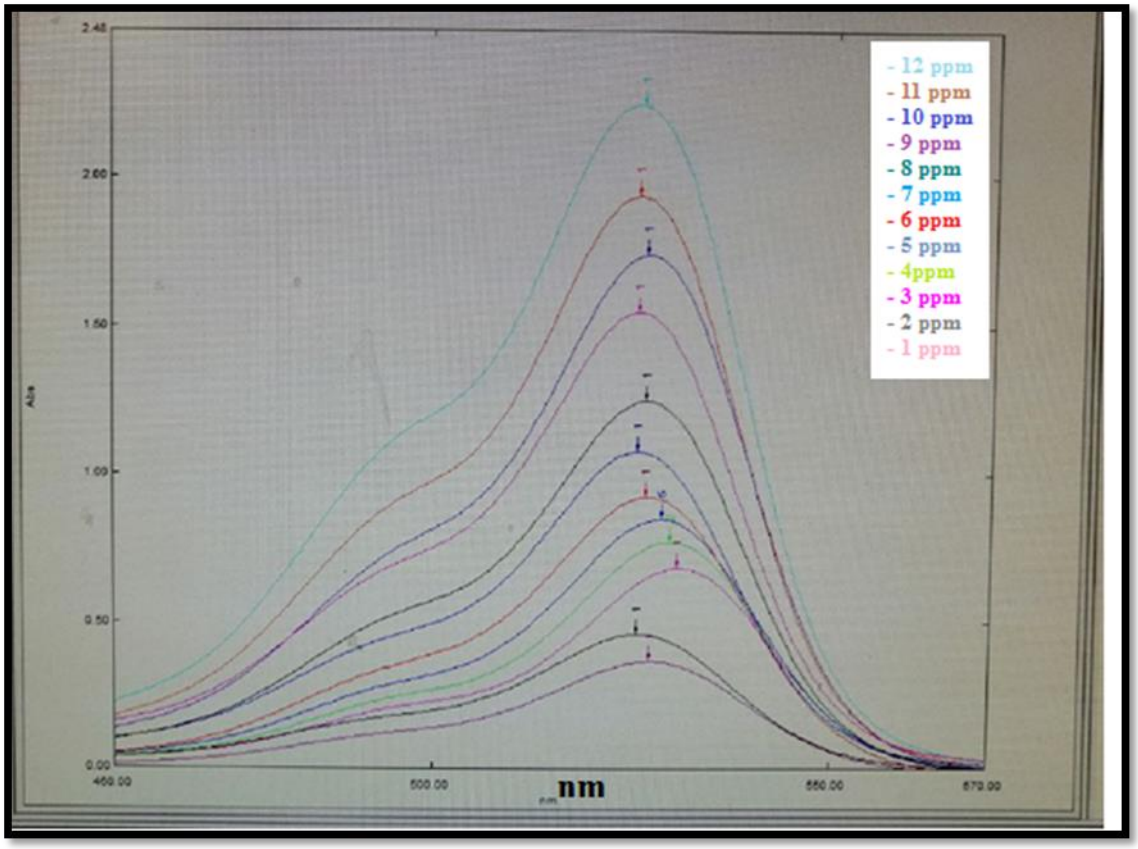

Figure (6-2): UV-visible spectra for Rhodamine 6G at different concentrations.

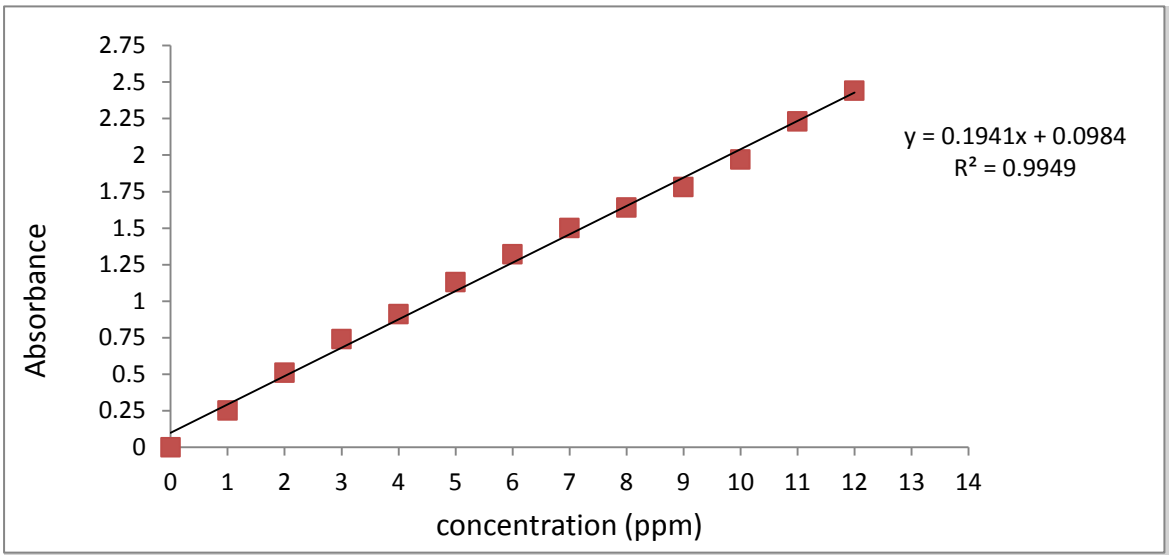

Figure (7-2): Calibration curve for different concentrations of Rhodamine 6G dye recorded at 524 nm.

2.11.2.Effect of Initial Concentration (ppm) of Rhodamine 6G dye on the adsorption to (0.1 gm) of Tertiary Nanocomposite Cu/ZnO-rGO

In this section, different concentration of Rhodamine 6G dye were suspended over 0.1 g of the nanocomposite at varying initial substratum concentrations (3, 5, 7, 10, and 12) ppm. The adsorption rate falls once the adsorbent is dosed at 0.1 g, the optimal pH is reached, the contact period is 60 minutes, and the temperature is 30 °C. This could be owing to the adsorbents' limited number of active sites, which become saturated at high concentrations [119].

2.11.3. Effect of the Dosage of (0.1 gm) Tertiary Nanocomposite Cu/ZnO-rGO on removel of Rhodamine 6G dye

Using several weights of Tertiary Nanocomposite Cu/ZnO-rGO (0.001, 0. 006, 0.02,0.07, and 0.1 g) of nanocomposite, a series of experimet were conducted to find the appropriate doses for the Nanocomposite record in the removal of the dye solution with 10 mL of 10 ppm. For a total of 60 minutes, these trials were conducted at 30 °C temperature [120].

2.11.4. Effect temperature on an adsorption of dye Rhodamine 6G on to(0.1 gm) of Tertiary Nanocomposite Cu/ZnO-rGO

A series of experiments were carried out using 0.1g of Cu/ZnO-rGO nanocomposite at pH 9 with different temperatures (15, 20, 25, and 30 °C) with constant stirring under normal atmospheric conditions for a total time of 60 minutes to study the effects of temperature on the adsorption of Rhodamine 6G dye solution over Cu/ZnO-rGO with dye concentration of 50 ppm. These experimet were carried out to see how

temperature affected on the rate of adsorption dye removal over Nanocomposite process [121].

2.11.5. Effect of pH of an Adsorption of Rhodamine 6G dye on (0.1 gm) of Tertiary Nanocomposite Cu/ZnO-rGO

A series of experimet were conducted in the pH values of (3,5, 7, 9, and 11) using HNO_3 and NH_3 (1M) to control on the media, 0.1 gm, Rhodamine 6G was removed from nanocomposite by varying the pH. Cu/ZnO-rGO nanocomposite and 10 mL dye aqueous solution at 10 ppm for 60 minutes at ambient temperature with steady stirring under normal air conditions [122].

2.12. Adsorption Isotherms

Adsorption isotherm: equilibria relationship between aqueous and adsorbent phases at a certain temperature, Langmuir and Freundlich models were used to explain the adsorption of Rhodamine 6G dye over Cu/ZnO-rGO nanocomposite. A research kinetics isotherm for adsorption Rhodamine 6G dye onto Cu/ZnO-rGO nanocomposite was carried out using the same approach as the equilibrium experiments. The concentrations of Rhodamine 6G dye were determined using UV-Vis light by measuring absorbance at 524nm, an adsorption quantity of Rhodamine 6G dye at time t, qt (mg g-1), and use following equations (2-5),(2-6) for calculated concentrations of Rhodamine 6G dye:

$$\mathbf{q_t} = \frac{(\mathbf{C_o} - \mathbf{C_t})\mathbf{V}}{\mathbf{W}} \qquad \text{……} \quad \textbf{(2-5)}$$

$$\mathbf{q_e} = \frac{(C_o - C_e) \times V}{W} \qquad \text{……...} \quad \textbf{(2-6)}$$

where **qt,qe** represent the quantity of Rhodamine 6G adsorbed over nanomaterials at a regular time and in equilibrium, **Co** and **Ce** represent the starting and final dye concentrations (ppm), **W** is the weight of the adsorbent (g) and **V** is the volume of the solution (L) [123].

2.12.1. Isotherm of Freundlich adsorption

Freundlich isotherm model is used to explain heterogeneous adsorbent surfaces with diverse adsorption sites, as well as multilayer adsorption. The non-linear form of the Freundlich isotherm is described by the equation:

$$q_e = k_F C_e^{1/n} \qquad \text{…… (2-7)}$$

$$\log q_e = \log K_F + 1/n \log C_e \qquad \text{…….. (2-8)}$$

Where **Kf** and n denote the Freundlich constants, **K** denotes the quantity of adsorption, and **n** denotes the degree of nonlinearity. The slope and intercept of a linear plot of log **qe** vs log **Ce** can be used to derive the values of **k** and **n**. Equation **(2-7)** can be linearized by taking the logarithm of both sides. Equation **(2-8)** is the form of the Freundlich model [124].

2.12.2. Isotherm of Langmuir adsorption

Langmuir isotherm assumes that adsorbent materials' surface sites are identical and equivalent, and that each molecule has the same sorption activation energy, resulting in inhomogeneous adsorption, monolayer surface coverage, and no interaction between the adsorbed species on the surface [125].

The Langmuir isotherm has the following mathematical expression:

$$\frac{ce}{qe} = \frac{1}{qm.kl} + \frac{ce}{qm} \qquad \text{…….. (2-9)}$$

qe is the quantity of dye per adsorbed during equilibrium, where **qm** is the absolute maximum of Rhodamine 6G adsorbed by unit mass of the catalyst and **KL** is the Langmuir constant. (mg. g−1) , the values of **KL** can be determined from the linear plot of **Ce/qe** versus **Ce**.

2.12.3. kinetic Modeling for Adsorption Rhodamine 6G dye over synthesized Nanocomposites.

In this study, two types of kinetic models were used to evaluate the adsorption rate Rhodamine 6G adsorption capacity over the prepared nanomaterials: pseudo-first order and pseudo-second-order kinetics.

The pseudo-first order model, often known as the Lagergren equation, can be written as Eq: (2-10).

$$\ln(q_t - q_e) = \ln(q_e) - k_1 t \qquad \text{……. (2- 10)}$$

Where **qe** and **qt** (mg/g) are the amounts of Rhodamine 6G adsorbed at equilibrium and at time **t** (min), respectively, **k1** (min-1) is the adsorption rate constant, **slope = -K1**, and **intercept = log qe** are the liner forms of the pseudo-second order model Eq: (2-11).

$$\frac{t}{q_t} = \frac{1}{k_2 q_e^2} + \frac{t}{q_e} \qquad \text{…….……. (2-11)}$$

The rate constant of the second-order equation (g/mg min) is **k2** (L.mol-1. min-1). **Slope =1/qe** and **intercept = 1/K2qe2** when plotting between **t/qt** and **t** [126].

2.12.4. Measurement of the Reaction Rate Constant

The reaction equilibrium rate after adsorption could be expressed in the following way:

$$\ln\left(\frac{C_0}{C_t}\right) = kt \qquad \text{…….. (2-12)}$$

Where **At** and **Ao** are the reactant concentrations at **t = t** and **t = 0**, respectively, and **K** and **t** are the apparent reaction rate constant and time. A slope of **K** is obtained by plotting ln **(Co/Ct)** versus **t** [127].

2.13. Antibacterial Activity of Synthesized Nanomaterials

Metallic NPs, in particular, were known to use various mechanisms of action to destroy bacteria. NPs have also been shown to infiltrate the cell wall of bacteria and create pores on the membrane's surface, leading in the production of free radicals that can harm the cell membrane12. Ions from NPs have been reported to disrupt enzyme production, produce oxidative stress (ROS), and inhibit DNA translation [128]. The agar diffusion method was used to calculate the inhibitory effect of the prepared compounds on these types of bacteria, which involves drilling three holes in the bacteria-cultured dishes and placing the prepared derivatives in the excavation of the bacteria-cultured varieties in three concentrations (10) mg/ml, 5 mg/ml, and 2.5 mg/ml). Place the dishes in a (37 °C) incubator for 24 hours before measuring the area of inhibition [129]. The antimicrobial effect of the produced nanoparticles were determined use agar diffusion the following procedure an experiment using bacterial isolates was performed , Ecoli and Staphylococcus aureus, which were donated by Babylon Women and Children Teaching Hospital in Babylon Governorate, Iraq. This bacterium was chosen because of its medical significance. Many diseases are caused by these diseases.

Chapter Two

Experimental part

3. Result and Discussion

3.1. Analysis of X-Ray Patterns

3.1.1.1 XRD Analyses of (ZnO, GO, and Cu Nanoparticles)

The crystal structure and crystal size of the particles were determined by XRD analysis. Figure (1-3 a) shown XRD pattern of the synthezied Zinc Oxide NPs From the analysis of X-ray diffraction patterns were calculated the peaks intensity, full width half maximum FWHM and the positions of the peaks ZnO NPs as shown in Table(1-3). according to crystal planes (100), (002), (101), (102), (110), (103), (200), (112) and (201).), XRD peaks at 2θ = 31.975°, 34.635°, 36.745°, 47.675°, 56.775°, 62.975°, 65.825°, 68.075°, and 68.275° correspond to (JCPSD card number. 2551-007-01). Scherer's equation [130] was used to calculate the mean particle size of NPS.The results were consistent with reported in International Centre for Diffraction Data ICDD (No.04-0813) for ZnO. Figure (1-3 b) GO powder showed a typical broad peak at (2Ɵ = 14.19°) attributed to (001) due to the creation of oxygen-containing clusters between its leaves, while Figure (1-3 c) shows for rGO, after the process of heat reduction, the sample peak moves to the right side at (2Ɵ = 25.625) and these values are identical to In comparison to those documented in the literature of both GO and rGO at [131]. The peaks at (36.4°, 47.4°, and 56.7°) correspond to the (111, 200, and 220) planes of the structure of copper nanoparticles, respectively,whereas the (62.9° and 69.1°) (311 and 222) planes.and was find suggest Cu impurities for biosynthesis see Figure (1-3 d). In comparison to those documented in the literature to synthesis copper

nanoparticale by biological method , all potential Cu Nps peaks are allocated (JCPDSNo-4-0836) [132].

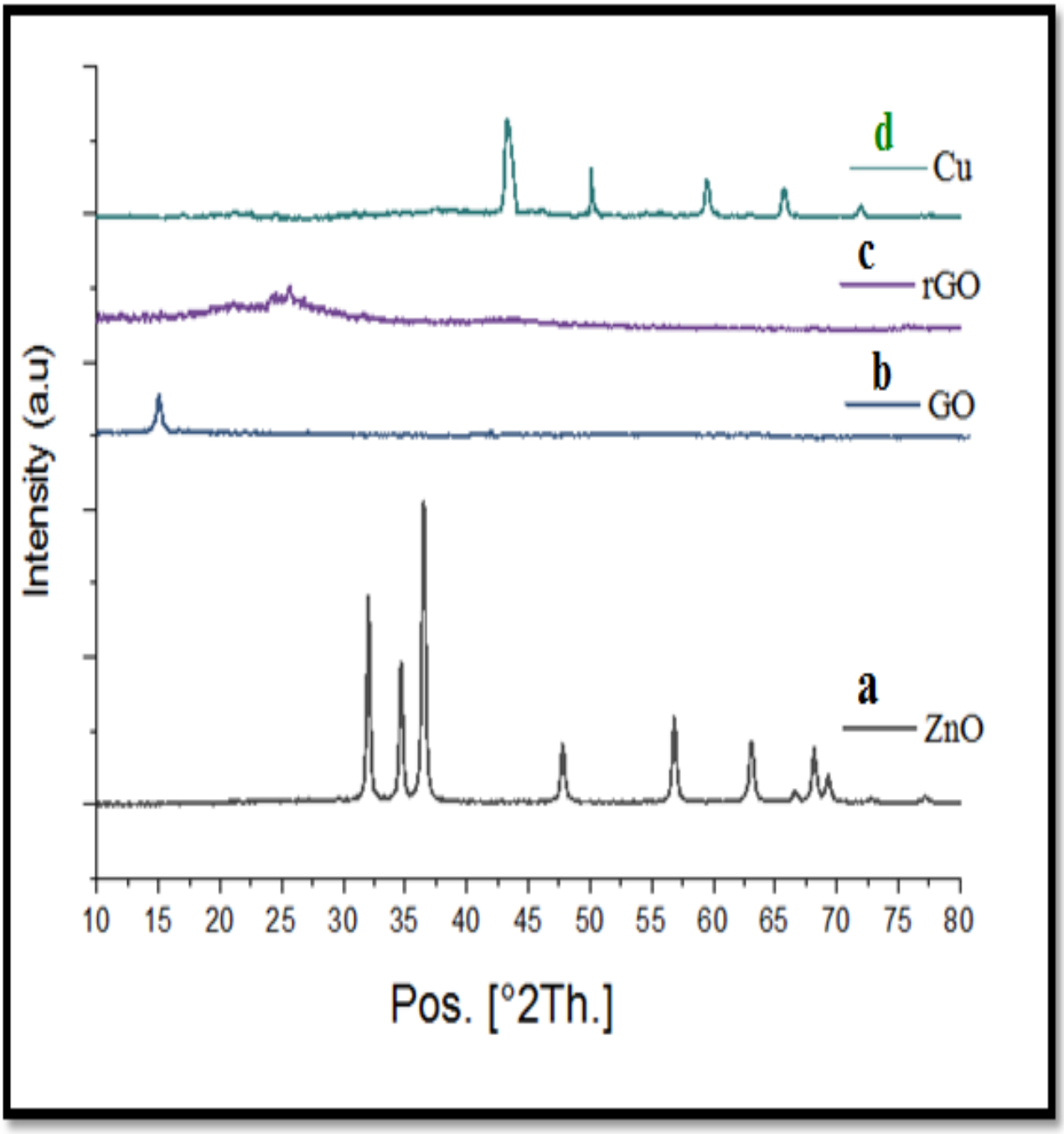

Figure (1-3): XRD patterns for (a)ZnO (b)GO (c) rGO and (d) Cu)NPs

3.1.2 X-rays Analyses of binary Cu/ZnO, ZnO/rGO , Cu/rGO nanocomposites ,and 0.1g Cu-ZnO/rGO tertiary nanomposite.

Figure (2-3 a) illustrates the XRD patterns of zinc oxide saturated with copper (Cu/ZnO). There are differ peak created after doped enters the ZnO structure . After the addition of doping cations, indicating crystal development or changes in crystal strains. There was also a minor shift in the peaks, XRD peaks at 2θ = (36.625°, 38.475°, 40.025°, 56.775°, 46.745°,56.775°, 63.075°, 68.825°, and 69.075°). This shift is also consistent with the compound's stress and the replacement of some zinc cations with copper in the nanoparticales [133].The FWHM was clearly reduced for the samples doped with a quantity of Cu compared to the undoped ZnO-NPs in compare with Figure (1-3) for ZnO NPs [134]. The XRD pattern of ZnO/rGO is given in Figure (6-3 b) With compare for XRD of ZnO in Figure (1-3) . There are no new crystal orientations or change in ZnO's preferred orientations as a result of RGO. Because rGO's diffractive intensity is identical to that described in the literature, no additional peak was identified in the XRD spectrum of ZnO/rGO composite. A peaks at (2Ɵ = 29.9, 32.6, 34.5, 47.3, 56.4, 62.6, 66.1, and 65.8°) as though they were crystal planes (100), (101), (102), (110), (103), (112), and (201) for ZnO/rGO, respectively. which matches the value on the standard card [135]. The (002) peak of rGO theoretically should have appeared in XRD diffraction of ZnO/rGO. Although, it is not visible in an equivalent structures, which indicates that the ZnO surface is sparsely coated by rGO.

The XRD data of pure Cu/rGO nanocomposites are shown in Figure (2-3 c) Cu/rGO composites have no copper oxide peaks when compared to pure Cu and rGO/Cu nanocomposites, and there are five reflection peaks at (2Θ = 43.13°, 50.03°, 59.38°, 65.63°, and 71.83°) that can be attributed to (111, 200, 220, 311, and 222) (JCPDS No. 65-9026), respectively. This lead to that nanocomposite's low rGO loading and carbon's short scattering length relative to copper nanoparticale [136].

Figure (2-3) displays the XRD patterns of Cu-ZnO/rGO nanocomposite of undoped ZnO/RGO, and it can be noticed that GO exhibits a significant diffraction peak at (2 Θ= 14.19°), which is attributed to GO's distinctive diffraction which represents the reduction of GO when exposed to the vapor of a strong reducing agent like hydrazine hydrate Figure (1-3).Furthermore, As illustrated in Figure (2-3 d)The XRD peak However, tertiary nanocomposites made of Cu, ZnO, and rGO have a lower intensity than binary nanocomposites and alone. In the binary nanocomposite Cu/ZnO, ZnO crystallites may have formed. In contrast to the binary nanocomposites, the ternary nanocomposites have substantially lower XRD peak intensities. This may be owing to the fact that the binary nanocomposites were coupled with rGO sheets, which somewhat altered the crystallite structure and created ternary nanocomposites. The slight shift in peak positions were observed with copper doping in ZnO indicating that all doped copper had gone to the substitution sites. According to their pattern, the binaries nanocomposites exhibit a minor shift. of planes (1 0 0), (0 0 2) and (1 0 1) towards higher angle side showing that Cu replaces Zn in the hexagonal lattice along with the c-axis and average size of tertiary nanocomposite is shown in Table (3-3) , These findings show that ZnO/rGO heterostructures

can be successfully formed. This suggests that following Cu doping the crystallinity of ZnO decreases [137].

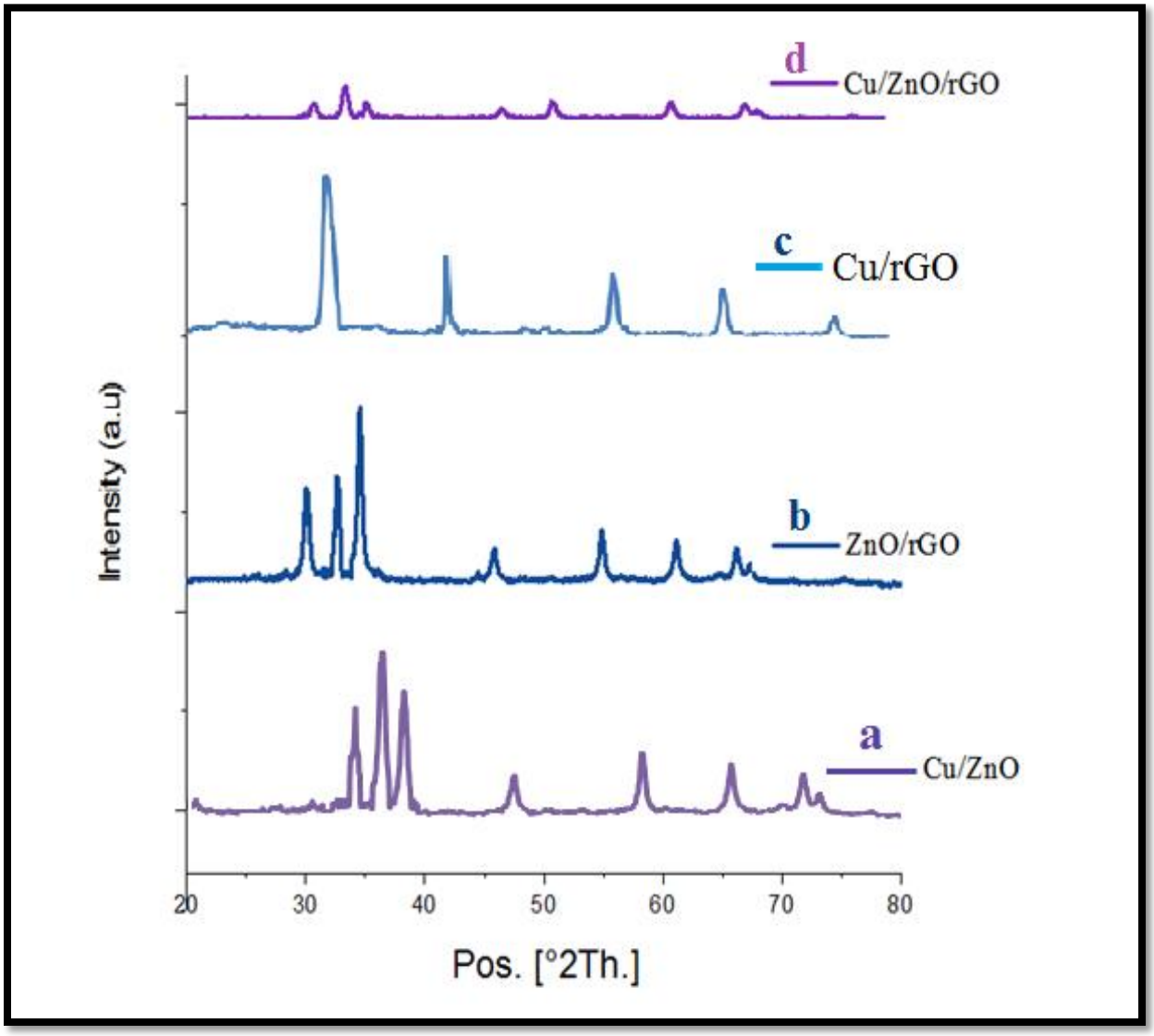

Figure (2-3):XRD patterns for (a)Cu/ZnO (b)ZnO/rGO (c)Cu/rGO binary Nanocomposite and (d)Cu/ZnO/rGO Tertiary Nanocomposite

Table (1-3): Average Crystal size (nm) of (Cu , ZnO, GO , and rGO NPs) Values of angels of diffraction 2θ (Deg.), Full width half maximum FWHM.

Sample	Position [2Θ]	FWHM	Size (nm)	Average Crystal size(nm)
Cu	71.89646	0.04977	49.58024	46.9777
	65.68777	0.01645	29.87514	
	59.44106	0.01371	54.4929	
	50.06619	0.00816	94.69004	
	43.33008	0.92422	6.250163	
ZnO	77.16859	0.34843	25.06158	33.91459
	69.28484	0.5439	29.16451	
	66.61001	0.49572	36.35955	
	63.07892	0.47623	27.54988	
	56.81904	0.41167	37.55724	
	47.77424	0.40842	43.06721	
	36.487	0.3757	36.99403	
	34.66168	0.36426	37.93177	
GO	14.98679	0.54597	14.05037	30.32576
	5.40281	2.50985	35.14996	
	71.1727	1.44221	41.77696	
rGO	25.5079	2.95457	34.5713	27.8401
	44.13162	11.72239	21.10889	

Table (2-3): Average Crystal size (nm) of (Cu/ZnO , Cu/rGO , and ZnO/rGO) Binary Nanocomposite Values of angels of diffraction 2θ (Deg.), Full width half maximum FWHM.

Sample	Position [2Θ]	FWHM	Size (nm)	Average Crystal size(nm)
Cu/ZnO	32.02638	0.45335	44.850727	31.25456198
	34.57898	0.50447	32.960811	
	36.48946	0.49298	85.950734	
	46.57685	0.8944	16.103116	
	47.77091	0.64926	58.220513	
	56.82693	0.58973	27.368088	
	63.08894	0.69417	25.177751	
	66.54437	0.71637	34.41239	
	67.31983	0.66991	74.57079	
	64.85179	1.1515	52.9307	
Cu/rGO	30.07138	0.62301	41.03084	43.96145
	32.65675	0.48802	83.69993	
	34.53823	0.5238	52.48863	
	44.46463	0.26694	31.23135	
	45.81489	0.60965	69.07872	
	54.8774	0.54899	78.32218	
	61.13916	0.63062	61.07828	
	66.22109	0.61777	85.18309	
	67.31983	0.66991	24.57079	
	64.85179	1.1515	42.9307	
ZnO/rGO	35.2209	4.03582	42.04149	38.00444
	22.97669	0.26458	80.28766	
	27.23569	2.33569	37.45941	
	31.42407	0.83457	49.77483	
	18.3431	0.41157	99.32759	
	37.83791	0.01281	86.9776	
	52.54848	0.41409	47.14942	
	55.45144	1.57503	25.63262	
	42.82257	0.7742	38.89527	
	14.15869	0.63314	32.49848	

Table (3-3): Average Crystal size (nm) of (Cu/ ZnO/rGO) Tertiary Nanocomposite Values of angels of diffraction 2θ (Deg.), Full width half maximum FWHM.

Sample	Position [2Θ]	FWHM	Size (nm)	Average Crystal size(nm)
Cu/ZnO/rGO	32.04545	0.71683	39.3902	23.77378
	26.3961	0.11124	63.94518	
	36.56494	0.68692	19.28525	
	34.79221	0.69655	29.362604	
	47.86364	0.80365	16.62941	
	52.36364	0.8941	15.42364	
	62.04545	0.73069	25.09464	
	68.66883	1.69537	21.70386	
	69.46753	1.48885	13.87076	
	77.37662	0.57234	23.03225	

3.2. Field Scanning Electron Microscopy (FE-SEM)

The morphology of the ZnO,Cu,GO,rGO, Cu/rGO , Cu/ ZnO, ZnO/rGO , and Cu-ZnO/rGO nancomposite, as well as the average particle sizes, were studied using Field Scanning Electron Microscopy (FE-SEM) Figures.

3.2.1. FE-SEM of ZnO, Cu , and GO Nanoparticales

All images at (200 nm) magnifications powder of alone ,binary and tertiary nanocomposite , FE-SEM was used to study the morphology of as-synthesized ZnO, Figure (3-3 a). shows particles of ZnO have spherical shaped and it relatively homogeneous they had a wide particle size variation from (58.9–98.5 nm) with well separated grain boundaries which is consistent with that obtained from XRD patterns by applying Scherer's equation , Formation of ZnO NPs with nanoscale dimensions with an average particle size around (53 nm) Figure (3-3 b) shows the copper nanoparticles. Image from a FE-SEM , copper nanoparticles looked to be clumped together. Hydroxyl groups in Ginger root extract may be responsible for agglomeration. which is consistent with that obtained from XRD patterns by applying Scherer's equation images of copper nanoparticles and revealed an average size of (46 nm) and a spherical shape it relatively homogeneous they had a wide particle size variation [138]. The FESEM image of Figure (3-3 c) shows the effective exfoliation of graphite oxide (GO) produced by graphite oxidation.A wrinkled surface characterizes the layering of the nanosheets' structure. According to Scherer's equation, GO nanosheets with a size range of (95.11 nm) have a porous structure .

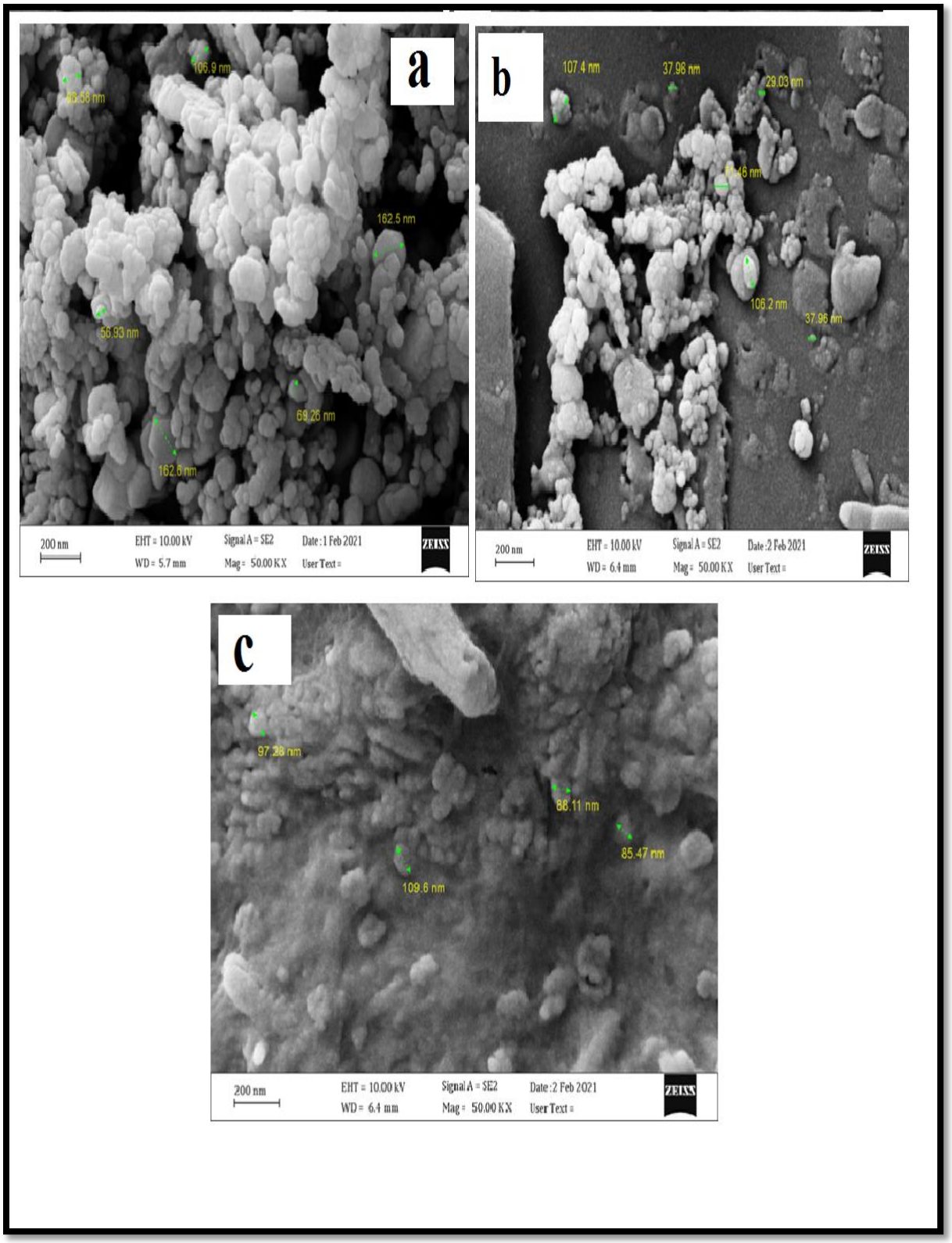

Figure (3-3): FE-SEM image for(a)ZnO (b)Cu (c)GO Nanoparticales

3.2.2. FE-SEM of binary Cu/ZnO ,Cu/rGO ,and ZnO/rGO Nanocomposite

FE-SEM is used to examine the apparent morphology of hydrothermally produced Cu-doped ZnO-NPs. are shown in Figure (4-3 a). The shape of ZnO appears to be nanorod that have been trimmed by the addition of Cu. Cu/ZnO diameters ranged size from (35- 96 nm) and average size by applying Scherer's equation (32 nm) .Cu-dopedZnO appeared to be smaller , isolated cotton packs arranged side by side at the bottom [139]. As the mass ratio binary of Cu/rGO is increased, Cu nanoparticles with sizes from (40-98 nm) grow on the surface of rGO nanosheets, as illustrated in Figure (4-3 b). and according to XRD average size by applying Scherer's equation was (63 nm) .These findings suggest that a simple thermal reduction approach can produce well dispersed Cu nanoparticles with a restricted size distribution in the rGO [140]. Figure (4-3 c). FE-SEM image of ZnO/rGO, show layer of rGO surface totally covered by ZnO seeds. ZnO nanoparticles on the rGO sheet have a size of (63-90 nm)and according to XRD average size by applying Scherer's equation was (68 nm) . Chemically bonded ZnO/rGO structure is formed when metal and metal oxide crystals are formed simultaneously in this one-step method. The interactions between Zn and oxygen-containing functional groups in rGO can carry out this activity [141].

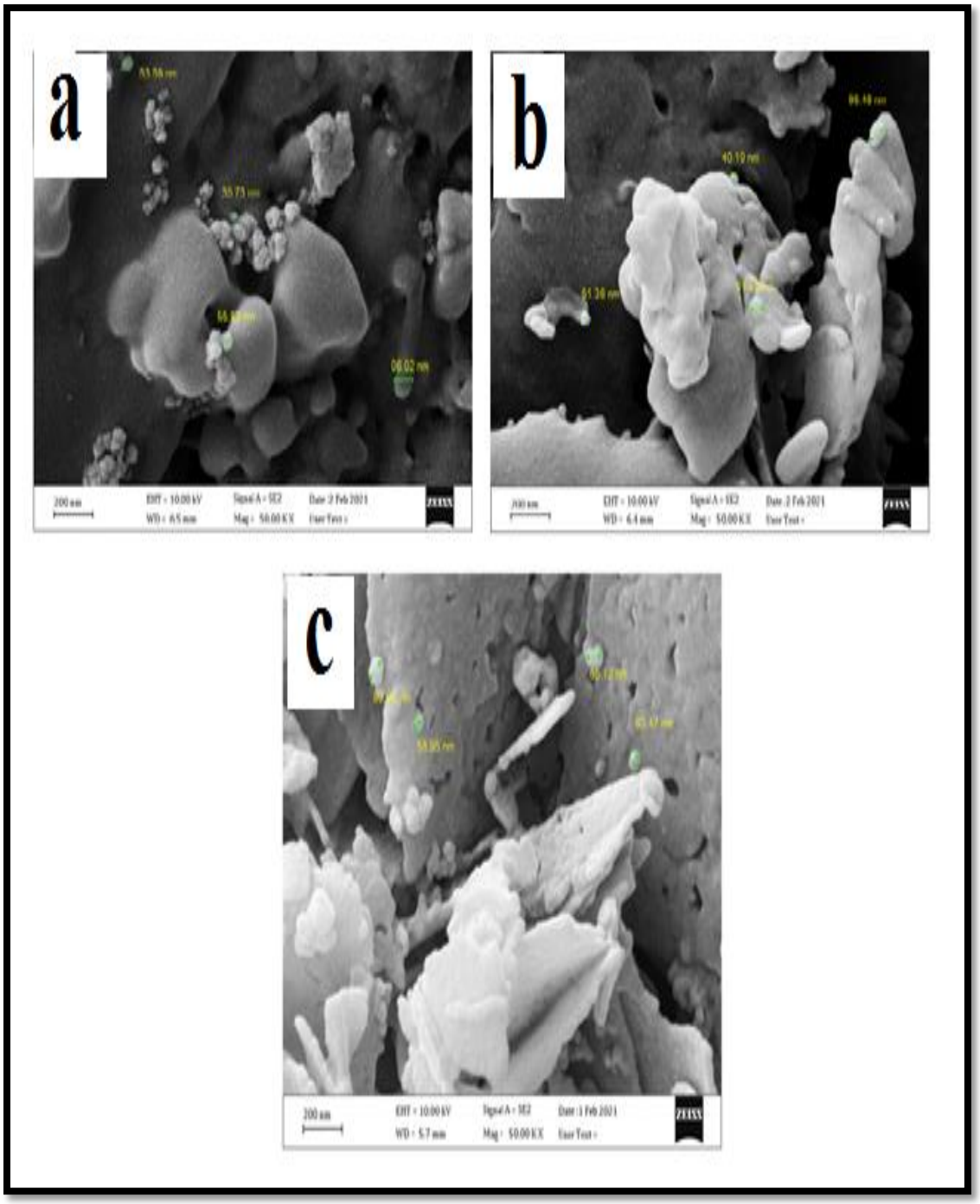

Figure (4-3):FE-SEM image binary for (a) Cu/ZnO (b)Cu/rGO (c)ZnO/rGO Nanocomposite

3.2.3. FE-SEM image of Tertiary Cu/ZnO/rGO Nanocomposite

Figure (5-3) shows FE-SEM image of tertiary Cu/ZnO/rGO nanocomposite sample In both heat and modified materials, agglomeration was observed following addition of rGO to Cu/ZnO after added Cu^{2+} ion and rGO nanosheets, A shape of ZnO crystals obviously changed, but it changed again after being coating and stabilizing on rGO nanosheets. Vander-Waals interaction on either A nano-lattice crystalline alter the growth mechanism of aggregations, according to a new study ZnO crystals and also the size of binary nanocomposite Cu/ZnO will decrease after doping by rGO as Shown that in Table (3-3). The average size of nanocompsites measured by FE-SEM was about (17-80 nm) and according to XRD average size by applying Scherer's equation it was (48 nm).Surface developer rGO promotes self-assembly of ZnO particles. On top of ZnO and Cu grains, rGO sheets appear to act as flat surface[142].

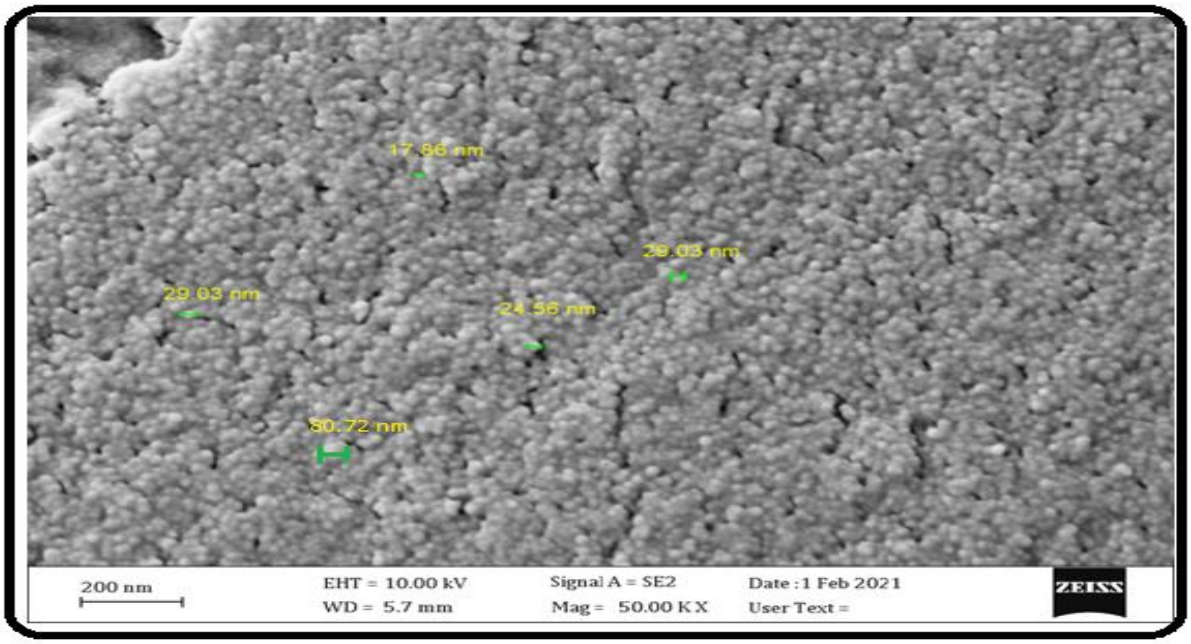

Figure (5-3): FE-SEM spectra for 0.1g Cu/ZnO/rGO Nanocomposite

3.3. Energy-dispersive X-rays (EDX) Analysis

3.3.1. EDX Analysis of (ZnO, Cu, and GO Nanoparticles)

The elemental composition of zinc and oxygen containing group in ZnO nanoparticles was determined using energy dispersive X-rays analysis (11-3 a). The examination yielded 81.2 weight percentages of zinc, 20.0 weight percentages of oxygen, and 5.9 weight percentages of carbon. Previous studies reported a weight percentage of zinc and a weight percentage of oxygen, and a similar pattern was found, but our investigation revealed the presence of carbon, which was owing to the use of zinc acetate dehydrate as a precursor for preparation of zinc oxide nanoparticles[143]. Figure (11-3 b) show aggregation of carbon and oxygen may be due to the presence of secondary metabolites in the Ginger root extract [144]. Shown EDX image of copper nanoparticle synthesized using Ginger root extract, EDX spectrum confirms and size of the nano-copper by this eco-friendly method weight percentage of copper element 71.2, carbon 16.4, and oxygen 9.9% Figure (11-3 C) EDX spectra of GO shows the presence of carbon, oxygen, sulphur, and chlorine. Sulfur and chlorine were present because rGO was made using a modified Hummers technique [145].

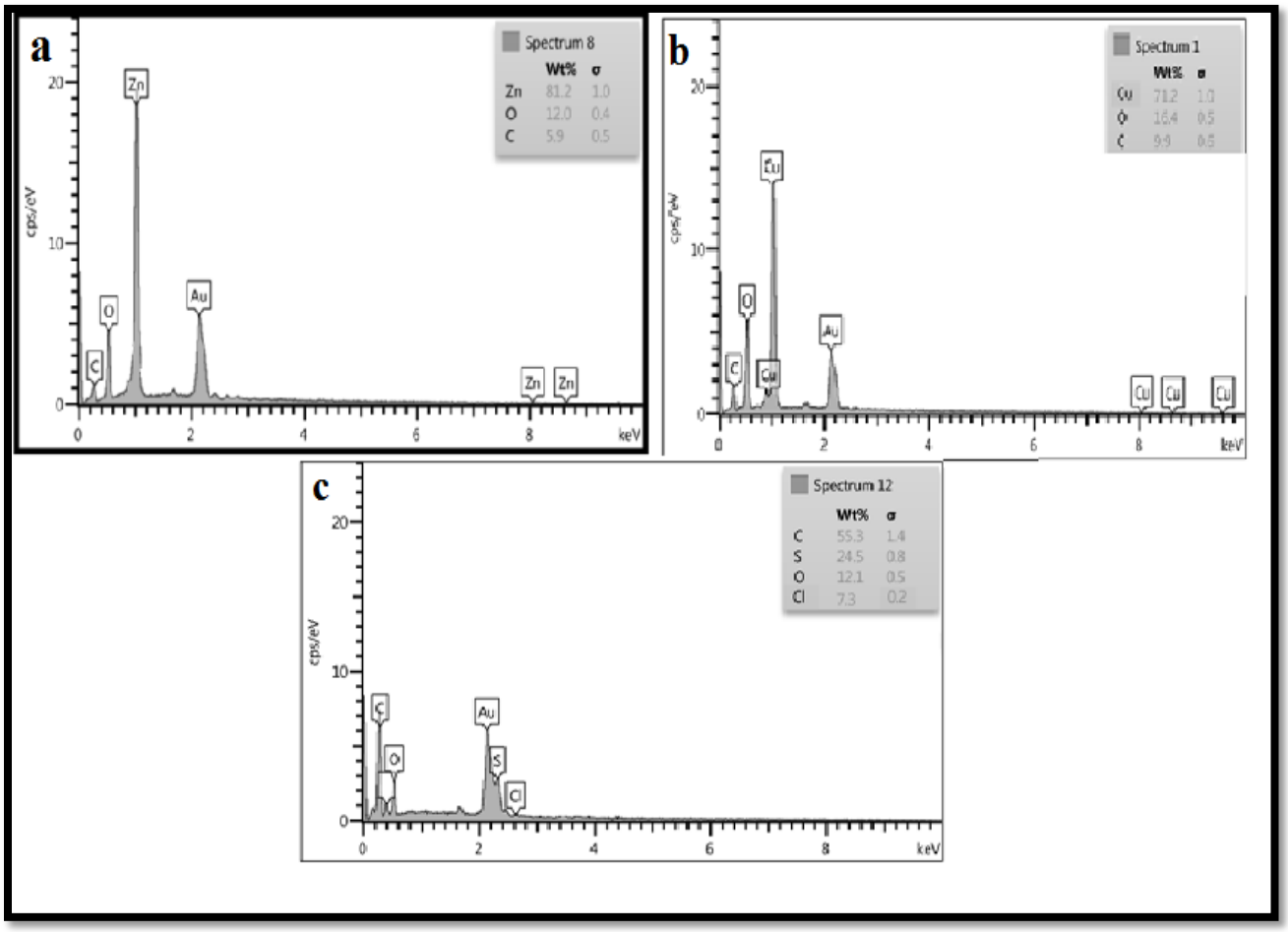

FIG. (6-3): EDX Image for (a) ZnO (b) Cu (c) GO Nanoparticale

3.3.2. EDX Analysis of binary (Cu/ZnO ,ZnO /rGO , and Cu/rGO Nanocomposites)

A chemical content and formation of the sample were investigated using EDX. Cu-doped ZnO nanoparticles Figure (12-3 a) shows a typical the EDX spectra of doping ZnO nanoparticles the presence of chemical components was confirmed (Zn=64.1 , O=33.3 percent ,Cu=14.8 percent) Carbon traces(C) , in additional to these chemical compounds was found on the substrate. The Zinc Oxide was found in the EDX peak locations, and the sharpness EDX peakes showed These findings are in line with those of prior

studies [146]. Figure (12-3 b) indicates that the ZnO/rGO EDX spectrum clearly shows that the sample was made up entirely of Zn and O. It was difficult to identify the relative concentration of oxygen to zinc, which suggested that the O element in ZnO bonds emerged in the ZnO structure, using EDX analysis. Meanwhile, the EDX spectrum of ZnO/rGO revealed the presence of (Zn= 57.3 wt%, O=23.0 wt%, and C=13.9 wt%) in all samples, indicating that the integration of ZnO into rGO by the hydrothermal technique was successful . EDX in the form (12-3 c) was used to examine Cu/rGO nanocomposite, and the results of sample were provided Cu = 71.1 percent, O=18.1 percent, and C = 5.8 percent are the weight ratios determined by EDX [147].

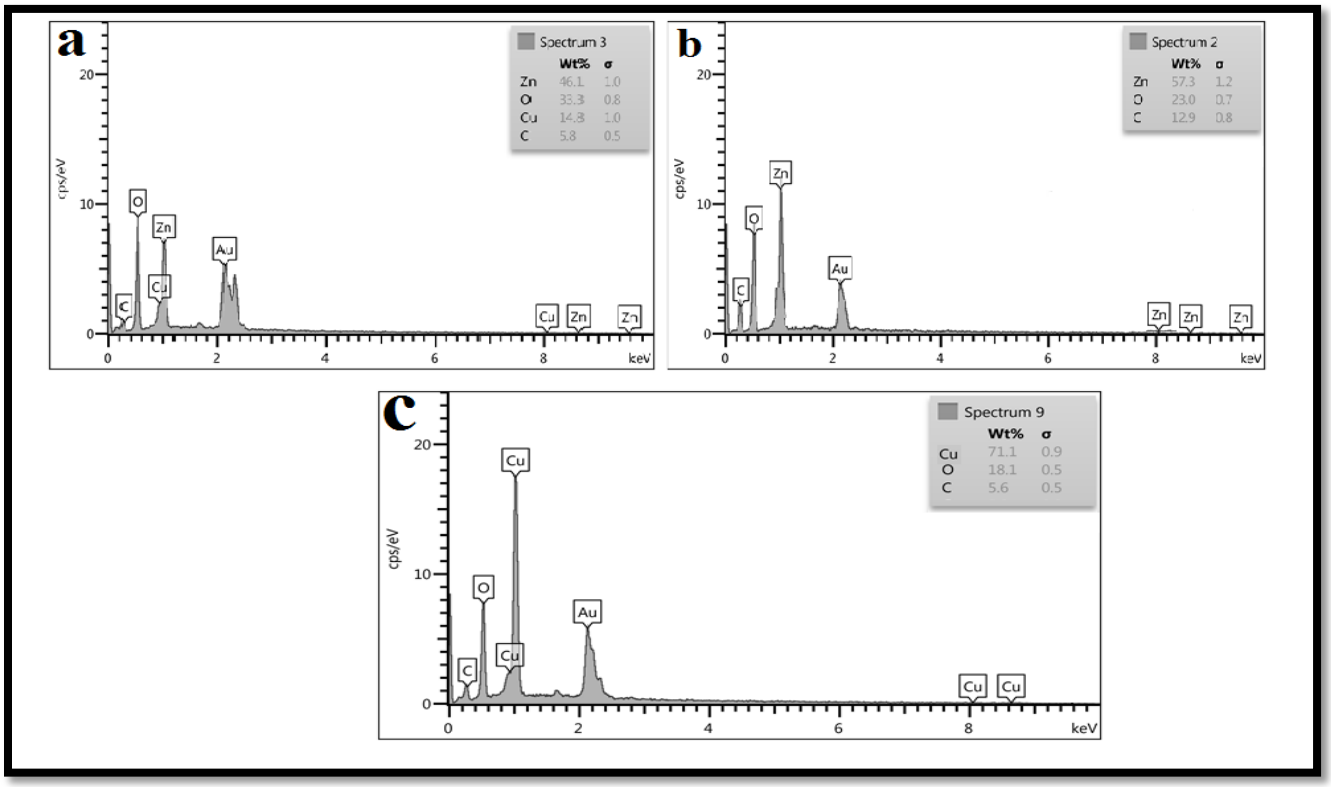

Figure (7-3): EDX spectra for binary (a)Cu/ ZnO (b) ZnO/rGO (c) Cu/rGO Nanocomposite

3.3.3. EDX Analysis of Tertiary (Cu/ZnO /rGO, Nanocomposites)

As shown in Figure (13-3), energy-dispersive X-ray spectroscopy (EDX) was used to determine the exact composition of the components present in the Cu/ZnO/rGO nanocomposite sample for an initial analysis of a nanocomposite sample, a random section was chosen. It was determined that the atomic structural of Cu/ZnO/rGO tertiary nanocomposite is approximately C (5.8%), O (33.3%), Cu (14.8%), and Zn (46.1%) of Weight the sample ,This is consistent with what is mentioned in the literatures [148].

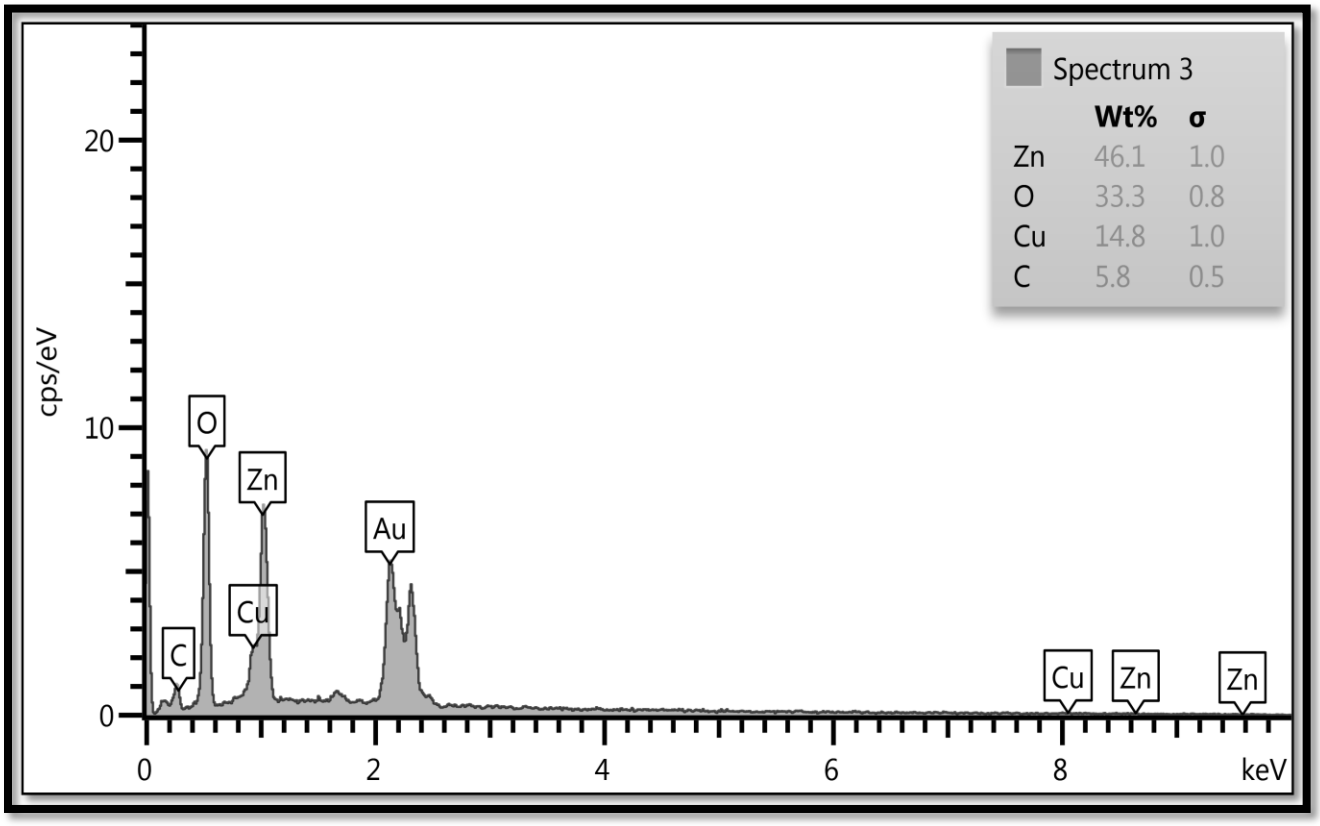

Figure (8-3): EDX spectra for Tertiary Cu/ZnO/rGO Nanocomposite

3.4. Fourier Transform Infrared Spectra (FT-IR)

3.4.1 FT-IR spectra of ZnO, Cu and GO Nanoparticales

Figures illustrate FTIR spectra for ZnO, Cu, and GO NPs. The precipition process is used to make ZnO, as shown in Figure (6 -3 a) Nanoparticle functional groups were identified via FT-IR analysis. The samples contain absorption peaks throughout the range of (3190, 1643, 1516, 1570, 1003, 802, 700, and 597 cm^{-1}) suggesting the distinctive functional group found in the produced zinc oxide nanoparticles at 468 cm^{-1} to the stretching vibration of the Zn-O bond. The 575.9 cm^{-1} absorption peak represents the metal-oxygen, (ZnO stretching vibrations) vibration mode. The Sharp peak in 1003 cm^{-1} is attributable to C-N bond stretching vibration of the primary amine or the C-O bond stretch vibration of a primary alcohol. The peak at 1570 cm^{-1} is responsible for the vibration modes of aromatic nitro compounds and alkyl. The peak at 3190 cm^{-1} is caused by hydroxyl molecules stretching [148,149]. There was a modest increase intensity after the production of copper nanoparticles, as shown in Figure (6-3 b) at 3624 cm^{-1}, which could be attributed to the binding of $[Cu(SO4)_2]^+$ groups to –OH. The carbonyl and carboxylate (CO) bands of the peptide bonds (tightening of amides) bands were assigned to the band at 1708 cm. The oxidation of –CO groups to the extract components caused a blue shift from 1541 to 1708 cm^{-1}, which was observed. Similarly, (bacterial) dimethyl alkane caused an increase in band intensity at 1236 cm^{-1} [150]. Cu NPs FTIR spectrum also suggests the possibility of copper ions interacting with ginger extract. At 489 cm^{-1}, no distinctive Cu_2O vibration was seen during the bioreduction phase [151,152]. Figure (6-3 c) shows FT-IR spectrum of GO, which has a high peak at 3367 cm^{-1} and additional weak intensity peaks

at 1730, 1626,1062, and 1053 cm^{-1}. OH groups, epoxy symmetric ring deformation, carboxylic acid stretching vibrational, ter-tiary C-OH groups, residual (sp^2) hybridized Carbon group post oxidation, graphitic carbon, and C-O stretching vibrations of alkoxy groups are represented by these peaks, sequentially [1

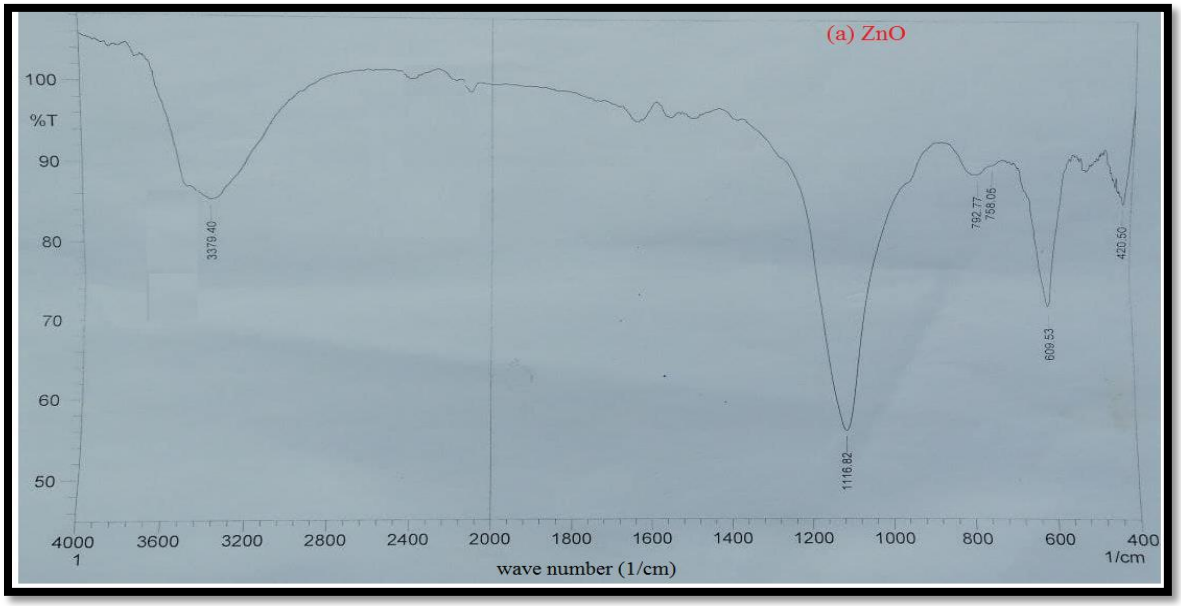

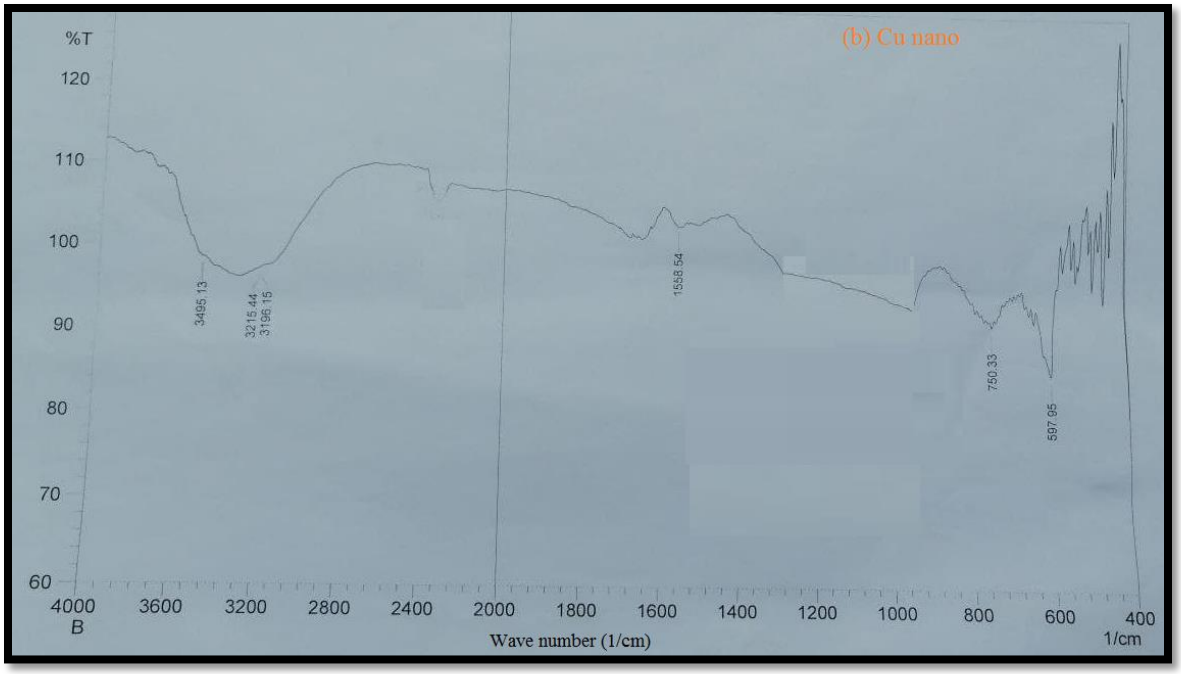

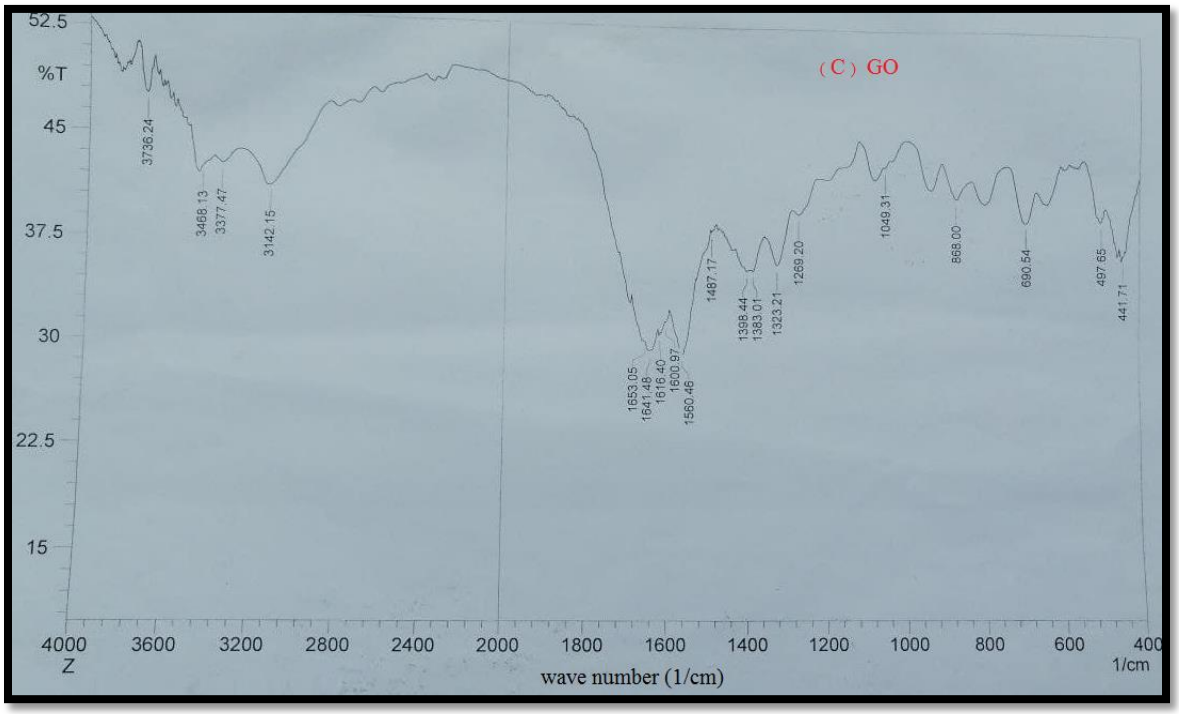

Figure (9-3): FT-IR Spectra for ZnO,Cu,and GO Nanoparticales

3.4.2. FT-IR Spectra of binary (Cu/ZnO , ZnO /rGO, and Cu/rGO) Nanocomposites

The Cu-doped ZnO nanocomposite was studied using FTIR (Figure 7-3). CuO and ZnO both have absorption signals in region (385–690 cm-1) that are due to metal-oxygen stretching vibrations. In bulk ZnO and CuO, however, the band shape is noticeably different: Cu-O oxide exhibits two bands with good resolution in 700 and 560 cm^{-1}. The broad unstructured absorption in 3379 cm^{-1}, which correlates to the O–H stretch vibration of hydroxyl group, and smaller bands in the spectrum of organic residues[154]. ZnO exhibits another broad, featureless connections round in 460–390 cm^{-1}, A broad structure less absorption at 3379 cm^{-1}, that corresponds to O–H . A broad ZnO vibration and a narrow strong Cu-O band in 420 $cm^{-1}$are also

observed. Cu-second O's mode, at around 609 cm^{-1}, is extremely weak and cannot be regarded significant [155].

Figure (10-3): FT-IR Spectra for binary Cu/ZnO Nanocomposite

FT-IR spectra of rGO was still covered by the oxygen functional groups (Figure 8-3). The oxygen functional groups are thought to act as metal ion anchor sites, increasing metal oxide dispersal. They were assigned a large and high maximum absorbance at 3396 cm-1 for the stretching vibrations of OH group. There are number of O-H bonds on the rGO surface, which could act as anchoring sites to hold ZnO nanoparticles at 620 cm-1 in situ. C-O absorbance peaks at 1072 cm-1 [156-160].

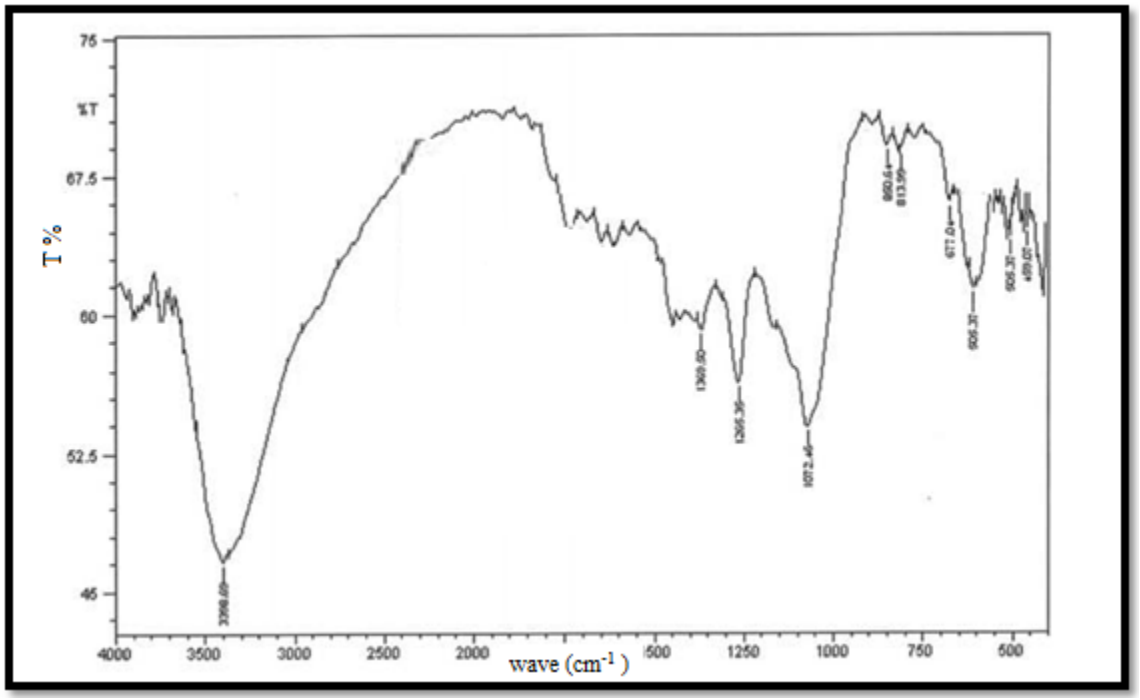

Figure (11-3): FT-IR Spectra for binary ZnO/rGO Nanocomposite

FTIR spectra of Cu–rGO nanocomposite are shown in (Figure 9-3), with peaks for O-H, C–O, C-OH, and C–O stretching bond vibrations at 3247, 1307, 1618, and 1039 cm-1, respectively, and some peaks for Cu–O stretching vibrations at 596, 530, 477, and 415 cm-1 [160].

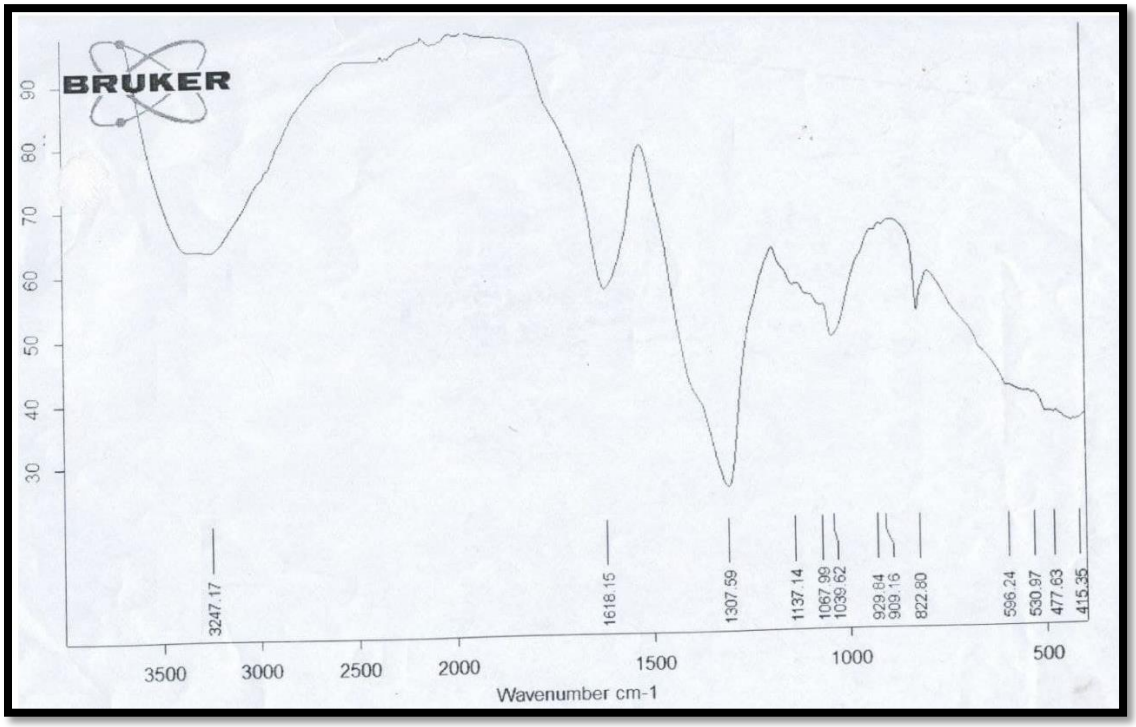

Figure (12-3): FT-IR Spectra for binary Cu/rGO Nanocomposite

3.4.3. FT-IR Spectra of Tertiary (Cu/ZnO /rGO) Nanocomposites

Figure (10-3) shows IR spectra for Cu/ZnO/rGO Nanocomposite, curves revealed that the spectrum of GO had an excessive amount groupings with oxygen as a component. The high absorption intensity wave at 3489 cm^{-1} in the rGO spectra was attributed to the O–H bond stretching

vibrations, which were mostly caused by C–OH and/or intercalated moisture. 1608 cm^{-1} and 1444 cm^{-1} were attributed to C–O and C=O bonds being stretched by the functional groups carboxylic and oxylic, respectively [161]. The signals pertaining to the carbonyl and hydroxyl groups have been reduced, indicating that the rGO sheets have been covered by Cu/ZnO and a ternary nanocomposite has formed. The Cu/ZnO–rGO nanocomposites had the same peaks as rGO, but there was a new broad peak at 694 cm1 that was attributable to Zn–O vibrations. These spectra results demonstrate that Cu/ZnO nanoparticles were attached to rGO sheets once more. FT-IR spectra for Cu/rGO, ZnO/rGO ,and Cu/ZnO/rGO exhibited Cu–O and Zn–O peaks in the region (694–400 cm^{-1}) [162]. Further, in the spectral of nanocomposites, C-O (1444 cm^{-1}) signals may be found, which are assumed to be induced by the migrating of functional groups (C–O or C–OH) to the borders of graphene sheets after thermal processing [163].

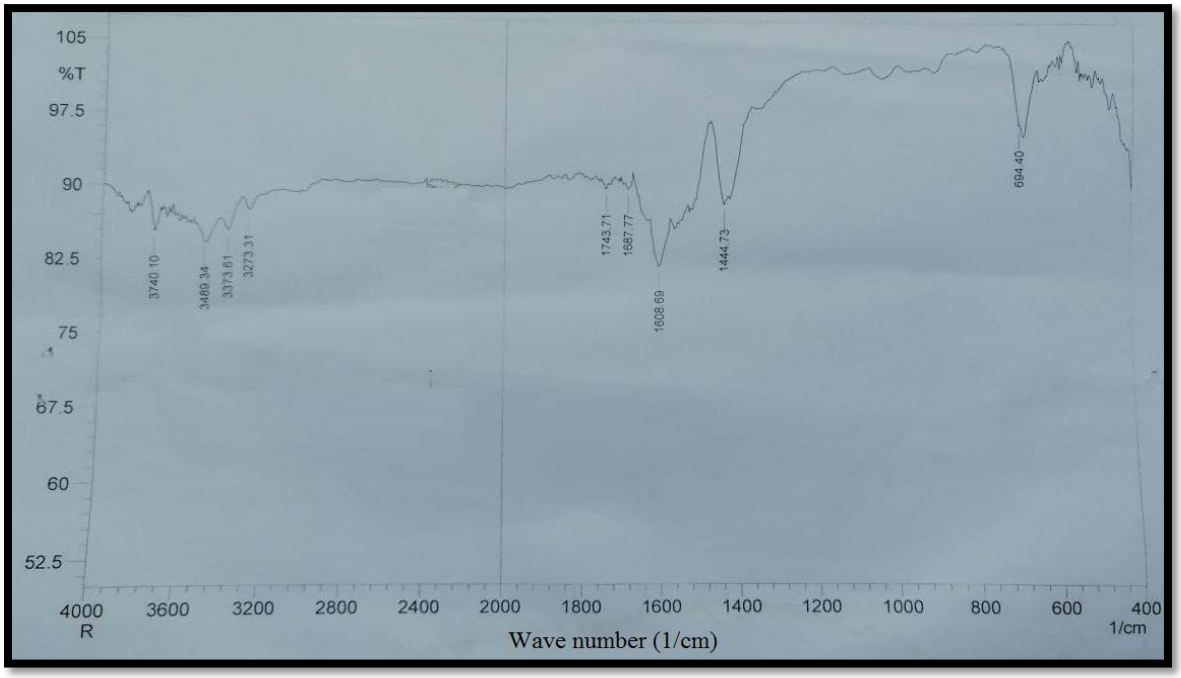

Figure (13-3):FT-IR Spectra for Tertiary Cu/ZnO/rGO Nanocomposite

3.5. Zeta Potential Analysis

The zeta potential of any particle in suspension, macromolecule, or material surface is a physical property. It may be used to improve suspension, emulsion, and protein solution formulations, anticipate improve layer and coat development by reducing contacts with substrates. Understanding the zeta potential might help you save time when creating trials formulations. It can also help with long-term stable forecasting. Determination of macromolecule charging, or more accurately protein charge, requires a very sensitive device, such as the new Zeta size, as well as a mechanism for reducing sample volume and avoiding degradation.

3.5.1. Zeta Potential Analysis of (ZnO, Cu, and GO) Nanoparticales

Figure (14-3) showing its zeta potential for ZnO NPs produced nanoparticles.Using the zeta sizer micro equipment, The analysis was done on liquid samples (Malvern). The incident laser beam induces the Brownian mobility of synthesized nanoparticles. The zeta potential displays both particle polydispersity and a high repulsive force [164]. The potential stabilization of a colloidal solution is indicated by the frequency of the zeta potential among both -50 and +50 mV. In a colloidal dispersion of ZnO NPs, aggregates can form. Aggregation is a mass of primary particles held together through strong chemical bonds, whereas agglomeration is a cluster of primary particles held together through weak van der Waals forces. The hydrodynamic size of the ZnO NPs demonstrated that they formed small aggregates when dispersed in water circumstances. The ZnO NPs' stability was determined to be -12.5 mV [165].

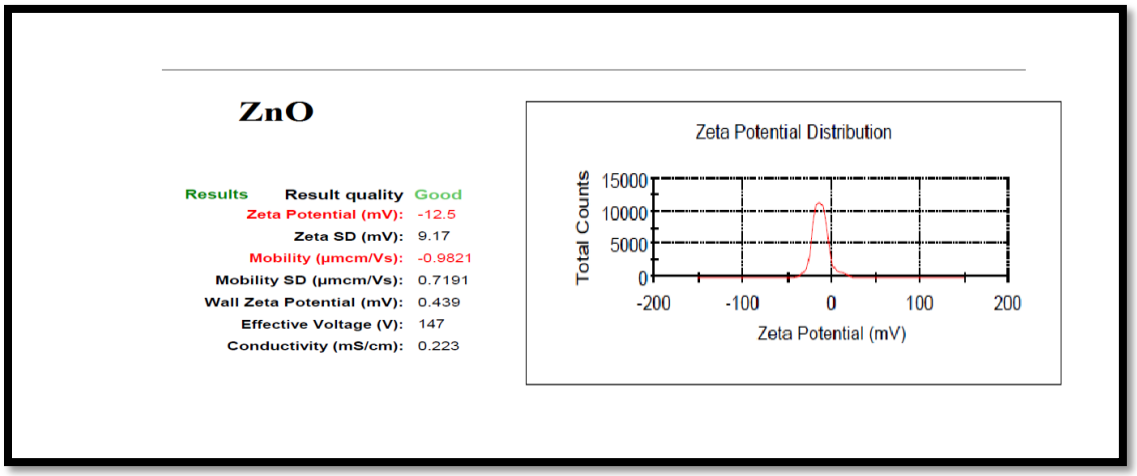

FIG. (14-3): Zeta Potential image for ZnO Nanoparticale

The results are shown in Figure (15-3), it is clear from the schematic diagram that the milling dissolves in water and the zeta potential value of the present copper nanoparticles is (2.77 mV) and to groups of carbohydrates and butene produced from the ginger plant during the biosynthesis of copper nanoparticles[166].

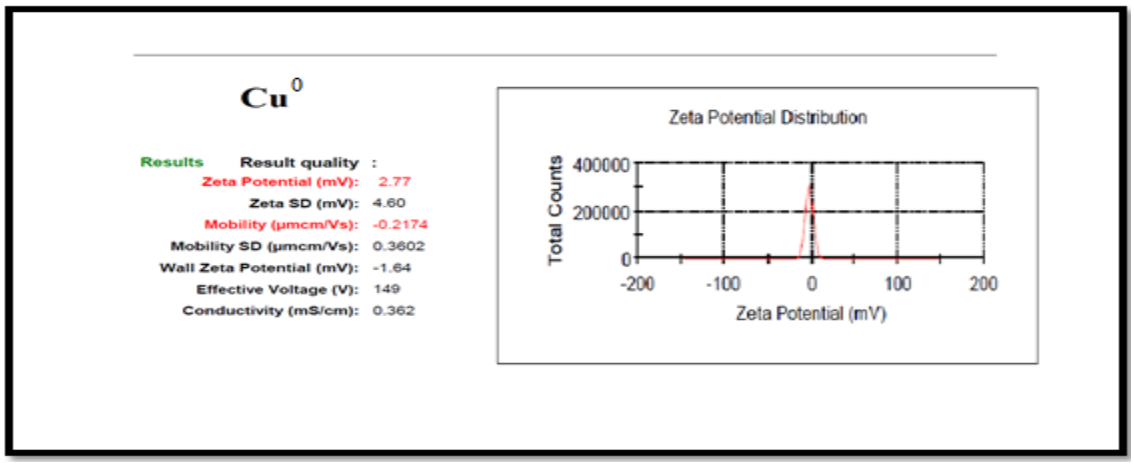

Figure (15-3): Zeta Potential spectra for Cu Nanoparticale

The spectra for GO (-15.4 mV) exhibit negatively charged nanoparticles, as illustrated in Figure (16-3) The stability of colloidal dispersions in water is related to these negative values [167].

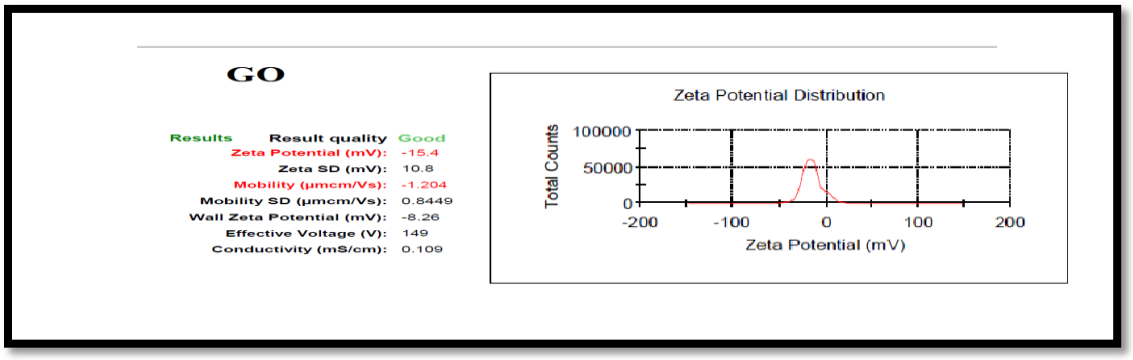

Figure (16-3): Zeta Potential spectra for GO Nanoparticale

3.5.2. Zeta Potential Analysis of binary (Cu/rGO, Cu/ZnO, and ZnO/rGO Nanocomposites)

Negative values of Zeta Potential for nanocomposite refer to the charge transfer and are connected to the stability of colloidal dispersions of NPs in double-distilled water. As a result, the stability of nanocomposite is determined by the composition of the nanocomposite matrix, which allows for charge transfer. Figure (17-3) shows the zeta potential values of samples distributed in double distilled water at room temperature. Cu/rGO (-19.7 mV) possessed negative charges, which can be seen in the sample [168].

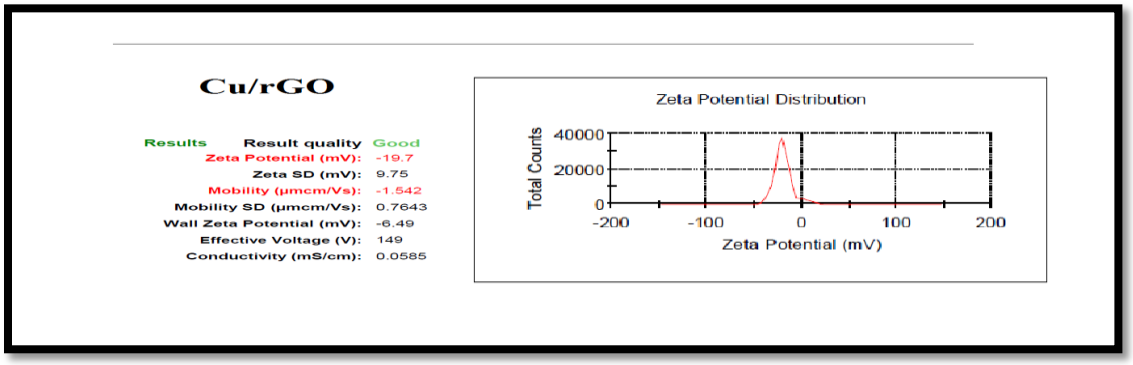

Figure (17-3): Zeta Potential spectra for binary Cu/rGO Nanocomposite

The investigation of zeta potential for Cu/ZnO binary nanocomposite is shown in Figure (18-3). Value of zeta potential increase with precence of containing oxygen group and addition of a divalent cations As Cu^{2+} .It is obvious from the diagram that milling dissolves in water. The measured zeta potential sample was found to have a value of (-16.8 mV) [169].

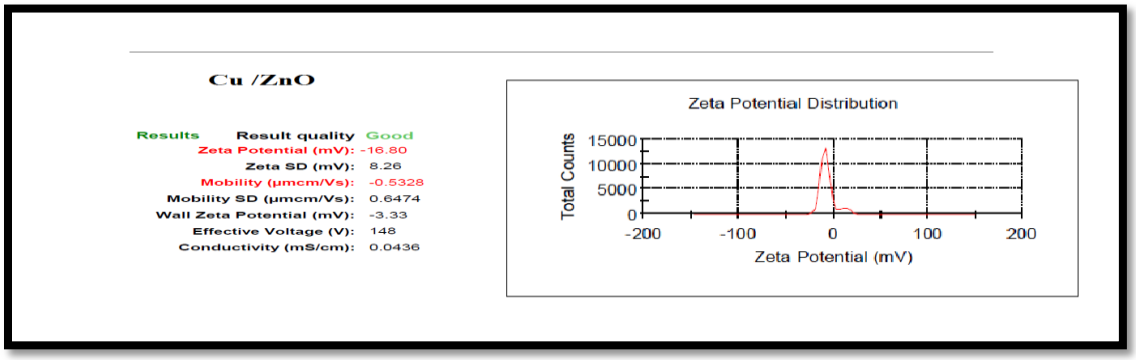

Figure (18-3): Zeta Potential spectra for binary Cu/ZnO Nanocomposite

The investigation of zeta potential for ZnO/rGO binary nanocomposite is shown in Figure (19-3). which indicates a high degree of stability in solution and more chances of aggregation, with a zeta potential (- 20.5 mV) the value of zeta will increase with found oxygen group and a divalent cations ,This is attributed to the effective electron collection and transportation characteristics of rGO [170].

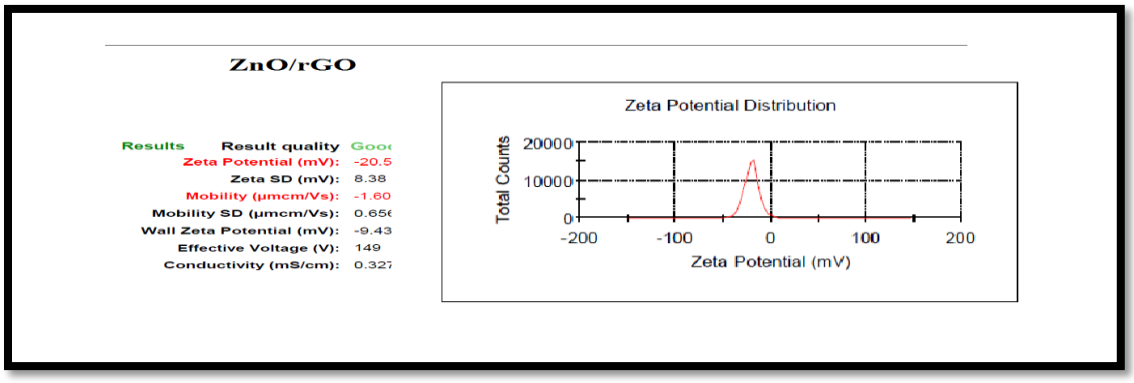

Figure (19-3): Zeta Potential spectra for binary ZnO/rGO Nanocomposite

3.5.3. Zeta Potential Analysis of Tertiary (Cu/ZnO /rGO) Nanocomposites

Zeta potential as a function of ionic strength. as expected, began to aggregate with increase in ionic strength with existence GO. Te addition of a divalent cations Cu^{2+} and Zn lead to stronger aggregation of the GO sheets and give the best zeta potential .A tertiary nanocomposite surface charge in Figure (20-3) demonstrated that the colloidal solution of produced nanocomposite was fairly stable, with a Zeta potentia of approximately (-27.4 mV). The stronger the colloidal stability of nanoscale materials, the higher the zeta potential (positive or negative) value [171] .

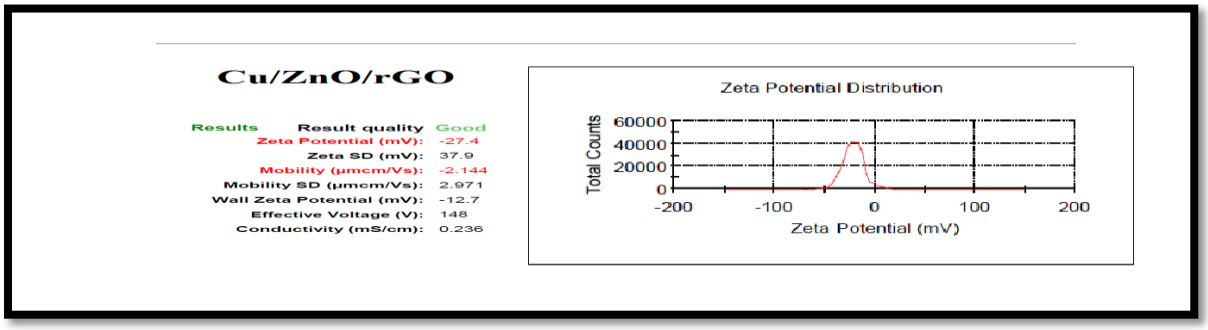

Figure(20-3): Zeta Potential image for Tertiary (Cu/ZnO/rGO) Nanocomposite

3.6. Brunauer–Emmett–Teller BET Surface Area

The surface area measurements for all synthesized nanomaterials table (4-3). shows (ZnO, Cu,GO, Cu/ZnO, ZnO/rGO, Cu/rGO, and Cu-ZnO/rGO) In comparison to other materials, the Cu/ZnO/rGO tertiary nanocomposite had a greater surface area, total pore volume, and the lowest pore size.

Table (4-3): Surface parameters of(Cu , ZnO , GO) Nanoparticales , binary (Cu/ZnO , Cu/rGO , ZnO/rGO) and Tertiary Cu/ZnO/rGO Nanocomposite

Sample	surface area BET [m2 g-1]	Total pore volume [cm3 g-1]	Mean pore diameter [nm]
Cu	10.282	0.028507	51.873
ZnO	11.071	0.019708	33.937
GO	18.898	0.069406	79.833
Cu/ZnO	26.847	0.12792	56.253
Cu/rGO	23.97	0.17413	68.724
ZnO/rGO	27.401	0.19597	58.232
Cu/ZnO/rGO	29.833	0.19406	22.566

3.7. Measuring of Band Gap Energy for Nanocomposite and Nanoparticle.

The band gap of the initial material NP and composite was calculated by using diffuse reflectance spectra as shown in Figure (21-3) and Figure (22-3) respectively indicating the reflectance spectra of Tertiary Nanocomposite in the wavelength (λ), the calculation of the band gap energy of the photo catalyst is given by blank equation [172]:

$$E_{bg} = h * C / \lambda \quad \text{……..} \quad \textbf{(3-1)}$$

$$E_{bg} = 1240 / \lambda \quad \text{…….} \quad \textbf{(3-2)}$$

Where λ is wavelength in nanometers (376,384, and 398 nm), the band gap energy of materiales that was measured by equation (3-1) equal to (3.29 ,3.22 , and 3.11 eV) for (ZnO ,Cu/ZnO ,ZnO/rGO) Consecutively .But at wavelength (411nm) Band gap energy of tertiary nanocomposite only that was measured by equation(3-2) equal to (3.01eV). This result indicates formation of new phase for tertiary Nanocomposite differe from intial Material.

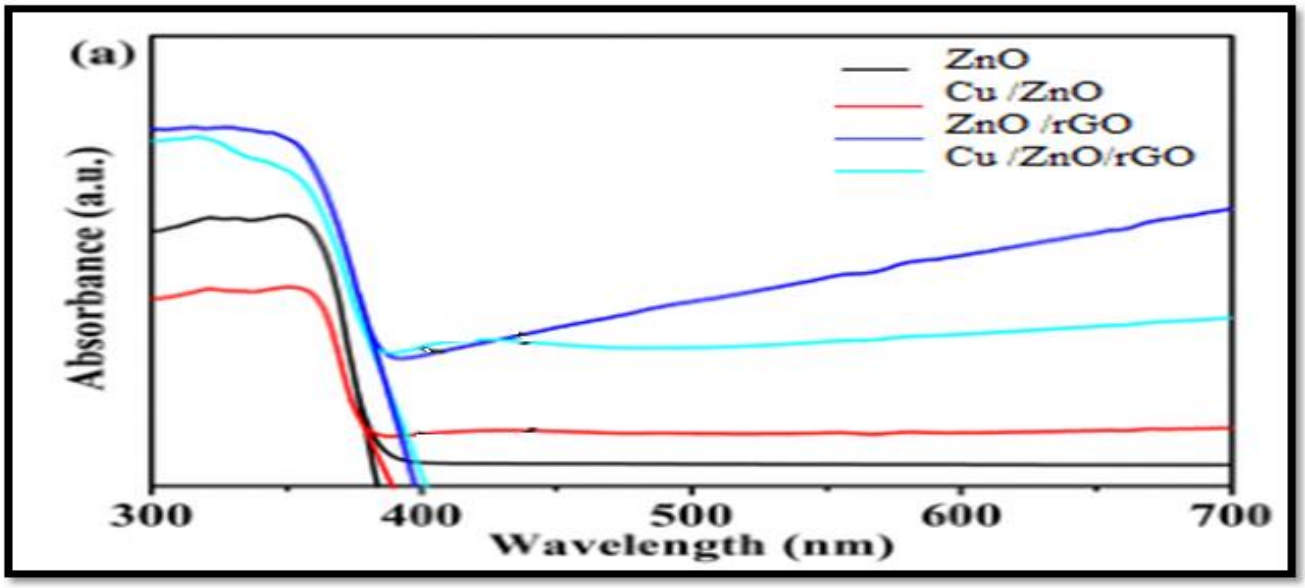

Figure (21-3):UV-Vis spectrum of nanomaterial

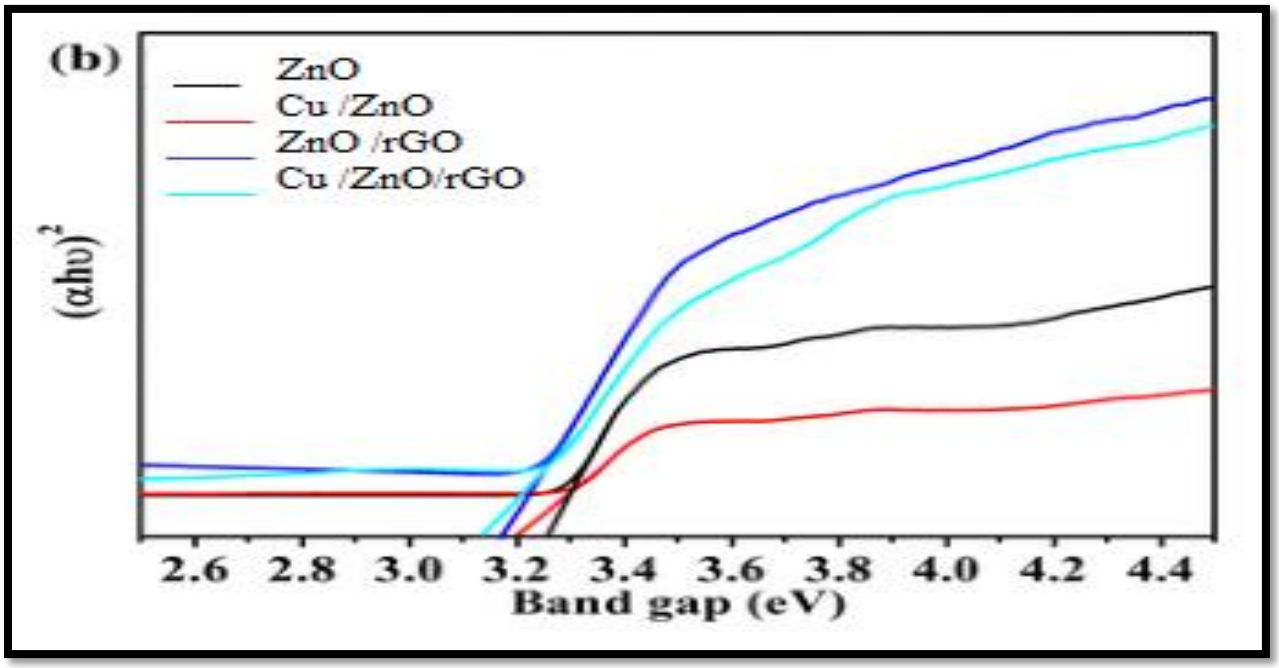

Figure (22-3): UV-Vis diffuse reflectance spectroscopy for nanomaterial

3.8 Antibacterial activity for Synthezied nanocomposite

The antibacterial activity of materials prepared was conducted using a circle diffusion approach. Cu/ZnO/rGO nano composites because of the high surface-to-volume relation and compact size, that allow them to contact closely with cell membranes, they have an antibacterial activity, and antimicrobial screening of Cu NPS has been considered in contrast to bacterial microorganisms such as E. coli and S. aureus. by Plate dispersion method [173]. By adding the mixed copper to the purified circuit and patiently administering it onto Mueller-Hinton agar plates, from the focal point of the plate to the plausible region, it is incubated for 24 hours at 37 °C. [174]. The restricted area were measured in millimeters, and the results was recorded. Boreholes were drilled using an antibacterial steel plug. 100 l of varying foci (0.25, 0.5, and 1.0 g/ml) of copper nanoparticles were put into each batch.

Chapter Three

Results and Discussion

4. Applications

4.1 Adsorption Activity of the Synthezied Nanomaterials

The adsorption capacity of the synthezied materials which include (Cu ,ZnO, GO, Cu-doped ZnO, Cu – doped rGO, ZnO - doped rGO and (Cu-ZnO/rGO) Naocomposite was explored by execution a few adsorption examinations of Rhodamine 6G color with these materials. As displayed in Table (4-1) and Figure (4-1) these outcomes it tends to be seen that, the best adsorption productivity was seen over Cu-ZnO/rGO in examination with different adsorbents under a similar adsorption conditions as (pH, color focus , weight of catalase ,temperature , and contact time) .This presumably emerges from high porosity of this tertiary composite in correlation with each of synthezied materials with its higher BET surface region in examination with different adsorbents that were utilized in this investigation The following equation was used to calculate dye removal efficiency:

Remaining percentage =A_t /A_o …….. (1-4)

Where the At, A0 is the final and the initial adsorption concentration of dye [175].

Table (1-4): Remaining percentage of Rhodamine 6G dye over prepared Nanomaterials

Time (min.)	Cu	ZnO	rGO	Cu/ZnO	Cu/rGO	ZnO/rGO	Cu/ZnO/rGO
	Remaining percentage $=A_t/A_O$						
0	1.0	1.0	1.0	1.0	1.0	1.0	1.0
15	0.8934	0.8883	0.8426	0.868	0.8477	0.893	0.852
30	0.8426	0.8375	0.7664	0.7512	0.7258	0.7411	0.736
45	0.7766	0.67	0.6142	0.67005	0.5989	0.5634	0.507
60	0.7411	0.5583	0.4365	0.5837	0.4771	0.3705	0.192

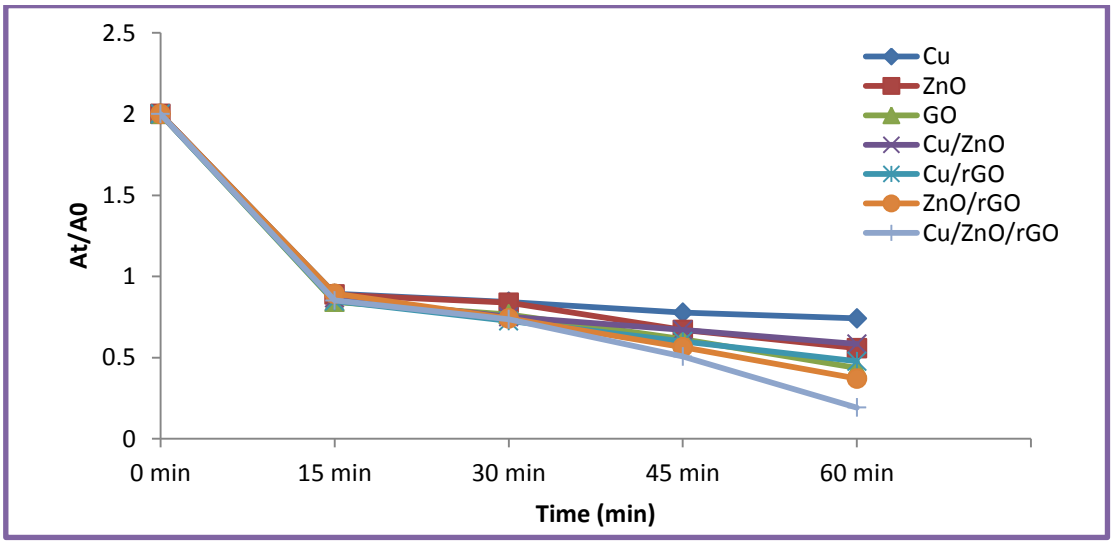

Figure (1-4 a): Remaining percentage of Rhodamine 6G dye over prepared Nanomaterials.

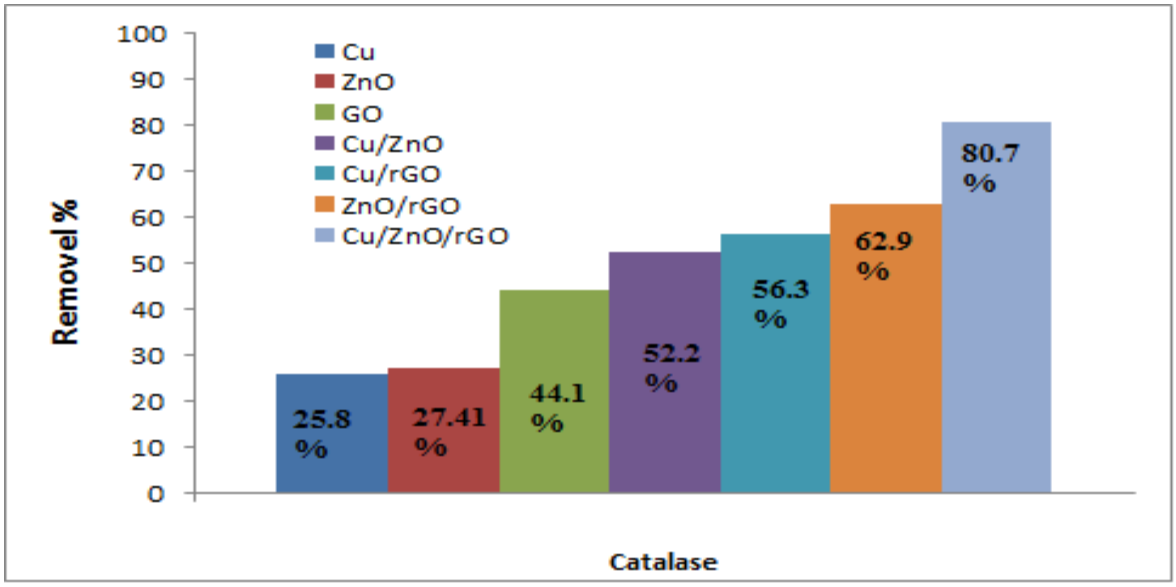

Figure (1-4 b): Removel percentage of Rhodamine 6G dye over prepared Nanomaterials.

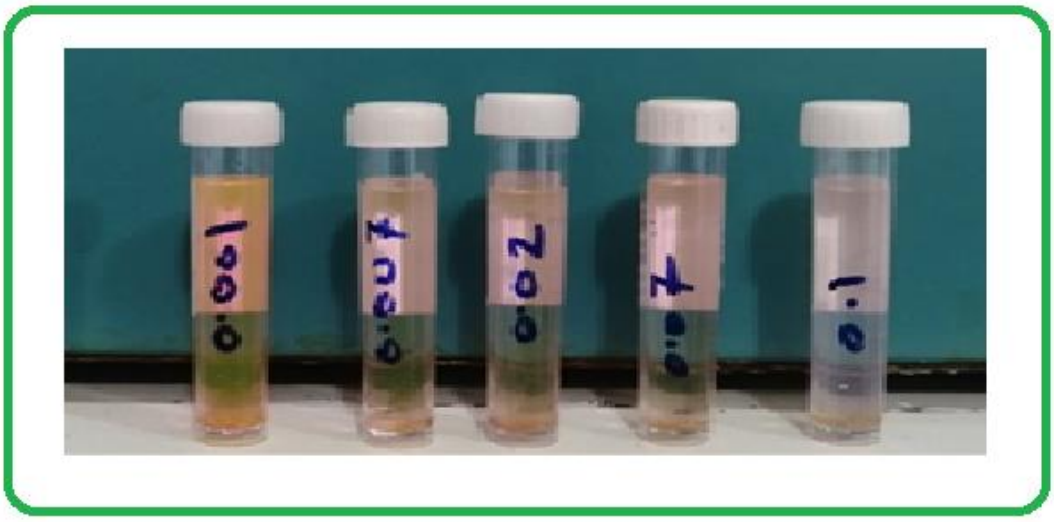

Figure (2-4): Remaining of Rhodamine 6G dye over Tertiary Nanocomposite after 60 min at different weight.

4.1.1. Catalyst Dosage Effects on Rhodamine 6G Dye Removal

The influence of catalyst dosage on the adsorbed of Rhodamine 6G pigment over the prepared catalysts was investigated using an experiment involving (0.001, 0.006, 0.02,0.07, and 0.1) g of Tertiary Nanocomposite Cu/ZnO/rGO, dye aqueous solution (10 mL, 10 ppm, at 30 OC), and continuous stirring under normal atmospheric conditions for 60 minutes. Table (2-4) and Figure (1-4) show the results of adsorption of Rhodamine 6G dye by this method (2-4). Increased catalyst dose, according to these findings, resulted in Dye removal efficiency has improved. Because an increase in adsorbent dose leads to a bigger surface area and, as a result, an increase in adsorption sites under the same adsorption conditions, this would result in the adsorption of more dye molecules on the catalyst surface [176].

Table (2-4): Remaining percentage of Rhodamine 6G dye over tertiary nanocomposite 0.1 g of Cu-ZnO / rGO at different Weight Dose

Time/min	0.1 gm	0.006 gm	0.02 gm	0.07 gm	0.001 gm
A_t/A_0					
0	1	1	1	1	1
15	0.852792	0.908629	0.93401	0.954315	0.969543
30	0.736041	0.741117	0.796954	0.827411	0.883249
45	0.507614	0.563452	0.639594	0.680203	0.791878
60	0.192893	0.446701	0.507614	0.57868	0.670051

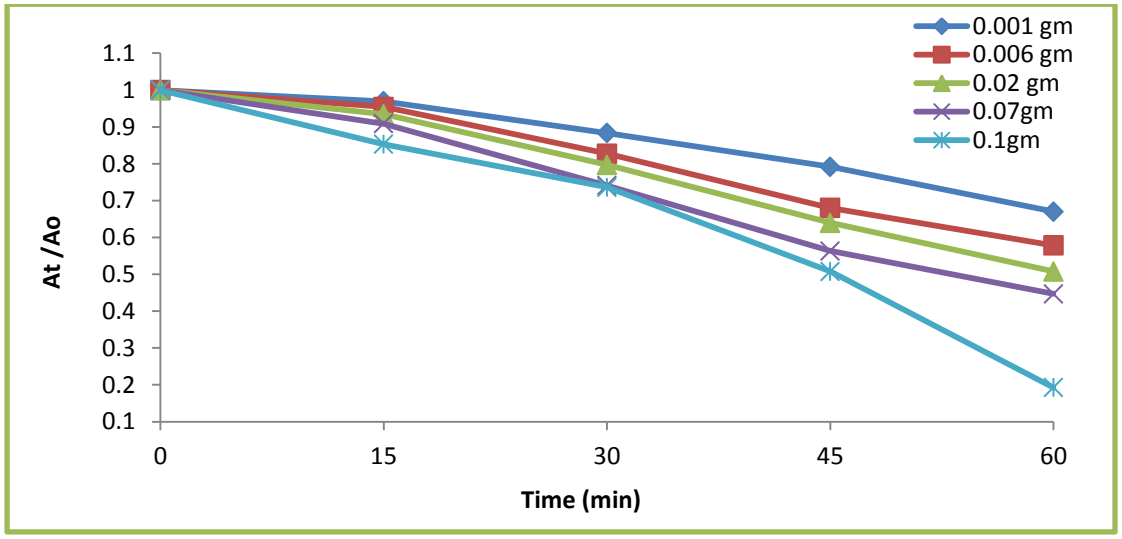

Figure (3-4): Effect of Weight of reaction mixture on efficiency adsorption of Rhodamine 6G dye on tertiary nanocomposite 0.1g Cu/ZnO/rGO.

4.1.2 . Effect of pH Solution on Rhodamine 6G Dye Removal from 0.1gm Cu-ZnO/rGO Tertiary Nanocomposite

A series of experiment were carried out to investigate effect of pH of reaction mixture pH on ability for Rhodamine 6G by dye adsorption removal over 0.1g of Cu-ZnO / rGO tertiary Nanocomposite. These tests were carried out with different pH dye solutions (3, 5, 7, 9, and 11). For each run, the same adsorption conditions were used. In each case, 0.1 g of catalyst was mixed with 10 mL of dye solution containing 10 ppm dyes for one hour at 25 C^{O}. The effects of pH on the reaction mixture are shown in Table (3-4) and Figure (3-4). According to these findings, the best clearance of Rhodamine 6G dye occurred at pH=9. The surface of the adsorbent becomes basic at pH values greater than pH=9, which can cause dye molecules to repel the adsorbent surface, reducing the efficacy of dye removal by adsorption. In contrast, in a too acidic environment

(pH=5), removal efficiency was lower than in a pH=9 environment, most likely due to competing adsorption of dye molecules with other negatively charged species such as chloride ions to the same adsorption sites at the surface [177].

Table (3-4): Remaining percentage of Rhodamine 6G dye over to tertiary nanocomposite 0.1 g Cu-ZnO / ZnO under different pH.

Time/min	pH=3	pH=5	pH=7	pH=9	pH=11
A_t/A_0					
0	1.00	1.00	1.00	1.00	1.00
15	0.86802	0.822335	0.781726	0.730964	0.84264
30	0.77665	0.659898	0.730964	0.690355	0.80203
45	0.664975	0.64467	0.685279	0.624365	0.736041
60	0.64467	0.604061	0.664975	0.548223	0.700508

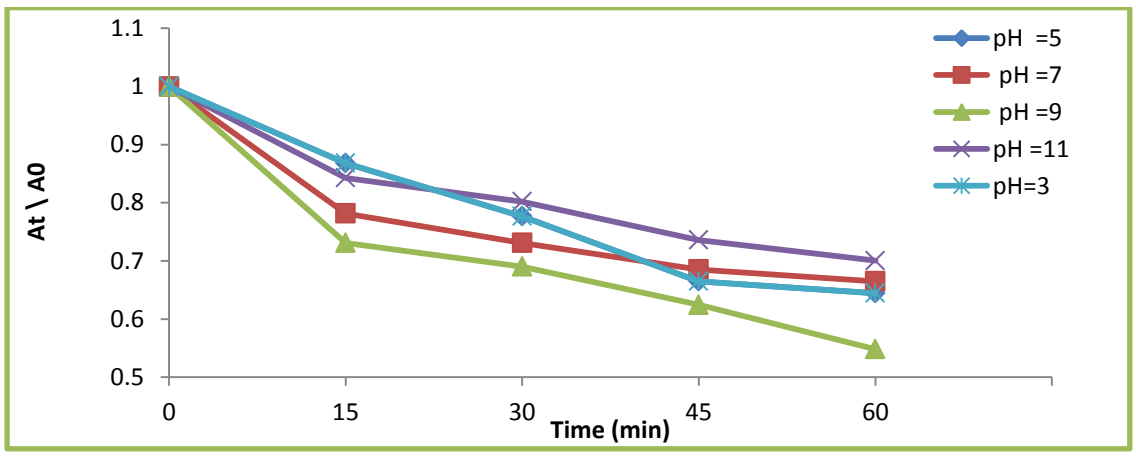

Figure (4-4): Effect of pH of reaction mixture on efficiency of adsorption of Rhodamine 6G dye over tertiary nanocomposite 0.1g Cu-ZnO/rGO.

4.1.3 Effect of Temperature on Adsorption Removal of adsorption of Rhodamine 6G dye over tertiary nanocomposite 0.1g Cu-ZnO/rGO

The effect of the temperature on Rhodamine 6G dye adsorption from an aqueous solution onto a tertiary nanocomposite 0.1g Cu-ZnO/rGO was investigated using studies carried out at temperature rang (15 – 30 °C). At same other experimental circumstances, pH dye solution was equal to (9) in room temp. for 1hour with dye concentration for 10 ppm and a catalyst weight of 0.1 g. Because the adsorption process is exothermic, an increase in temperature leads to an increase in the kinetic energy of the molecules, the adsorption of Rhodamine 6G decreases with increasing temperature, as shown that Figure (4-4) and inTable (4-4). adsorbed on adsorption surface, increasing the chances of them separating from the adsorption surface and returning to the solution. Furthermore, high temperatures influence the adsorbent's solubility, and if the solubility increases with temperature, the adsorption decreases [178].

Table (4-4): Remaining percentage of Rhodamine 6G dye over to tertiary composite 0.1 g Cu/ZnO / rGO under different temperature.

Time/min	15 °C	20 °C	25 °C	30 °C
		A_t/A_0		
0	1.00	1.00	1.00	1.00
15	0.979695	0.944162	0.918782	0.888325
30	0.944162	0.893401	0.807107	0.715736
45	0.908629	0.84264	0.695431	0.624365
60	0.832487	0.77665	0.57868	0.492386

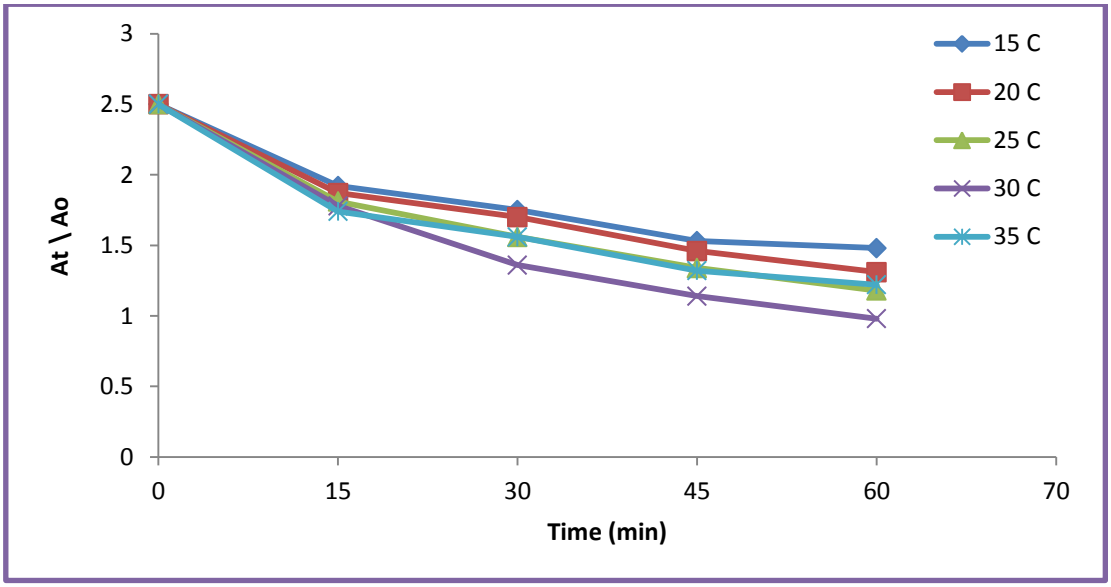

Figure (5-4): Effect of Temperature of reaction mixture on efficiency of adsorption of Rhodamine 6G dye over tertiary composite 0.1g Cu-ZnO/rGO.

4.1.4.Effect of Initial Dye Concentration of Rhodamine 6G for Adsorption efficiency Over Tertiary nanocomposite 0.1 g Cu/ZnO/rGO.

Several concentrations of Rhodamine 6G dye (3, 5, 7, 10, 12) ppm were used with the weight optimal (0.1) g of catalyst. Because particales of tertiary nanocomposite 0.1 g Cu/ZnO/rGO.contain efficient adsorption sites, the adsorption process increased when the starting concentration of Rhodamine 6G dye was increased. Table (5-4) and Figure (5-4) (5-4) Based on these findings, the best beginning dye concentration is (10 ppm). Because all of the ions present in the solution can interact with the nanocomposite's binding sites, the adsorption ratio emerges for Cu/ZnO/rGO at high low concentrations compared to high dye concentrations. The saturation of the adsorption sites causes higher dye

concentrations for the same nanocomposite and decreased adsorption yield [179].

Table (5-4): Remaining percentage of of Rhodamine 6G dye over tertiary composite 0.1g Cu-ZnO/rGO. under at different dye concentration.

Time/min	5 ppm	7 ppm	10 ppm	12 ppm
A_t/A_0				
0	1.00	1.00	1.00	1.00
15	0.42132	0.48731	0.791878	0.873604
30	0.380711	0.426396	0.629442	0.675635
45	0.258883	0.370558	0.497462	0.57868
60	0.243655	0.365482	0.187817	0.431472

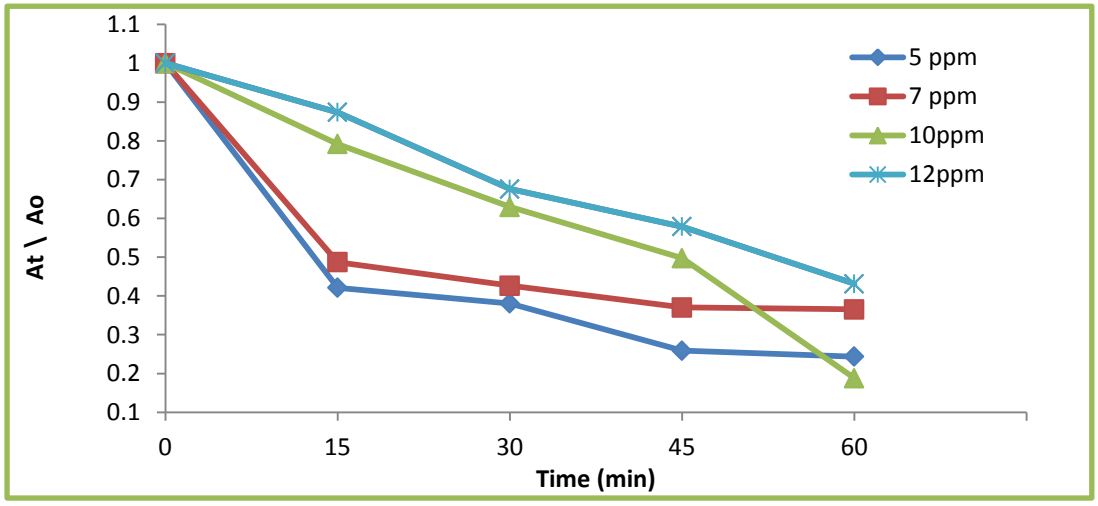

Figure (6-4): Effect of dye concentration of reaction mixture on efficiency of Rhodamine 6G dye over tertiary nanocomposite 0.1g Cu-ZnO/rGO.

4.2 Adsorption isotherms and kinetic models:

4.2.1. Adsorption Isotherms for Adsorption of Rhodamine 6G dye over tertiary composite 0.1g Cu-ZnO/rGO.

Freundlich and Langmuir adsorption model was used to examine adsorption isotherms for Rhodamine 6G dye adsorption over a tertiary composite of 0.1 g Cu-ZnO/rGO. Figures 1 and 2 show these isotherms (4-6 and 4-7). Table (7-4) lists the parameters of the two isotherms.

Table (6-4): Freundlich and Langmuir parameters for adsorption of Rhodamine 6G over 0.1 g Cu-ZnO/rGO.

Adsorption isotherm	parameters	Cu\ZnO\rGO
Freundlich	Kf	1.043758439
	n	1.0713
	R2	0.9961
Langmuir	Qm	6.802721088
	KL	0.1338554
	R2	0.9945

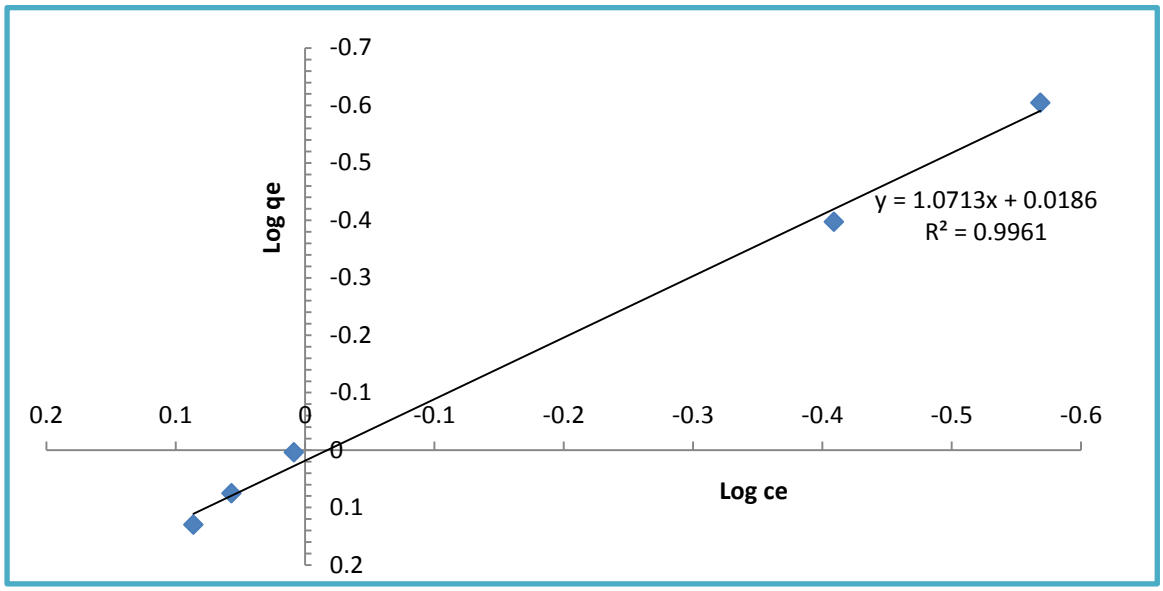

Figure (7-4): Freundlich adsorption isotherm for Rhodamine 6G dye over tertiary nanocomposite 0.1 g Cu-ZnO/rGO.

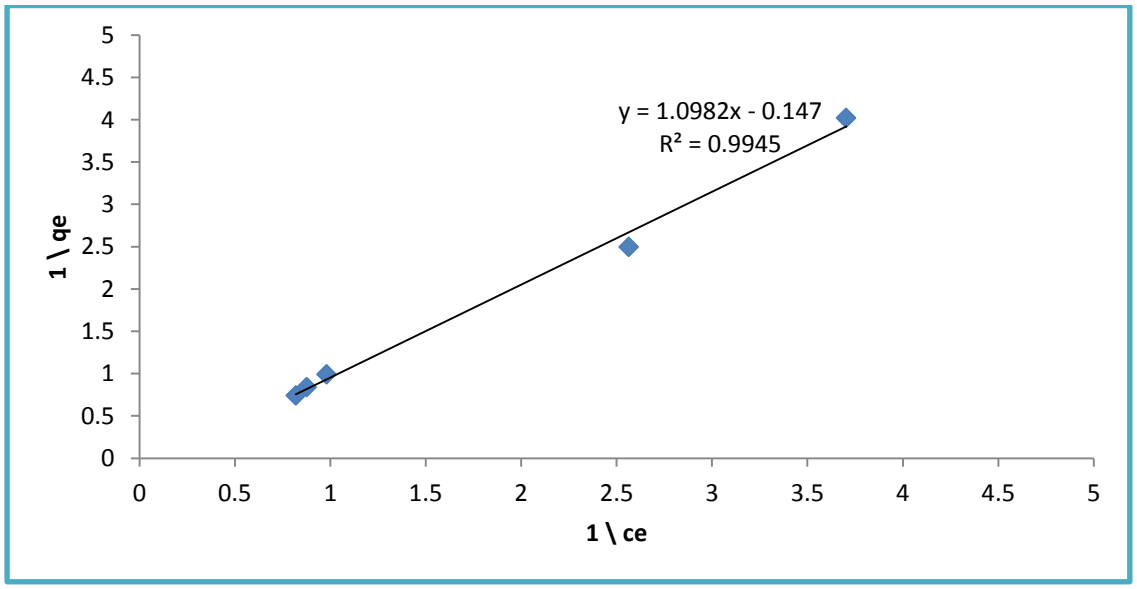

Figure (8-4): Langmuir adsorption isotherm for Rhodamine 6G dye over Tertiary nanocomposite 0.1 g Cu-ZnO/rGO.

Table 4-5 shows that the value of the correction factor (R^2) isotherm for Freundlich is larger than the value of the correlation factor R^2 for the Langmuir isotherm, indicating that the reaction follows the Freundlich

isotherm in this situation. The value of (n), which denotes the number of adsorption layers, has been changed (1.0713). This indicates that the adsorption took place in monolayers [180].

4.2.2.Kinetics of adsorption for Rhodamine 6G dye over Tertiary nanocomposite 0.1 g Cu-ZnO/rGO.

Adsorbents for obtaining information about kinetic parameters. kinetics model for (the pseudo first order) , (pseudo second order) was applying. Tables (4-5) and (4-6), Figure (4-5), and Table (4-6) show various rate constants calculated from slopes and intercepts, as well as correlation coefficients (4-6) Figure 4-6 shows a pseudo-second order plot with a higher correlation coefficient (R^2) and a computed adsorption capacity value that is closer to the empirically measured value (4-5). That means model (pseudo second order) more closely describes kinetic information [181]. The value of the rate constant (k) for adsorption reactions was calculated from the slope of plots between ln Ct/Co versus duration of adsorption reaction displayed in Figure (4-8), yielding 0.0027 min^{-1}[182].

Table (7-4) and Table (8-4): Adsorption parameters for the adsorption of Rhodamine 6G over tertiary nanocomposite 0.1 g Cu-ZnO/rGO at different adsorbent dose

Kinetic Model- pseudo 1st order				
Weight (gm)	**eq.exp (mg\g)**	**qe.cal. (mg\g)**	**K1 (min^{-1})**	**R^2**
0.001	51	137.3044	0.000972	0.8417
0.006	16.166	23.46711	0.0005	0.9292
0.02	6.35	11.16965	0.000663	0.8918
0.07	1.48	4.293061	0.001108	0.911
0.1	1.59	1.995511	0.000412	0.9303

Kinetic Model- pseudo 2st order				
Weight (gm)	**eq.exp (mg\g)**	**qe.cal. (mg\g)**	**K2 (g/mg.min)**	**R^2**
0.001	51	129.8701	0.000136	0.8141
0.006	16.166	44.84305	0.000403	0.7722
0.02	6.35	24.3309	0.000731	0.8565
0.07	1.48	4.264392	0.004329	0.723
0.1	1.59	8.143322	0.002134	0.9324

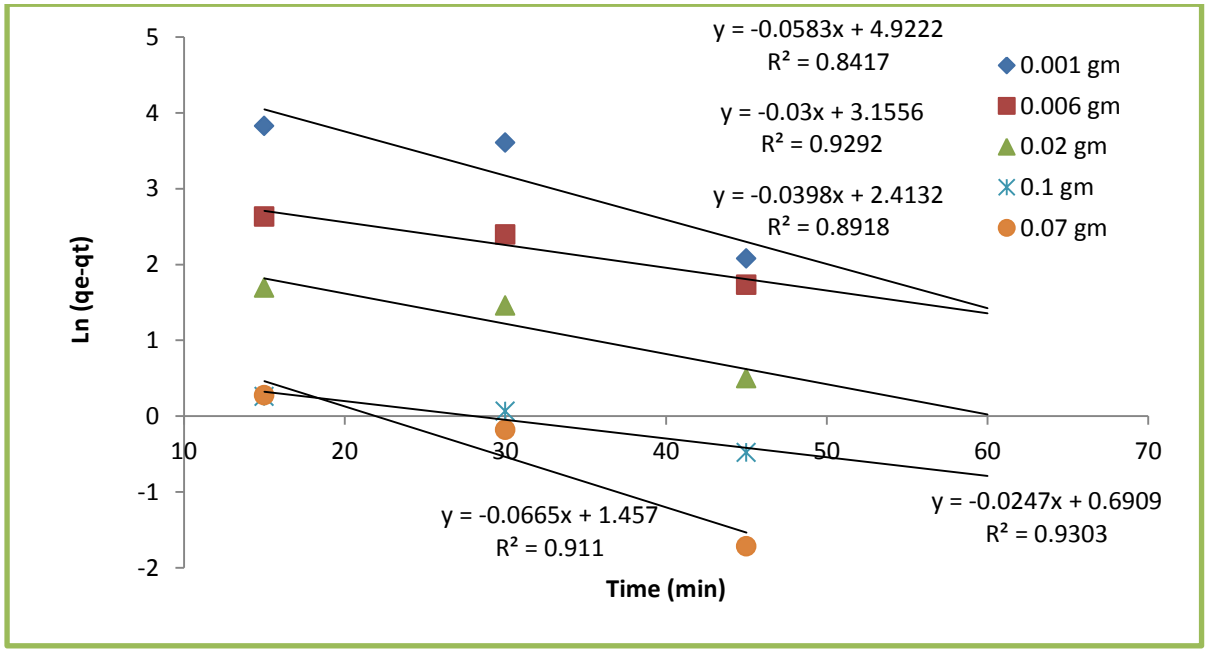

Figure (9-4): Plot of kinetic model for pseudo first order ,of adsorption for Rhodamine 6G over tertiary nanocomposite Cu-ZnO/rGO at conditions reaction, adsorbent dose (0.001-0.1 g), initial [Rhodamine 6G] 10 ppm, pH 9 and 30 °C.

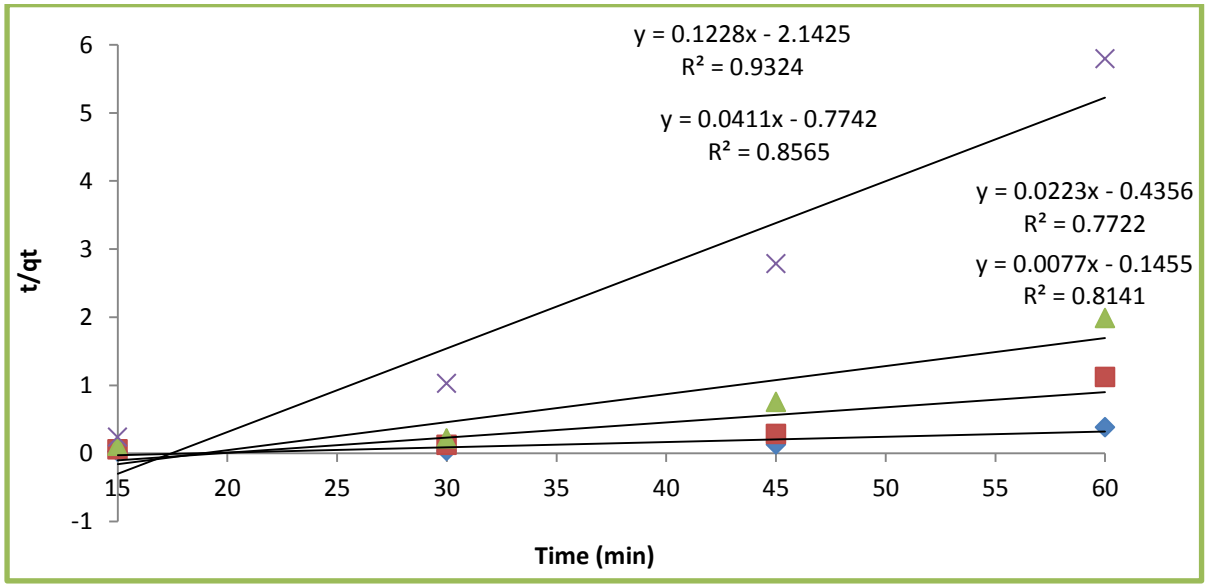

Figure (10-4): Plot of kinetic model for pseudo Second order,for adsorption for Rhodamine 6G over tertiary nanocomposite Cu-ZnO/rGO at conditions reaction, adsorbent dose (0.001- 0.1 g), initial [Rhodamine 6G] 10 ppm, pH 9 and 30 °C.

4.3. Antibacterial activity of the Synthezied Nanomaterials

Gram-positive and Gram-negative bacteria strains were gathered from Babylon Women and Children Hospital's laboratories, and the results revealed the influence of these materials' nanocomposites on (Gram-ve) bacteria that were present with E. coli, and (Gram+ve) bacteria ware represented by S. aurous. aureus is a kind of bacteria.To investigate how different Cu/rGO, ZnO/rGO, Cu/ZnO, and Cu/ZnO/rGO ratios affected (Gram-Ve) E. coli, as well as gram-positive S. aureus to learn more about the inhibitory mechanisms at work. each of (E. coli) and (S. aureus). treated with foure nanocomposites (1-10 mg) in aureus cultures and measured bacterial growth in an incubeter for 24 hours at 37 °C. In the MIC test for bacteria with these Cu/rGO, ZnO/rGO, Cu/ZnO, and Cu/ZnO/rGO nanomateriales in Table (7-4) and Figure (11-4) indicated the largest inhibition area for Escherichia coli (11 mm) and S. aureus (10.5 mm) using Cu/ZnO/rGO tertiary nanocomposite compared to synthetic nanocomposites becouseit have smaller partical size of these material then it can iner into bacteria and inhibition active protein these types bacteria.

Table (9-4): Inhibition zones (mm) of neat , Cu/ZnO, Cu/rGO , ZnO/rGO, and Cu-ZnO/rGO against S. aurous and E coli bacteria

Types of bacteria	Inhibition zone(mm)			
	Cu/ZnO (10mg/ml)	Cu/rGO (10mg/ml)	ZnO/rGO (10mg/ml)	Cu/ZnO/rGO (10mg/ml)
S. aureus	6.5 mm	5.8 mm	7.2 mm	9.6 mm
E. Coli	10 mm	8.4 mm	11 mm	13.2 mm

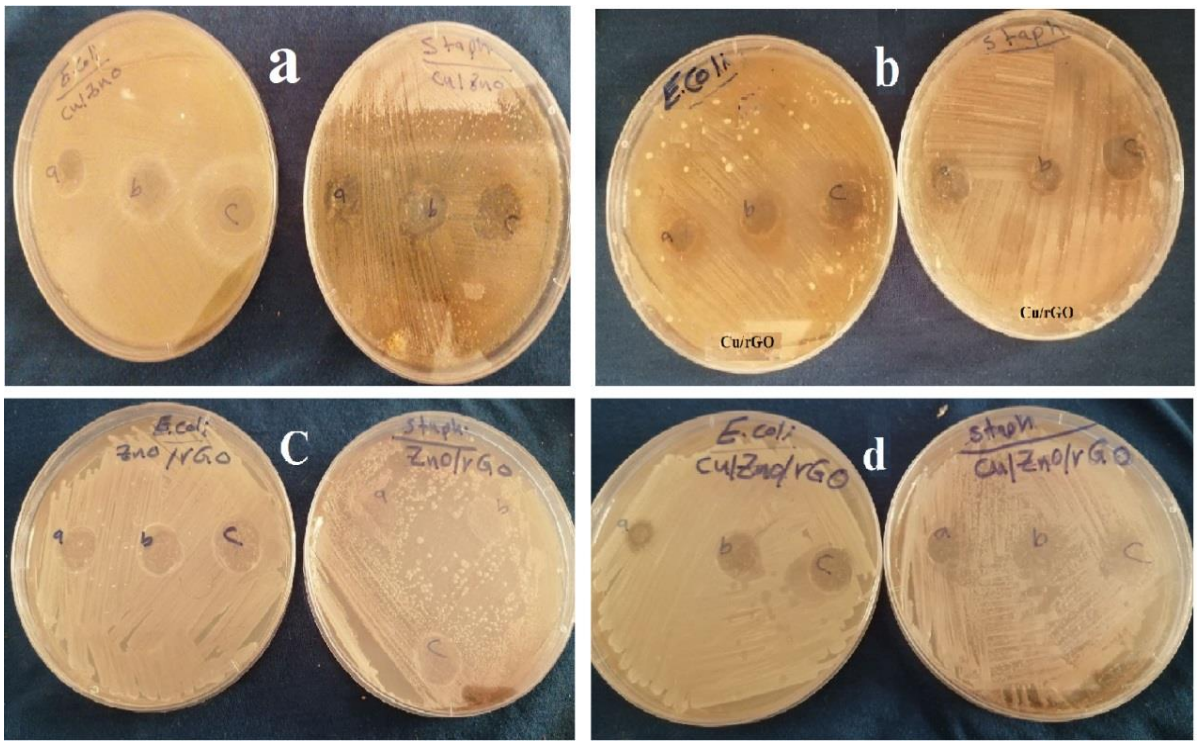

Figure (11-4): Inhibition zones (mm) of (a) Cu/ZnO ,(b) Cu/rGO,(c) ZnO/rGO and (d) Cu/ZnO/rGO against E. coli bacteria and S. aurous bacteria.

4.4. Conclusion.

1. In this work, Copper nanoparticles have been successfully synthesized by environmentally friendly method , ZnO and GO nanoparticles were successfully synthesized.
2. binary system Cu/ZnO, Cu/rGO , and ZnO/rGO and tertiary system Cu-ZnO/rGO of nanocomposite were successfully synthesized.
3. The best efficiency is 80.7 % adsorption process of Tertiary nanocomposite ability of (0.1 gm) to remove Rhodamine 6G dye at 30 °C.
4. The kinetics Model of the reaction was identified and it was found to be of the pseduo second order , according to Frandluich isotherm .
5. The action of bacteria was inhibited, and the nanocomposite show inhibition of the activity of (Gram-positive and Gram-negative bacteria) was able to kill colonies of them with a size of (13.2 mm) of E.Coli and (9.6 mm) S.aureus of the total colony size of bacteria in the dish compared with other nanoparticles.
6. According to adsorption isotherms for adsorption of (R 6G) dye over Cu/ZnO/rGO and the obtained result user fitted with Frandluich adsorption isotherm.
7. It is agree with pseduo second order K_2 (gm/mg.min).
8. It is with pseduo 1^{st} order in solution.

4.5 Recommendations to Future Studies

Many recommendations for future research initiatives can be utlined in this study:

1. Examination adsorption of Rhodamine 6G dye with another type of tertiary catalyst, comparing the results with the current study.
2. Examination adsorption of other dyes with the same type of Tertiary catalyst.
3. Study of the adsorption efficiency of the synthezied catalystes with the other dyes
4. Investigation use of these catalysts to improve adsorption processes and prevent the activity from these material against viruses and microbes.
5. Comparing and contrasting current synthesis methods and orientation towards the biosynthesis of some catalysts because it is an environmentally friendly way and at a lower cost.

References

References

[1] Chen, Guanying, Jangwon Seo, Chunhui Yang, and Paras N. Prasad. "Nanochemistry and nanomaterials for photovoltaics." *Chemical Society Reviews* 42, no. 21 (2013): 8304-8338.

[2] Prasad, Ram, Atanu Bhattacharyya, and Quang D. Nguyen. "Nanotechnology in sustainable agriculture: recent developments, challenges, and perspectives." *Frontiers in microbiology* 8 (2017): 1014.

[3] Duhan, Joginder Singh, Ravinder Kumar, Naresh Kumar, Pawan Kaur, Kiran Nehra, and Surekha Duhan. "Nanotechnology: The new perspective in precision agriculture." *Biotechnology Reports* 15 (2017): 11-23.

[4] Gaur, Parul. "Nanotechnology Applications in the Sectors of Renewable Energy Sources." *Smart Nanotechnology with Applications*. CRC Press, (2020) :71-85.

[5] Camargo, Pedro Henrique Cury, Kestur Gundappa Satyanarayana, and Fernando Wypych. "Nanocomposites: synthesis, structure, properties and new application opportunities." *Materials Research* 12, no. 1 (2009): 1-39.

[6] Duan, Ke, Yijun Li, Li Li, Yujin Hu, and Xuelin Wang. "Pillared graphene as excellent reinforcement for polymer-based nanocomposites." *Materials & Design* 147 (2018): 11-18.

[7] Modi, Ashish, Nikhil Koratkar, Eric Lass, Bingqing Wei, and Pulickel M. Ajayan. "Miniaturized gas ionization sensors using carbon nanotubes." *Nature 424*, no. 6945 (2003): 171-174.

[8] Pandya, Shivani, S. Jani, A. Chavan, A. K. Singh, S. Bhatt, *et al.* "Nanocomposites and IT'S application-review." *International Journal of Pharmaceutical Sciences and Research* 4, no. 1 (2013): 19-28.

[9] Zaleska-Medynska, Adriana, Martyna Marchelek, Magdalena Diak, and Ewelina Grabowska. "Noble metal-based bimetallic nanoparticles: the effect

of the structure on the optical, catalytic and photocatalytic properties." *Advances in colloid and interface science* 229 (2016): 80-107.

[10] Daniel, Marie-Christine, and Didier Astruc. "Gold nanoparticles: assembly, supramolecular chemistry, quantum-size-related properties, and applications toward biology, catalysis, and nanotechnology." *Chemical reviews* 104, no. 1 (2004): 293-346.

[11] Pandya, Shivani, S. Jani, A. Chavan, A. K. Singh, S. Bhatt, *et al* "Nanocomposites and IT'S application-review." *International Journal of Pharmaceutical Sciences and Research* 4, no. 1 (2013): 19-28.

[12] Paul, Donald R., and Lioyd M. Robeson. "Polymer nanotechnology: nanocomposites." *Polymer* 49.15 (2008): 3187-3204.

[13] Ozin, Geoffrey A. "Nanochemistry: synthesis in diminishing dimensions." *Advanced Materials* 4.10 (1992): 612-649.

[14] Gubin, S. P., G. Yu Yurkov, and I. D. Kosobudsky. "Nanomaterials based on metal-containing nanoparticles in polyethylene and other carbon-chain polymers." *International Journal of Materials and Product Technology* 23.1-2 (2005): 2-25.

[15] Tang, X. Z., P. Kumar, S. Alavi, and K. P. Sandeep. "Recent advances in biopolymers and biopolymer-based nanocomposites for food packaging materials." *Critical reviews in food science and nutrition* 52, no. 5 (2012): 426-442.

[16] Suchanek, Wojciech, and Masahiro Yoshimura. "Processing and properties of hydroxyapatite-based biomaterials for use as hard tissue replacement implants." *Journal of Materials Research* 13.1 (1998): 94-117.

[17] Iravani, Siavach, Hassan Korbekandi, Seyed Vahid Mirmohammadi, and Behzad Zolfaghari. "Synthesis of silver nanoparticles: chemical,

physical and biological methods." *Research in pharmaceutical sciences* 9, no. 6 (2014): 385.

[18] Kardani, A., and A. Montazeri. "Metal-matrix nanocomposites under compressive loading: Towards an understanding of how twinning formation can enhance their plastic deformation." *Scientific Reports* 10.1 (2020): 1-15..

[19] Camargo, Pedro Henrique Cury, Kestur Gundappa Satyanarayana, and Fernando Wypych. "Nanocomposites: synthesis, structure, properties and new application opportunities." *Materials Research* 12.1 (2009): 1-39.

[20] Rane, Ajay Vasudeo, Krishnan Kanny, V. K. Abitha, and Sabu Thomas. "Methods for synthesis of nanoparticles and fabrication of nanocomposites." In *Synthesis of inorganic nanomaterials*, pp. 121-139. Woodhead Publishing, 2018.

[21] Choa, Y-H., J-K. Yang, B-H. Kim, Y-K. *et al.* "Preparation and characterization of metal/ceramic nanoporous nanocomposite powders. " *Journal of Magnetism and Magnetic Materials* 266, no. 1-2 (2003): 12-19.

[22]Patel, Murlidhar. "Mechanical Behaviors of Ceramic Particulate Reinforced Aluminium Metal Matrix Composites–A Review." *Int. Res. J. Eng. Technol* 7.1 (2020): 201-204.

[23] Li, Xiaochun, Yong Yang, and Xudong Cheng. "Ultrasonic-assisted fabrication of metal matrix nanocomposites." *Journal of Materials Science* 39.9 (2004): 3211-3212.

[24] El-Eskandarany, M. Sherif. "Mechanical Milling: A Superior Nanotechnological Tool for Fabrication of Nanocrystalline and Nanocomposite Materials." *Nanomaterials* 11.10 (2021): 2484.

[25] Creighton, J. R., and P. Ho. "Introduction to chemical vapor deposition (CVD)." *Chemical vapor deposition* 2 (2001): 1-22.

References

[27] Joseph, M. C., C. Tsotsos, M. A. Baker, P. J. Kench, *et al.* "Characterisation and tribological evaluation of nitrogen-containing molybdenum–copper PVD metallic nanocomposite films." *Surface and Coatings Technology* 190, no. 2-3 (2005): 345-356.

[28] Rane, Ajay Vasudeo. "Methods for synthesis of nanoparticles and fabrication of nanocomposites." *Synthesis of inorganic nanomaterials.* Woodhead Publishing, (2018). 121-139.

[29] Scallan, Elaine, Robert M. Hoekstra, Frederick J. Angulo, Robert V. Tauxe, *et al.* "Foodborne illness acquired in the United States—major pathogens." *Emerging infectious diseases* 17, no. 3 (2011): 7.

[30] Nakahira, Atsushi, and Koichi Niihara. "Sintering behaviors and consolidation process for Al2O3/SiC nanocomposites." *Journal of the Ceramic Society of Japan* 100.1160 (1992): 448-453.

[31] Sternitzke and Martin. "Structural ceramic nanocomposites." *Journal of the European Ceramic Society* 17.9 (1997): 1061-1082.

[32] Verdejo, Raquel. "Graphene filled polymer nanocomposites." *Journal of Materials Chemistry* 21.10 (2011): 3301-3310.

[33] Utracki, Leszek A. "Clay-containing polymeric nanocomposites and their properties." *IEEE Electrical Insulation Magazine* 26.4 (2010): 8-15.

[34] Ray, Suprakas Sinha. "Recent Trends and Future Outlooks in the Field of Clay-Containing Polymer Nanocomposites." *Macromolecular Chemistry and Physics* 215.12 (2014): 1162-1179.

[35] Alexandre, Michael, and Philippe Dubois. "Polymer-layered silicate nanocomposites: preparation, properties and uses of a new class of materials." *Materials science and engineering*: R: Reports 28.1-2 (2000): 1-63.

References

[36] Carrado, Kathleen A., and Langqiu Xu. "In situ synthesis of polymer−clay nanocomposites from silicate gels." *Chemistry of materials* 10.5 (1998): 1440-1445.

[37] Ver Avadhani, Chilukuri, Yoshiki Chujo, Koji Kuraoka, and Tetsuo Yazawa. "Polyamide-silica gel hybrids containing metal salts: Preparation via the sol-gel reaction." *Polymer bulletin* 38, no. 5 (1997): 501-508.

[38] Tyulenev, M., S. Zhironkin, and O. Litvin. "The low-cost technology of quarry water purifying using the artificial filters of overburden rock." *Pollution Research* 34.4 (2015): 825-830.

[39] Stone, Vicki, Bernd Nowack, Anders Baun, Nico van den Brink, Frank von der Kammer, *et al.* "Nanomaterials for environmental studies: classification, reference material issues, and strategies for physico-chemical characterisation." *Science of the total environment* 408, no. 7 (2010): 1745-1754.

[40] Sathiyapriya, R., V. Hariharan, K. Prabakaran, M. Durairaj, and V. Aroulmoji. "Nanotechnology in Materials and Medical Sciences." *International journal of advanced Science and Engineering* (2019).

[41] Abdin, Zainul, Mohammad A. Alim, Rahman Saidur, Monirul R. Islam, *et al*. "Solar energy harvesting with the application of nanotechnology." *Renewable and sustainable energy reviews* 26 (2013): 837-852.

[42] Koç, Pınar, and Ahmet Gülmez. "Analysis of relationships between nanotechnology applications, mineral saving and ecological footprint: Evidence from panel fourier cointegration and causality tests." *Resources Policy* 74 (2021): 102373.

References

[43] Peng, Zan, Xiaojuan Liu, Wei Zhang, Zhuotong Zeng, *et al.* "Advances in the application, toxicity and degradation of carbon nanomaterials in environment: A review." *Environment international* 134 (2020): 105298.

[44] Paul, Sanjib K., Himjyoti Dutta, Laxmi Narayan Sethi, and Sujit Kumar Ghosh. "Nanosized Zinc Oxide: Super-functionalities, present scenario of application, safety issues, and future prospects in food processing and allied industries." *Food Reviews International* 35, no. 6 (2019): 505-535.

[45] Kołodziejczak-Radzimska, Agnieszka, and Teofil Jesionowski. "Zinc oxide—from synthesis to application: a review." *Materials* 7.4 (2014): 2833-2881.

[46] Padmavathy, Nagarajan, and Rajagopalan Vijayaraghavan. "Enhanced bioactivity of ZnO nanoparticles—an antimicrobial study." *Science and technology of advanced materials* (2008)..

[47] Malhotra, Satinder Pal Kaur, and T. K. Mandal. "Zinc oxide nanostructure and its application as agricultural and industrial material." Contaminants in *Agriculture and Environment*: Health Risks and Remediation 1 (2019): 216.

[48] Qin, Xuesi, *et al.* "Effect of oxidation condition on growth of N: ZnO prepared by oxidizing sputtering Zn-N film." *Nanoscale research letters* 11.1 (2016): 1-8.

[49] Zak, A. Khorsand, WH Abd Majid, M. Ebrahimizadeh Abrishami, and Ramin Yousefi. "X-ray analysis of ZnO nanoparticles by Williamson–Hall and size–strain plot methods." *Solid State Sciences* 13, no. 1 (2011): 251-256.

[50] Mohan, Ananthu C., and B. Renjanadevi. "Preparation of zinc oxide nanoparticles and its characterization using scanning electron microscopy

(SEM) and X-ray diffraction (XRD)." *Procedia Technology* 24 (2016): 761-766.

[51] Huang, Feng, Zhang Lin, Wenwen Lin, Jiye Zhang, Kai Ding, Yonghao Wang, Qinghong Zheng et al. "Research progress in ZnO single-crystal: growth, scientific understanding, and device applications." *Chinese Science Bulletin* 59, no. 12 (2014): 1235-1250.

[52] Moon, Wei Chek. "A review on interesting properties of chicken feather as low-cost adsorbent." *International Journal of Integrated Engineering* 11.2 (2019).

[53] Sharma, Rahul, and Parveen Saini. "Graphene-based composites and hybrids for water purification applications." *Diamond and Carbon Composites and Nanocomposites*. IntechOpen, 2016.

[54] Wang, Jianlong, and Xuan Guo. "Adsorption isotherm models: Classification, physical meaning, application and solving method." *Chemosphere* 258 (2020): 127279.

[55] Tennakone, K., A. R. Kumarasinghe, and P. M. Sirimanne. "Dye sensitization of low-bandgap semiconductor electrodes: cuprous oxide photocathode sensitized with methyl violet." *Semiconductor science and technology* 8.8 (1993): 1557.

[56] Chatti, Ravikrishna, Sadhana S. Rayalu, Nidhi Dubey, Nitin Labhsetwar, and Sukumar Devotta. "Solar-based photoreduction of methyl orange using zeolite supported photocatalytic materials." *Solar energy materials and solar cells* 91, no. 2-3 (2007): 180-190.

[57] Belghiti, N., M. Bennani, M. Hamidi, S. M. Bouzzine, and M. O. H. "New compounds based on anthracene as a good candidate for organic dye-sensitized solar cells: Theoretical investigations." *African Journal of Pure and Applied Chemistry* 6, no. 14 (2012): 164-172.

References

[58] O'Neill, Cliona, Freda R. Hawkes, Dennis L. Hawkes, Nidia D. Lourenço, *et al.* "Colour in textile effluents–sources, measurement, discharge consents and simulation: a review." *Journal of Chemical Technology & Biotechnology*: International Research in Process, Environmental & Clean Technology 74, no. 11 (1999): 1009-1018.

[59] Barzan, M., and F. Hajiesmaeilbaigi. "Investigation the concentration effect on the absorption and fluorescence properties of Rhodamine 6G dye." *Optik* 159 (2018): 157-161.

[60] Zehentbauer, Florian M., Claudia Moretto, Ryan Stephen, Thangavel Thevar, John R. Gilchrist, *et al.* "Fluorescence spectroscopy of Rhodamine 6G: Concentration and solvent effects." Spectrochimica Acta Part A: *Molecular and Biomolecular Spectroscopy* 121 (2014): 147-151.

[61] Kutushov, M., and O. Gorelik. "Low concentrations of Rhodamine-6G selectively destroy tumor cells and improve survival of melanoma transplanted mice." *Neoplasma* 60, no. 3 (2013): 262-273.

[62] Sabir, Sidra, Muhammad Arshad, and Sunbal Khalil Chaudhari. "Zinc oxide nanoparticles for revolutionizing agriculture: synthesis and applications." *The Scientific World Journal* 2014 (2014).

[63] Özgür, and Ümit, "A comprehensive review of ZnO materials and devices." *Journal of applied physics* 98.4 (2005): 11.

[64] Wu, Qingzhi. "Amino acid-assisted synthesis of ZnO hierarchical architectures and their novel photocatalytic activities." *Crystal Growth and Design* 8.8 (2008): 3010-3018.

[65] Tian, Jianjun, Qifeng Zhang, Lili Zhang, Rui Gao, Laifa Shen, Shengen Zhang, Xuanhui Qu, and Guozhong Cao. "ZnO/TiO_2 nanocable structured photoelectrodes for CdS/CdSe quantum dot co-sensitized solar cells." *Nanoscale* 5, no. 3 (2013): 936-943.

References

[66] Talam, Satyanarayana, Srinivasa Rao Karumuri, and Nagarjuna Gunnam. "Synthesis, characterization, and spectroscopic properties of ZnO nanoparticles." *International Scholarly Research Notices* 2012 (2012).

[67] Rajendra, Radhai, C. Balakumar, Hasabo A. Mohammed Ahammed, S. Jayakumar, and E. Rajesh. "Use of zinc oxide nano particles for production of antimicrobial textiles." *International Journal of Engineering, Science and Technology* 2, no. 1 (2010): 202-208.

[68] Kumar, KH Sudheer, N. Dhananjaya, and LS Reddy Yadav. "E. tirucalli plant latex mediated green combustion synthesis of ZnO nanoparticles: Structure, photoluminescence and photo-catalytic activities." *Journal of Science: Advanced Materials and Devices* 3.3 (2018): 303-309.

[69] Madathil, Aneesh N. Pacheri, K. A. Vanaja, and M. K. Jayaraj. "Synthesis of ZnO nanoparticles by hydrothermal method." *International Society for Optics and Photonics*. 6639, (2007):66390.

[70] Novoselov, and Konstantin S. "A roadmap for graphene." *nature* 490.7419 (2012): 192-200.

[71] Weiss, Nathan O., Hailong Zhou, Lei Liao, Yuan Liu, Shan Jiang, *et al.* "Graphene: An Emerging Electronic Material (Adv. Mater. 43/2012)." *Advanced Materials* 24, no. 43 (2012): 5776-5776.

[72] Huang, Cancan, Chun Li, and Gaoquan Shi. "Graphene based catalysts." *Energy & Environmental Science* 5.10 (2012): 8848-8868.

[73] Liu, Yuxin, Xiaochen Dong, and Peng Chen. "Biological and chemical sensors based on graphene materials." *Chemical Society Reviews* 41.6 (2012): 2283-2307.

References

[74] Sun, Yiqing, Qiong Wu, and Gaoquan Shi. "Graphene based new energy materials." *Energy & Environmental Science* 4.4 (2011): 1113-1132.

[75] Wassei, Jonathan K., and Richard B. Kaner. "Oh, the places you'll go with graphene." *Accounts of chemical research* 46.10 (2013): 2244-2253.

[76] Aggarwal, Nupur, *et al.* "Investigation of room temperature ferromagnetic behaviour in dilute magnetic oxides." *Integrated Ferroelectrics* 186.1 (2018): 10-16.

[77] Nomura, Kenji, Hiromichi Ohta, Kazushige Ueda, Toshio Kamiya, Masahiro Hirano, and Hideo Hosono. "Thin-film transistor fabricated in single-crystalline transparent oxide semiconductor." *Science* 300, no. 5623 (2003): 1269-1272.

[78] Osmond, Megan J., and Maxine J. Mccall. "Zinc oxide nanoparticles in modern sunscreens: an analysis of potential exposure and hazard." *Nanotoxicology* 4.1 (2010): 15-41.

[80] Gawande, Manoj B., Anandarup Goswami, François-Xavier Felpin, and Tewodros Asefa, "Cu and Cu-based nanoparticles: synthesis and applications in catalysis." *Chemical reviews* 116, no. 6 (2016): 3722-3811.

[81] Bramhanwade and Kavita, "Fungicidal activity of Cu nanoparticles against Fusarium causing crop diseases." *Environmental chemistry letters* 14.2 (2016): 229-235.

[82] Selvam, Kandasamy, Chinnappan Sudhakar, Thangasamy Selvankumar, *et al*. "Biomimetic synthesis of copper nanoparticles using rhizome extract of Corallocarbus epigaeus and their bactericidal with photocatalytic activity." *SN Applied Sciences* 2, no. 6 (2020): 1-7.

[83] Tadyszak, Krzysztof, Jacek K. Wychowaniec, and Jagoda Litowczenko. "Biomedical applications of graphene-based structures." *Nanomaterials* 8.11 (2018): 944.

References

[84] Yang, Zhoufei, Jiarui Tian, Zefang Yin, Chaojie Cui, Weizhong ,*et al.* "Carbon nanotube-and graphene-based nanomaterials and applications in high-voltage supercapacitor: a review." *Carbon* 141 (2019): 467-480.

[85] Craciun, Monica Felicia, Sven Rogge, M-JL den Boer, Serena Margadonna, *et al.* "Electronic Transport through Electron-Doped Metal Phthalocyanine Materials." *Advanced Materials* 18, no. 3 (2006): 320-324.

[86] Zhou, Yong, Qiaoliang Bao, Lena Ai Ling Tang, Yulin Zhong, and Kian Ping Loh. "Hydrothermal dehydration for the ―green‖ reduction of exfoliated graphene oxide to graphene and demonstration of tunable optical limiting properties." *Chemistry of Materials* 21, no. 13 (2009): 2950-2956.

[87] Zhang, Yiteng, Gennady P. Berman, and Sabre Kais. "The radical pair mechanism and the avian chemical compass: Quantum coherence and entanglement." *International Journal of Quantum Chemistry* 115.19 (2015): 1327-1341.

[88] Look, David C. "Recent advances in ZnO materials and devices." *Materials Science and Engineering*: B 80.1-3 (2001): 383-387.

[89] Uhm, Young Rang, Byung Sun Han, Chang Kyu Rhee, and Sun Ju Choi. "Photocatalytic characterization of Fe-and Cu-doped ZnO nanorods synthesized by cohydrolysis." *Journal of Nanomaterials* 2013 (2013).

[90] Shukla, R. K., Anchal Srivastava, Nishant Kumar, Akhilesh Pandey, and Mamta Pandey. "Optical and Sensing Properties of Cu Doped ZnO Nanocrystalline Thin Films." *Journal of Nanotechnology* (2015).

[91] Alinezhad, Heshmatollah, and Sahar Mohseni Tavakkoli. "Efficient and convenient synthesis of 1, 8-dioxodecahydroacridine derivatives using Cu-doped ZnO nanocrystalline powder as a catalyst under solvent-free conditions." *The Scientific World Journal 2013* (2013).

References

[92] Tan, Ping, Jian Sun, Yongyou Hu, Zheng Fang, Qi Bi, Yuancai Chen, and Jianhua Cheng. "Adsorption of $Cu^{2+,}$ Cd^{2+} and Ni^{2+} from aqueous single metal solutions on graphene oxide membranes." *Journal of hazardous materials* 297 (2015): 251-260.

[93] Zhang, Yu, Sui Zhang, Jie Gao, and Tai-Shung Chung. "Layer-by-layer construction of graphene oxide (GO) framework composite membranes for highly efficient heavy metal removal." *Journal of membrane science* 515 (2016): 230-237.

[94] Durmus, Zehra, Belma Zengin Kurt, and Ali Durmus. "Synthesis and characterization of graphene oxide/zinc oxide (GO/ZnO) nanocomposite and its utilization for photocatalytic degradation of basic fuchsin dye." ChemistrySelect 4.1 (2019): 271-278.

[95] Qin, Jiaqian, Xinyu Zhang, Chengwu Yang, Meng Cao, Mingzhen Ma, and Riping Liu. "ZnO microspheres-reduced graphene oxide nanocomposite for photocatalytic degradation of methylene blue dye." *Applied Surface Science* 392 (2017): 196-203.

[96] Kuntal, Dheeraj, Swati Chaudhary, ABV Kiran Kumar, R. Megha, CH VV Ramana, YT Ravi Kiran, Sabu Thomas, and Daewon Kim. "rGO/ZnO nanorods/Cu based nanocomposite having flower shaped morphology: Ac conductivity and humidity sensing response studies at room temperature." *Journal of Materials Science: Materials in Electronics* 30, no. 16 (2019): 15544-15552.

[197] Phan and Duy-Thach."Black P/graphene hybrid: A fast response humidity sensor with good reversibility and stability." *Scientific reports* 7.1 (2017): 1-7.

References

[98] Zhang, Dongzhi, Hongyan Chang, Peng Li, Runhua Liu, and Qingzhong Xue. "Fabrication and characterization of an ultrasensitive humidity sensor based on metal oxide/graphene hybrid nanocomposite." *Sensors and Actuators B: Chemical* 225 (2016): 233-240.

[99] Yang, Hui, Qiangqiang Ye, Ruixue Zeng, Junkai Zhang, Lei Yue, Ming Xu, Zhi-Jun Qiu, and Dongping Wu. "Stable and fast-response capacitive humidity sensors based on a ZnO nanopowder/PVP-RGO multilayer." *Sensors* 17, no. 10 (2017): 2415.

[100]He, Shiying, "High efficient visible-light photocatalytic performance of Cu/ZnO/rGO nanocomposite for decomposing of aqueous ammonia and treatment of domestic wastewater." *Frontiers in chemistry* 6 (2018): 219.

[101] Liu, Li, Shouchun Li, Juan Zhuang, Lianyuan Wang, Jinbao Zhang, Haiying Li, Zhen Liu, Yu Han, Xiaoxue Jiang, and Peng Zhang. "Improved selective acetone sensing properties of Co-doped ZnO nanofibers by electrospinning." *Sensors and actuators B: chemical* 155, no. 2 (2011): 782-788.

[102] Azam, Ameer, Arham S. Ahmed, Mohammad Oves, Mohammad S. Khan, Sami S. Habib, and Adnan Memic. "Antimicrobial activity of metal oxide nanoparticles against Gram-positive and Gram-negative bacteria: a comparative study." *International journal of nanomedicine* 7 (2012): 6003.

[103] Chong, Yu, Cuicui Ge, Ge Fang, Renfei Wu, He Zhang, Zhifang Chai, Chunying Chen, and Jun-Jie Yin. "Light-enhanced antibacterial activity of graphene oxide, mainly via accelerated electron transfer." *Environmental science & technology* 51, no. 17 (2017): 10154-10161.

[104] Pathiraja, Inoka Kumari. "Removal of acid yellow 25 dye onto chitin extracted from waste crab legs and study of adsorption isotherms and

kinetics of AY25 dye adsorption." PhD diss., Southern Illinois University at Edwardsville, 2014.

[97] Sharma, Ponchami, and Manash R. Das. "Removal of a cationic dye from aqueous solution using graphene oxide nanosheets: investigation of adsorption parameters." *Journal of Chemical & Engineering Data* 58.1 (2013): 151-158.

[98] Modwi, A., M. A. Abbo, E. A. Hassan, O. K. Al-Duaij, and Ammar Houas. "Adsorption kinetics and photocatalytic degradation of malachite green (MG) via Cu/ZnO nanocomposites." *Journal of environmental chemical engineering* 5, no. 6 (2017): 5954-5960.

[99] Khani, Rouhollah, Batoul Roostaei, Ghodsieh Bagherzade, and Maryam Moudi. "Green synthesis of copper nanoparticles by fruit extract of Ziziphus spina-christi (L.) Willd.: Application for adsorption of triphenylmethane dye and antibacterial assay." *Journal of Molecular Liquids* 255 (2018): 541-549.

[100] Wong, Ka Kan, Annie Ng, in i Chen, ip Hang Ng, u Hang Leung, Kam Hong Ho, Aleksandra B. Djuri i et al. "Effect of nO nanoparticle properties on dye-sensitized solar cell performance." *ACS applied materials & interfaces* 4, no. 3 (2012): 1254-1261.

[101]Aragaw, Belete Asefa, and Atsedemariam Dagnaw. "Copper/reduced graphene oxide nanocomposite for high performance photocatalytic methylene blue dye degradation." *Ethiopian Journal of Science and Technology* 12.2 (2019): 125-137.

[102] Mandal, Sujoy Kumar, Kajari Dutta, Saptarshi Pal, Sumit Mandal, Avigyan Naskar, Pabitra Kumar Pal, T. S. Bhattacharya et al. "Engineering of ZnO/rGO nanocomposite photocatalyst towards rapid degradation of toxic dyes." *Materials Chemistry and Physics* 223 (2019): 456-465.

References

[103] Jilani, Asim, Mohd Hafiz Dzarfan Othman, Mohammad Omaish Ansari, Mohammad Oves, Syed Zajif Hussain, *et al.*. "Structural and optical characteristics, and bacterial decolonization studies on non-reactive RF sputtered Cu–ZnO@ graphene based nanoparticles thin films." *Journal of Materials Science* 54, no. 8 (2019): 6515-6529.

[104] Muzaffar, S., M. Naeem Aslam, S. Rehman, S. Umer, S. Ahmed, and H. Anwar. "A simple and low-cost purification method for microbial-free water using zinc oxide nanoparticles." In *IOP Conference Series: Materials Science and Engineering*, vol. 863, no. 1(2020). 012037.

[105] Romadhan, Muhammad Fajri, Nurgaha Edhi Suyatma, and Fahim Muchammad Taqi. "Synthesis of ZnO nanoparticles by precipitation method with their antibacterial effect." *Indonesian Journal of Chemistry* 16.2 (2016): 117-123.

[106] Abbas, Adel H., and Nada Y. Fairouz. "Characterization, biosynthesis of copper nanoparticles using ginger roots extract and investigation of its antibacterial activity." *Materials Today: Proceedings* (2021).

[107] Devi, R. Shruthi, M. Jeevitha, S. Preetha, and S. Rajeshkumar. "Free Radical Scavenging Activity of Copper Nanoparticles Synthesized from Dried Ginger." *Journal of Pharmaceutical Research International* (2020): 1-7.

[108] Santamaría-Juárez, Guillermo, Estela Gómez-Barojas, Enrique Quiroga-González, Enrique Sánchez-Mora, *et al.* "Safer modified Hummers' method for the synthesis of graphene oxide with high quality and high yield." *Materials Research Express* 6, no. 12 (2020): 125631.

[109] Alam, Syed Nasimul, Nidhi Sharma, and Lailesh Kumar. "Synthesis of graphene oxide (GO) by modified hummers method and its thermal

reduction to obtain reduced graphene oxide (rGO)." *Graphene* 6.1 (2017): 1-18.

[110] Basha, Mubarak Ali Muhamath, and Saranya Rishikesan. "Synthesis, Characterization and Evaluation of Antimicrobial, Antioxidant & Anticancer Activities of Copper Doped Zinc Oxide Nanoparticles." *Acta Chimica Slovenica* 67.1 (2020): 235-245.

[111] Ravi, K., B. Sathish Mohan, G. Satya Sree, I. Manga Raju, K. Basavaiah, *et al.* "ZnO/RGO nanocomposite via hydrothermal route for photocatalytic degradation of dyes in presence of visible light." *Int J Chem Stud* 6, no. 6 (2018): 20-26.

[112] Nie, Haibin, Licai Fu, Jiajun Zhu, Wulin Yang, Deyi Li, and Lingping Zhou. "Excellent tribological properties of lower reduced References

graphene oxide content copper composite by using a one-step reduction molecular-level mixing process." *Materials* 11, no. 4 (2018): 600.

[113] He, Shiying, Pengfu Hou, Evangelos Petropoulos, Yanfang Feng, Yingliang Yu,*et al.* "High efficient visible-light photocatalytic performance of Cu/ZnO/rGO nanocomposite for decomposing of aqueous ammonia and treatment of domestic wastewater." *Frontiers in chemistry* 6 (2018): 219.

[114] Meva, Francois Eya'ane. "Silver and palladium nanoparticles produced using a plant extract as reducing agent, stabilized with an ionic liquid: sizing by X-ray powder diffraction and dynamic light scattering." *Journal of Materials Research and* Technology 8.2 (2019): 1991-2000.

[115] Qiao, Yu, Xiangchao Meng, and Zisheng Zhang. "A new insight into the enhanced visible light-induced photocatalytic activity of NaNbO3/Bi2WO6 type-II heterostructure photocatalysts." *Applied Surface Science* 470 (2019): 645-657.

[116] Farrokhi, Mehrdad, Seyydeh-Cobra Hosseini, Jae-Kyu Yang, and Mehdi Shirzad-Siboni. "Application of ZnO–Fe 3 O 4 nanocomposite on the removal of azo dye from aqueous solutions: kinetics and equilibrium studies." *Water, Air, & Soil Pollution* 225, no. 9 (2014): 1-12.

[117] Adepu, Ajay Kumar, Suresh Siliveri, Suman Chirra, Srinath Goskula, *et al*. "A novel porous Fe3O4/Titanosilicate/g-C3N4 ternary nanocomposites: Synthesis, characterization and their enhanced photocatalytic activity on Rhodamine B degradation under sunlight irradiation." *Journal of Water Process Engineering* 34 (2020): 101141.

[118] Gomri, Fatima, Gisèle Finqueneisel, Antonio Gil, and Mokhtar Boutahala. "Adsorption of Rhodamine 6G and humic acids on composite bentonite–alginate in single and binary systems." *Applied Water Science* 8, no. 6 (2018): 1-10.

[119] Ahmadi, Shahin, and Chinenye Adaobi Igwegbe. "Adsorptive removal of phenol and aniline by modified bentonite: adsorption isotherm and kinetics study." *Applied Water Science* 8.6 (2018): 1-8.

[120] Waheeb, Azal Shakir, Hassan Abbas Habeeb Alshamsi, Mohammed Kassim Al-Hussainawy, and Haider Radhi Saud. "Myristica fragrans Shells as Potential Low Cost Bio-Adsorbent for the Efficient Removal of Rose Bengal from Aqueous Solution: Characteristic and Kinetic Study." *Indonesian Journal of Chemistry* (2019).

[121] Mohammad, Emman J., Salih H. Kathim, and Abbas J. Attiah. "Removal of Bismarck Brown G Dye from Simulated Industrial Wastewaters over (Co, Ni) 3O4/Al2O3 Co-Catalyst." *Babylon Univ. Pure Appl*. Sci 25.2 (2017): 504-514.

References

[122] FP de Sá, Fernando Pereira, Beatriz Nogueira Cunha, and Liliane Magalhães Nunes. "Effect of pH on the adsorption of Sunset Yellow FCF food dye into a layered double hydroxide (CaAl-LDH-NO3)." *Chemical Engineering Journal* 215 (2013): 122-127.

[123] Toor, Manjot, and Bo Jin. "Adsorption characteristics, isotherm, kinetics, and diffusion of modified natural bentonite for removing diazo dye." *Chemical Engineering Journal* 187 (2012): 79-88.

[124] Nanta, Phawinee, Kittiwut Kasemwong, and Wanwisa Skolpap. "Isotherm and kinetic modeling on superparamagnetic nanoparticles adsorption of polysaccharide." *Journal of environmental chemical engineering* 6.1 (2018): 794-802.

[125] Beyki, Mostafa Hossein, Sarina Ehteshamzadeh Ganjbakhsh, Sara Minaeian, and Farzaneh Shemirani. "Clean approach to synthesis of graphene like CuFe2O4@ polysaccharide resin nanohybrid: Bifunctional compound for dye adsorption and bacterial capturing." *Carbohydrate polymers* 174 (2017): 128-136.

[126] Gupta , Susmita Sen, and Krishna G. Bhattacharyya. "Kinetics of adsorption of metal ions on inorganic materials: a review." *Advances in colloid and interface science* 162.1-2 (2011): 39-58.

[127] Takahashi, Yusuke, Shiro Kubuki, Kazuhiko Akiyama, Katalin Sinkó, Ernő Kuzmann, *et al*. "Visible light activated photo-catalytic effect and local structure of iron silicate glass prepared by sol-gel method." *Hyperfine Interactions* 226, no. 1 (2014): 747-753.

[128] Bankier, Claire, R. K. Matharu, Y. K. Cheong, G. G. Ren, *et al*. "Synergistic antibacterial effects of metallic nanoparticle combinations." *Scientific reports* 9, no. 1 (2019): 1-8.

References

[129] Steffy, Katherin, G. Shanthi, Anson S. Maroky, and S. Selvakumar. "Synthesis and characterization of ZnO phytonanocomposite using Strychnos nux-vomica L.(Loganiaceae) and antimicrobial activity against multidrug-resistant bacterial strains from diabetic foot ulcer." *Journal of advanced research* 9 (2018): 69-77.

[130] Muhammad, Wali, Naimat Ullah, Muhammad Haroon, and Bilal Haider Abbasi. "Optical, morphological and biological analysis of zinc oxide nanoparticles (ZnO NPs) using Papaver somniferum L." *RSC advances* 9, no. 51 (2019): 29541-29548.

[131] Chen, Youhu, Yufang Niu, Tian Tian, Juan Zhang, Lu-Chang Qin *,et al.* "Microbial reduction of graphene oxide by Azotobacter chroococcum." *Chemical Physics Letters* 677 (2017): 143-147.

[132] Bahrami, Amir, Iraj Kazeminezhad, and Yaser Abdi. "Pt-Ni/rGO counter electrode: electrocatalytic activity for dye-sensitized solar cell." *Superlattices and Microstructures* 125 (2019): 125-137.

[133] Sampath, Malathi, Ramya Vijayan, Ezhilarasu Tamilarasu, Abiraman Tamilselvan, and Balasubramanian Sengottuvelan. "Green synthesis of novel jasmine bud-shaped copper nanoparticles." *Journal of Nanotechnology* 2014 (2014).

[134] Ma, Zhanhong, Fengzhang Ren, Xiaoli Ming, Yongqiang Long, and Alex A. Volinsky. "Cu-doped ZnO electronic structure and optical properties studied by first-principles calculations and experiments." *Materials* 12, no. 1 (2019): 196.

[135] Yusoff, Farhanini, Ngai Tze Khing, Lee Pak Sang, Nurul'ain Basyirah Muhamad, and Noorashikin Md Saleh. "The electrochemical behavior of zinc oxide/reduced graphene oxide composite electrode in dopamine." *Malaysian Journal of Analytical Sciences* 22, no. 2 (2018): 227-237.

References

[136] Zhang, Qi, Qin Luo, Zhenbo Qin, Lei Liu, Zhong Wu, Bin Shen, and Wenbin Hu. "Self-assembly of graphene-encapsulated Cu composites for nonenzymatic glucose sensing." *ACS omega* 3, no. 3 (2018): 3420-3428.

[137] Shewale, Prashant Shivaji, and Kwang-Seok Yun. "Synthesis and characterization of Cu-doped ZnO/RGO nanocomposites for room-temperature H2S gas sensor." *Journal of Alloys and Compounds* 837 (2020): 155527.

[138] Pudukudy, Manoj, and Zahira Yaakob. "Facile synthesis of quasi spherical ZnO nanoparticles with excellent photocatalytic activity." *Journal of Cluster Science* 26.4 (2015): 1187-1201.

[139] Yan, Wen, Yutang Liu, Shirin Mansooridara, Atoosa Shahriyari Kalantari, *et al.* "Chemical characterization and neuroprotective properties of copper nanoparticles green-synthesized by nigella sativa L. seed aqueous extract against methadone-induced cell death in adrenal phaeochromocytoma (PC12) cell line." *Journal of Experimental Nanoscience* 15, no. 1 (2020): 280-296.

[140] Neelgund, Gururaj M., and Aderemi Oki. "Graphene-coupled zno: A robust nir-induced catalyst for rapid photo-oxidation of cyanide." *ACS omega* 2.12 (2017): 9095-9102.

[141] Khalid, Awais, Pervaiz Ahmad, Abdulrahman I. Alharthi, Saleh Muhammad, Mayeen Uddin Khandaker, *et al.* "Synergistic effects of Cu-doped ZnO nanoantibiotic against Gram-positive bacterial strains." *Plos one* 16, no. 5 (2021): e0251082.

[142] Huang, Xiubing, Guixia Zhao, and Xiangke Wang. "Fabrication of reduced graphene oxide/metal (Cu, Ni, Co) nanoparticle hybrid composites

via a facile thermal reduction method." *RSC Advances* 5.62 (2015): 49973-49978.

[143] Asgharian, Maedeh, Mohsen Mehdipourghazi, Behnam Khoshandam, and Narjes Keramati. "Photocatalytic degradation of methylene blue with synthesized rGO/ZnO/Cu." *Chemical Physics Letters* 719 (2019): 1-7.

[144] Raj, L. F., and E. Jayalakshmy. "A biogenic approach for the synthesis and characterization of zinc oxide nanoparticles produced by Tinospora Cordifolia." *Int J Pharm Pharm Sci* 7 (2015): 384-386.

[145] Wu, Shuang, Shanmugam Rajeshkumar, Malini Madasamy, and Vanaja Mahendran. "Green synthesis of copper nanoparticles using Cissus vitiginea and its antioxidant and antibacterial activity against urinary tract infection pathogens." *Artificial Cells, Nanomedicine, and Biotechnology* 48, no. 1 (2020): 1153-1158.

[146] Bano, N., I. Hussain, A. M. El-Naggar, and A. A. Albassam. "Reduced graphene oxide nanocomposites for optoelectronics applications." *Applied Physics A* 125, no. 3 (2019): 1-7.

[147] Khan, S. A., F. Noreen, S. Kanwal, and G. Hussain. "Comparative synthesis, characterization of Cu-doped ZnO nanoparticles and their antioxidant, antibacterial, antifungal and photocatalytic dye degradation activities." *Dig J Nanomater Biostruct* 12, no. 3 (2017): 877-89.

[148] Pang, Yean Ling, Su Fang Tee, Steven Lim, Ahmad Zuhairi Abdullah, Hwai Chyuan Ong, *et al.* "Enhancement of photocatalytic degradation of organic dyes using ZnO decorated on reduced graphene oxide (rGO)." *Desalination Water Treat* 108 (2018): 311-321.

[149] Ahmadi, Fatemeh, and Shahram Ghasemi. "Electrophoretic deposition of copper–copper hydroxide/graphene oxide nanocomposite for

supercapacitor." *Journal of Materials Science: Materials in Electronics* 2 9076-9067 :(2018) 9.11.

[150] Kuntal, Dheeraj, Swati Chaudhary, ABV Kiran Kumar, R. Megha, CH VV Ramana, *et al.*. "rGO/ZnO nanorods/Cu based nanocomposite having flower shaped morphology: Ac conductivity and humidity sensing response studies at room temperature." *Journal of Materials Science: Materials in Electronics* 30, no. 16 (2019): 15544-15552.

[151] Jayarambabu, N., B. Siva Kumari, K. Venkateswara Rao, and Y. T. Prabhu. "Germination and growth characteristics of mungbean seeds (Vigna radiata L.) affected by synthesized zinc oxide nanoparticles." *International Journal of Current Engineering and Technology* 4, no. 5 (2014): 2347-5161.

[152] Joseph, Akancha Teresa, and B. Prakash, S.; "Plant synthesis and characterization of copper nanoparticles with Allium sativum and its antibacterial activity." *Int J. Sci. M. Technol* 4 (2016): 463–472

[153] Hasnain, Reza, Dalal Z. Hussain and Mustafa F. Hakani. "Biosynthesis of copper nanoparticles using aqueous Tilia extract: antimicrobial and anticancer activities." *Helion* 4.12 (2018): e01077.

[154] Johra, Fatima Tuz, and Woo-Gwang Jung. "Hydrothermally reduced graphene oxide as a supercapacitor." *Applied Surface Science* 357 (2015): 1911-1914.

[155] Kalpana, V. N., Poulami Chakraborthy, V. Palanichamy, and V. Devi Rajeswari. "Synthesis and characterization of copper nanoparticles using Tridax procumbens and its application in degradation of bismarck brown." *Analysis* 10 (2016): 17.

[156] Pashchanka, Mikhail, Rudolf C. Hoffmann, Aleksander Gurlo, Janine C. Swarbrick, Jayaprakash Khanderi, Jörg Engstler, *et al*. "Amolecular

approach to Cu doped ZnO nanorods with tunable dopant content." *Dalton Transactions* 40, no. 16 (2011): 4307-4314.

[157] Sarkar, Chandrama, and Swapan K. Dolui. "Synthesis of copper oxide/reduced graphene oxide nanocomposite and its enhanced catalytic activity towards reduction of 4-nitrophenol." *RSC advances* 5.75 (2015): 60763-60769.

[158] Marcano, Daniela C., Dmitry V. Kosynkin, Jacob M. Berlin, Alexander Sinitskii, Zhengzong Sun, *et al*. "Improved synthesis of graphene oxide." *ACS nano* 4, no. 8 (2010): 4806-4814.

[159] Asgar, Hassnain, Kashif Mairaj Deen, and Waseem Haider. "Estimation of electrochemical charge storage capability of ZnO/CuO/reduced graphene oxide nanocomposites." *International Journal of Energy Research* 44.3 (2020): 1580-1593

[160] Malvern Instruments, L. "Zeta Potential: An Introduction in 30 Minutes." *Malvern Instruments*. Report nr mrk 654 (2012): 6.

[161] Cui, Chang-Wei, Chao Yang, Jun Bao, Xie-Jun Huang, Xiao-Fei Zeng, and Jian-Feng Chen. "Monodispersed ZnO Nanoparticle-Poly (methyl methacrylate) Composites with Visible Transparency for Ultraviolet Shielding Applications." *ACS Applied Nano Materials* 3, no. 9 (2020): 9026-9034.

[162] Senthilkumar, N., E. Vivek, M. Shankar, M. Meena, M. Vimalan, and I. Vetha Potheher. "Synthesis of ZnO nanorods by one step microwave-assisted hydrothermal route for electronic device applications." *Journal of Materials Science: Materials in Electronics* 29, no. 4 (2018): 2927-2938.

References

[163] Cuevas, R."Extracellular biosynthesis of copper and copper oxide nanoparticles by Stereum hirsutum, a native white-rot fungus from chilean forests." *Journal of Nanomaterials* 2015 (2015).

[164] El-Shafai, Nagi M., Mohamed E. El-Khouly, Maged El-Kemary, Mohamed S. Ramadan, and Mamdouh S. Masoud. "Graphene oxide–metal oxide nanocomposites: fabrication, characterization and removal of cationic rhodamine B dye." *RSC advances* 8, no. 24 (2018): 13323-13332.

[165] El-Shafai, Nagi M. "Investigation of a novel (GO@ CuO. γ-Al2O3) hybrid nanocomposite for solar energy applications." *Journal of Alloys and Compounds* 856 (2021): 157463.

[166] Sapkota, B. B., and S. R. Mishra. "A simple ball milling method for the preparation of p-CuO/n-ZnO nanocomposite photocatalysts with high photocatalytic activity." *Journal of nanoscience and nanotechnology* 13.10 (2013): 6588-6596.

[167] Sood, Kritika, Jasreen Kaur, Harpreet Singh, Shailendra Kumar Arya, and Madhu Khatri. "Comparative toxicity evaluation of graphene oxide (GO) and zinc oxide (ZnO) nanoparticles on Drosophila melanogaster." *Toxicology reports* 6 (2019): 768-781.

[168] Ahamed, Maqusood. "SnO2-Doped ZnO/reduced graphene oxide nanocomposites: synthesis, characterization, and improved anticancer activity via oxidative stress pathway." *International Journal of Nanomedicine* 16 (2021): 89

[169] Sayğılı, Hasan. "Hydrothermal synthesis of magnetic nanocomposite from biowaste matrix by a green and one-step route:

characterization and pollutant removal ability." *Bioresource technology* 278 (2019): 242-247.

References

[170] Saranyaadevi, K., V. Subha, RS Ernest Ravindran, and S. Renganathan. "Synthesis and characterization of copper nanoparticle using Capparis zeylanica leaf extract." *Int J Chem Tech Res* 6, no. 10 (2014): 4533-4541.

[171] Bo Zhong, Jun, Jian zhang Li, Xi yang He, Jun Zeng, Yan Lu, Wei Hu, and Kun Lin. "Improved photocatalytic performance of Pd-doped ZnO." *Current Applied Physics* 12, no. 3 (2012): 998-1001.

[172] Wang, Lizhuo, Jinhui Zhao, Huimin Liu, and Jun Huang. "Design, modification and application of semiconductor photocatalysts." *Journal of the Taiwan Institute of Chemical Engineers* 93 (2018): 590-602.

[173] van den Bijllaardt, Wouter, Maarten J. Schijffelen, Ron W. Bosboom, James Cohen Stuart, *et al.* "Susceptibility of ESBL Escherichia coli and Klebsiella pneumoniae to fosfomycin in the Netherlands and comparison of several testing methods including Etest, MIC test strip, Vitek2, Phoenix and disc diffusion." *Journal of Antimicrobial Chemotherapy* 73, no. 9 (2018): 2380-2387.

[174] Hsueh, Yi-Huang, Chien-Te Hsieh, Shu-Ting Chiu, and Wan-Ju Ke. "Antibacterial property of composites of reduced graphene oxide with nano-silver and zinc oxide nanoparticles synthesized using a microwave-assisted approach." *International journal of molecular sciences* 20, no. 21 (2019): 5394.

[175] Ahmed, Dooraid N., Laith A. Naji, Ayad AH Faisal, Nadhir Al-Ansari, and Mu Naushad. "Waste foundry sand/MgFe-layered double hydroxides composite material for efficient removal of Congo red dye from aqueous solution." *Scientific Reports* 10, no. 1 (2020): 1-12.

136

[167] Mall, Indra Deo, Vimal Chandra Srivastava, and Nitin Kumar Agarwal. "Adsorptive removal of Auramine-O: Kinetic and equilibrium study." *Journal of Hazardous materials* 143.1-2 (2007): 386-395.

[177] Kausar, Abida, Munawar Iqbal, Anum Javed, Kiran Aftab, Haq Nawaz Bhatti, and Shazia Nouren. "Dyes adsorption using clay and modified clay: a review." *Journal of Molecular Liquids* 256 (2018): 395-407.

[178] Mohammad, Eman J., Abbas J. Lafta, Salih H. Kahdem, and Ayad F. Alkaim. "Enhancement the photocatalytic activity of Zinc Oxide surface by combination with Functionalized and non-Functionalized Activated Carbon." *Int J ChemTech Res* 9, no. 12 (2016): 656.

[179] Maderova, Z., E. Baldikova, K. Pospiskova, I. Safarik, and M. Safarikova. "Removal of dyes by adsorption on magnetically modified activated sludge." *International journal of Environmental science and technology* 13, no. 7 (2016): 1653-1664.

[180]. Liu, Xin, and Lingfan Zhang. "Removal of phosphate anions using the modified chitosan beads: adsorption kinetic, isotherm and mechanism studies." *Powder Technology* 277 (2015): 112-119.

[181] Fu, Jianwei, *et al.* "Adsorption of methylene blue by a high-efficiency adsorbent (polydopamine microspheres): kinetics, isotherm, thermodynamics and mechanism analysis." *Chemical Engineering Journal* 259 (2015): 53-61.

[182] Kaur, Jagdeep, Manoj Sharma, and O. P. Pandey. "Synthesis, characterization, photocatalytic and reusability studies of capped ZnS nanoparticles." *Bulletin of Materials Science* 37.4 (2014): 931-940.

الخلاصة:

تتضمن هذه الدراسة تخليق مركبات وجسيمات النانوية مثل التخليق الحيوي لجسيمات النحاس النانوية (Cu NPs) ، باستخدام مستخلص جذر الزنجبيل ، باستخدام نهج الترسيب فقط باستخدام (هيبتا هيدرات كبريتات الزنك) (ZnSO4.7H2O) كطريقة غير ضارة بالبيئة ، وتخليق جسيمات أوكسيد الزنك (ZnO NPs) عن طريق الترسيب . ثم بعد ذلك بطريقة اخرى تم اقترن جسيمات أوكسيد الزنك بالنحاس لانتاج المركبات النانوية الثنائية Cu / ZnO NPs بالطريقة الحرارية المائية .

تقترن هذه الأنظمة الثنائية النانوية بأوكسيد الجرافين المختزل (rGO) من أجل الحصول على المتراكب الثلاثي النانوي (Cu / ZnO / rGO) تم قياس جزء من فعاليته الفيزيائية والبيولوجية.

تم التحقيق من المواد المخلقة باستخدام تقنيات مختلفة مثل(X-Ray Diffract (X-Ray ,المجهر الإلكتروني (FE- SEM) ، تشتيت الطاقة - الأشعة السينية (EDX) ،جهد زيتا ، الأشعة تحت الحمراء (FTIR) ، و Brunaueres Emmett Teller (BET) المساحة السطحية .و تم قياس قوة زيتا عند حوالي (-27.4 مللي فولت) ،مساحة سطح BET [29.833 م ^{2} جم $^{-1}$] ومتوسط حجم الكريستال (23.77 نانومتر) .

كما تم فحص كفاءة امتصاص صبغة (الرودامين G 6)على كل هذه المواد وتم تسجيل أفضل نسبة إزالة للصبغة هي (% 80.7) عن المعلق المستخدم لهذه المواد باستخدام المتراكب النانوي الثلاثي بوزن 0.1 غم ، ودرجة حموضة 9 ودرجة حرارة 30 درجة مئوية ولمدة 60 دقيقة. في هذا السياق تم الأخذ بعين الاعتبار ظروف الامتزاز المختلفة مثل تأثير درجة الحرارة ، وزن كتلة المواد المستخدمة ، زمن التلامس، تركيز الصبغه ، ودرجة الحموضة لخليط التفاعل.

تم فحص كل من الايزوثيرم (لانجموير وفرندلش) وأظهرت النتائج التي تم الحصول عليها أنها كانت أكثر ملاءمة مع فرندلش وكانت حركية التفاعل من الدرجة الثانية الكاذبة .

كذلك تم التحقق من تثبيط نشاط سلالتين من بكتريا الأشريكية القولونية (الإشريكية القولونية (السالبة جرام) وبكتريا المكورات العنقودية الذهبية (الموجبة جرام) بتراكيز مختلفة من (2.5_ 10 ملغم / مل) من المركبات والجسيمات النانوية المخلقة وأظهرت أفضل منطقة تثبيط للمتراكب الثلاثي (Cu/ZnO / rGO)النانوي واعطى تركيز(10 ملغم / مل) أعلى منطقة تثبيط (13.2 ملم) ضد بكتيريا E. coli و(9.6 ملم) ضد بكتريا S. aurous

جمهورية العراق
وزارة التعليم العالي والبحث العلمي
جامعة بابل - كلية العلوم
قسم الكيمياء

تخليق المتراكب النانوي الثلاثي Cu/ZnO/rGO وتطبيقاته على ازالة صبغة الرودامين 6G من المحلول المائي والفعالية ضد البكتريا

رسالة مقدمة

إلى مجلس كلية العلوم – جامعة بابل

كجزء من متطلبات نيل درجة الماجستير في العلوم \ الكيمياء

تقدم بها

عادل حمزة عباس حسون

بكالوريوس علوم كيمياء- جامعة القادسية 2013

بأشراف

الأستاذ الدكتور ندى يحيى فيروز

١٤٤٣هـ ٢٠٢١م